

THE UNIVERSITY OF ALBERTA

A STUDY OF THE (${}^3\text{He},n$) REACTION ON SOME
 $1p$ SHELL NUCLEI

by



Tung - Hong Hsu

A THESIS

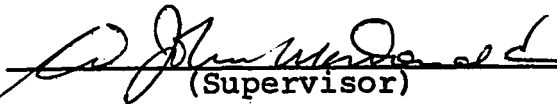
SUBMITTED TO THE FACULTY OF GRADUATE STUDIES
IN PARTIAL FULFILLMENT OF THE REQUIREMENTS FOR THE DEGREE
OF DOCTOR OF PHILOSOPHY

DEPARTMENT OF PHYSICS
EDMONTON, ALBERTA

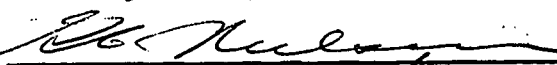
Spring, 1969

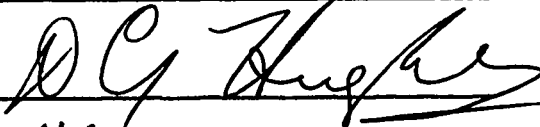
UNIVERSITY OF ALBERTA
FACULTY OF GRADUATE STUDIES

The undersigned certify that they have read, and recommend to the Faculty of Graduate Studies for acceptance, a thesis entitled A STUDY OF THE ($^3\text{He},n$) REACTION ON SOME $1p$ SHELL NUCLEI, submitted by Tung-Hong Hsu in partial fulfillment of the requirements for the degree of Doctor of Philosophy.

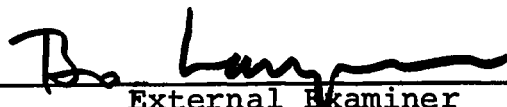


(Supervisor)





Edmonton



External Examiner

Date 15 Jan. 1969

ACKNOWLEDGEMENTS

I would like to thank my supervisor, Dr. W. J. McDonald, for his encouragement and support in the course of this work. Thanks are extended to Dr. G. C. Nielson for his interest in the work and patience in reading the manuscript.

I am especially grateful to Dr. J. L. Honsaker for his assistance in collecting data and many illuminating discussions.

I wish to thank Dr. W. Davies and Mr. N. Davison, who made available the running Yates DWBA and Hauser-Feshbach computer codes.

Thanks are extended to the software staff, Dr. W. K. Dawson and Mr. J. F. Easton, for providing an excellent data acquisition system, and also to the hardware staff Messrs. J. B. Elliot and L. Holms.

Thanks are also due to Mrs. L. Watson for her expeditious typing of this thesis.

Finally, I wish to acknowledge the financial support provided by the University of Alberta throughout the course of this work.

ABSTRACT

The reaction $^{11}\text{B}(^3\text{He},n)^{13}\text{N}$, $^{12}\text{C}(^3\text{He},n)^{14}\text{O}$ and $^{13}\text{C}(^3\text{He},n)^{15}\text{O}$ have been investigated by the neutron time-of-flight method. Precise reaction Q values and the corresponding excitation energies for ^{13}N (up to 12.937 MeV level) and ^{15}O (up to 9.665 MeV level) have been measured.

For the $^{11}\text{B}(^3\text{He},n)^{13}\text{N}$, neutron yield leading to 0.0 state, 2.358, 7.145, and 7.363 MeV were measured at 90° lab. angle, at ^3He bombarding energies between 5.4 to 6.45 MeV. Angular distributions of the neutrons leading to the 0.0, 2.358, 3.502, 6.353, 6.875, 7.145, 7.363, 9.476, 10.381 and 11.878 MeV levels were studied at $E_{^3\text{He}} = 6.49, 6.1, \text{ and } 4.7 \text{ MeV}$.

For the $^{13}\text{C}(^3\text{He},n)^{15}\text{O}$, neutron yields leading to 0.0, 6.183, 7.286, 7.570, 8.750, 9.498, 9.612 and 9.665 MeV states were measured at 0° at bombarding energies between 5.5 and 6.5 MeV. Neutron angular distributions for the ground state 6.183, 6.790, 6.869, 7.286, 7.570, 8.750, 8.926, 8.974, 9.498, and 9.611 MeV levels were studied at $E_{^3\text{He}} = 5.0$ and 6.2 MeV. Also, a relative angular distribution for $^{12}\text{C}(^3\text{He},n)^{14}\text{O}$ was obtained at $E_{^3\text{He}} = 6.1 \text{ MeV}$.

The simplified plane wave double stripping theory of Newns (NE 60) the diffraction model of Dar (DA 64), and the DWBA theory of Rook and Mitra (RO 64) were employed for explanation of angular distributions. To see how important is the contribution from the compound nucleus formation, the Hauser and Feshbach calculations were also performed for individual distributions. Reasonable agreement between direct reaction theories and experimental results suggests that for most of

the transitions studied, the direct interaction is predominant.

Based on a direct interaction model for the transition to the 8.926 MeV level of ^{15}O , the spin and parity can be re-assigned as $\frac{1}{2}^-$ instead of $\frac{1}{2}^+$ (AJ 62). Also, both the 9.498 and 9.612 MeV levels of ^{15}O were assigned as $j^\pi = \frac{3}{2}^-, \frac{5}{2}^-$.

TABLE OF CONTENTS

	Page
INTRODUCTION	i
CHAPTER I THE REACTION MECHANISM	1
1. Direct Interaction and Compound Nucleus Formation	1
2. The Plane Wave Born Approximation	2
3. The Distorted Wave Born Approximation	6
4. The Diffraction Model	8
5. Other Consideration on the DI Mechanism	10
6. Compound Nucleus Formation	11
CHAPTER II THE EXPERIMENTAL METHODS	13
1. The Neutron Time-of-Flight Systems	13
2. The Neutron Detectors	16
3. The Target Assembly	17
4. The Data Extractions	20
CHAPTER III THE RESULTS (I) $^{11}\text{B}(^3\text{He},n)^{13}\text{N}$ REACTION	24
1. General Background	24
2. The Energy Levels and Their Excitation Curves	25
3. The Analysis	28
4. Levels of ^{13}N	36
CHAPTER IV RESULTS (II) $^{13}\text{C}(^3\text{He},n)^{15}\text{O}$ AND $^{12}\text{C}(^3\text{He},n)^{14}\text{O}$	50
1. General Background	50
2. The Energy Levels and Their Excitation Curves	51
3. Analysis of the $^{13}\text{C}(^3\text{He},n)^{15}\text{O}$ and $^{12}\text{C}(^3\text{He},n)^{14}\text{O}$ Results	56
4. Levels of ^{15}O	60

	Page
CHAPTER V CONCLUSIONS	79
APPENDIX I THE TARGET THICKNESS MEASUREMENTS	83
1. The Boron 11 Target	83
2. The Carbon 13 Target	85
APPENDIX II THE Q VALUES MEASUREMENTS	89
APPENDIX III TABLES OF CROSS SECTIONS	92
REFERENCES	

FIGURES

	Page
Fig. 1. Block diagram of electronics system	14
2. A typical figure of merit curve for the n - γ discriminator circuit	21
3. A neutron time-of-flight spectrum for the $^{11}\text{B}(^3\text{He},n)^{13}\text{N}$ reaction at $E_{^3\text{He}} = 6.1$ MeV	26
4. The 90° neutron yield curves of $^{11}\text{B}(^3\text{He},n)^{13}\text{N}$ for the 0.0, 2.358, 7.145, 7.363 MeV levels of ^{13}N , and to an unresolved 3.502 + 3.55 MeV level	29
5. Neutron angular distribution of the ground state of ^{13}N for $E_{^3\text{He}} = 6.49$ MeV	37
6. Neutron angular distribution of the ground state of ^{13}N for $E_{^3\text{He}} = 6.1$ MeV	37
7. Neutron angular distribution of the ground state of ^{13}N for $E_{^3\text{He}} = 4.7$ MeV	37
8. Neutron angular distribution of the 2.358 MeV level of ^{13}N for $E_{^3\text{He}} = 6.49$ MeV	39
9. Neutron angular distribution of the 2.358 MeV level of ^{13}N for $E_{^3\text{He}} = 6.1$ MeV	39
10. Neutron angular distribution of the 2.358 MeV level of ^{13}N for $E_{^3\text{He}} = 4.7$ MeV	39
11. Neutron angular distribution of the unresolved levels 3.502 + 3.55 MeV of ^{13}N for $E_{^3\text{He}} = 6.49$ MeV	41
12. Neutron angular distribution of the unresolved levels 3.502 + 3.55 MeV of ^{13}N for $E_{^3\text{He}} = 6.1$ MeV	41
13. Neutron angular distribution of the unresolved levels 3.502 + 3.55 MeV of ^{13}N for $E_{^3\text{He}} = 4.7$ MeV.	41
14. Neutron angular distribution of the 6.353 MeV level of ^{13}N for $E_{^3\text{He}} = 6.1$ MeV	42
15. Neutron angular distribution of the 6.353 MeV level of ^{13}N for $E_{^3\text{He}} = 4.7$ MeV	42
16. Neutron angular distribution of the 6.875 MeV level of ^{13}N for $E_{^3\text{He}} = 6.1$ MeV	42
17. Neutron angular distribution of the 6.875 MeV level of ^{13}N for $E_{^3\text{He}} = 4.7$ MeV	42

18. Neutron angular distribution of the 7.145 MeV level of ^{13}N for $E_{3\text{He}} = 6.1$ MeV 42
19. Neutron angular distribution of the 7.145 MeV level of ^{13}N for $E_{3\text{He}} = 4.7$ MeV 42
20. Neutron angular distribution of the 7.363 MeV level of ^{13}N for $E_{3\text{He}} = 6.1$ MeV 45
21. Neutron angular distribution of the 7.363 MeV level of ^{13}N for $E_{3\text{He}} = 4.7$ MeV 45
22. Neutron angular distribution of the 9.476 MeV level of ^{13}N for $E_{3\text{He}} = 6.49$ MeV 47
23. Neutron angular distribution of the 9.476 MeV level of ^{13}N for $E_{3\text{He}} = 6.1$ MeV 47
24. Neutron angular distribution of the 9.476 MeV level of ^{13}N for $E_{3\text{He}} = 4.7$ MeV 47
25. Neutron angular distribution of the 11.878 MeV level of ^{13}N for $E_{3\text{He}} = 6.1$ MeV 47
26. Neutron angular distribution of the 11.878 MeV level of ^{13}N for $E_{3\text{He}} = 4.7$ 47
27. Neutron angular distribution of the 10.381 MeV level of ^{13}N for $E_{3\text{He}} = 6.49$ MeV 49
28. Neutron angular distribution of the 10.381 MeV level of ^{13}N for $E_{3\text{He}} = 6.1$ MeV 49
29. Neutron angular distribution of the 10.381 MeV level of ^{13}N for $E_{3\text{He}} = 4.7$ MeV 49
30. A time-of-flight spectrum for the $^{13}\text{C}(^3\text{He},n)^{15}\text{O}$ reaction of $E_{3\text{He}} = 5.0$ MeV 52
31. The 0° neutron yield curves of $^{13}\text{C}(^3\text{He},n)^{15}\text{O}$ for the 0.0, 6.183, 7.286 and 7.570 MeV levels 55
32. The 0° neutron yield curves of $^{13}\text{C}(^3\text{He},n)^{15}\text{O}$ for the 8.75, 9.498, 9.612 and 9.665 MeV levels 55
33. The 0° neutron yield curves of $^{13}\text{C}(^3\text{He},n)^{15}\text{O}$ for the unresolved levels of 8.926 + 8.974, 6.79 + 6.87 and 5.188 + 5.240 MeV 55
34. Neutron angular distribution of the ground state of ^{14}O for $E_{3\text{He}} = 6.1$ MeV 57
35. Neutron angular distribution of the ground state of ^{15}O for $E_{3\text{He}} = 6.2$ MeV 62

36. Neutron angular distribution of the ground state of ^{15}O for $E_{3\text{He}} = 5.0$ MeV 62
37. Neutron angular distribution of the unresolved 5.188 and 5.240 MeV levels of ^{15}O for $E_{3\text{He}} = 6.2$ MeV 62
38. Neutron angular distribution of the unresolved 5.188 and 5.240 MeV levels of ^{15}O for $E_{3\text{He}} = 5.0$ MeV 64
39. Neutron angular distribution of the 6.183 MeV level of ^{15}O for $E_{3\text{He}} = 6.2$ MeV 64
40. Neutron angular distribution of the 6.183 MeV level of ^{15}O for $E_{3\text{He}} = 5.0$ MeV 66
41. Neutron angular distribution of the 6.790 MeV level of ^{15}O for $E_{3\text{He}} = 5.0$ MeV 66
42. Neutron angular distribution of the 6.869 MeV level of ^{15}O for $E_{3\text{He}} = 5.0$ MeV 68
43. Neutron angular distribution of the 7.286 MeV level of ^{15}O for $E_{3\text{He}} = 6.2$ MeV 68
44. Neutron angular distribution of the 7.286 MeV level of ^{15}O for $E_{3\text{He}} = 5.0$ MeV 70
45. Neutron angular distribution of the 7.570 MeV level of ^{15}O for $E_{3\text{He}} = 6.2$ MeV 70
46. Neutron angular distribution of the 7.570 MeV level of ^{15}O for $E_{3\text{He}} = 5.0$ MeV 72
47. Neutron angular distribution of the 8.750 MeV level of ^{15}O for $E_{3\text{He}} = 6.2$ MeV 72
48. Neutron angular distribution of the 8.750 MeV level of ^{15}O for $E_{3\text{He}} = 5.0$ MeV 73
49. Neutron angular distribution of the 8.926 MeV level of ^{15}O for $E_{3\text{He}} = 6.2$ MeV 73
50. Neutron angular distribution of the 8.926 MeV level of ^{15}O for $E_{3\text{He}} = 5.0$ MeV 75
51. Neutron angular distribution of the 9.974 MeV level of ^{15}O for $E_{3\text{He}} = 6.2$ MeV 75
52. Neutron angular distribution of the 8.974 MeV level of ^{15}O for $E_{3\text{He}} = 5.0$ MeV 75

53.	Neutron angular distribution of the 9.498 MeV level of ^{15}O for $E_{3\text{He}} = 6.2$ MeV	77
54.	Neutron angular distribution of the 9.498 MeV level of ^{15}O for $E_{3\text{He}} = 5.0$ MeV	77
55.	Neutron angular distribution of the 9.611 MeV level of ^{15}O for $E_{3\text{He}} = 6.2$ MeV	77
56.	Neutron angular distribution of the 9.611 MeV level of ^{15}O for $E_{3\text{He}} = 5.0$ MeV	77
57.	Neutron angular distribution of the 9.665 MeV level of ^{15}O for $E_{3\text{He}} = 6.2$ MeV	78
58.	$^{11}\text{B}(^3\text{He},n)^{13}\text{N}$ reaction transition strength	80
59.	$^{13}\text{C}(^3\text{He},n)^{15}\text{O}$ reaction transition strength	80
60.	Neutron time-of-flight spectra from $^{11}\text{B}(\alpha,n)^{14}\text{C}$ used for the ^{11}B target thickness measurement	84
61.	Resonances used for the ^{13}C target thickness measurements	87

TABLES

		Page
Table 1.	Systems Used for Measurements	18
2.	Source of Cross Section Error	23
3.	Energy Levels of ^{13}N	27
4.	Some Optical Model Potentials for the Entrance Channel	33
5.	Optical Model Parameters Used in the $^{11}\text{B}(^3\text{He},n)^{13}\text{N}$ DWBA Calculation	34
6.	Parameters used for $^{11}\text{B}(^3\text{He},n)^{13}\text{N}$ HF Calculations	35
7.	Energy Levels of ^{15}O	53
8.	L Values for $^{13}\text{C}(^3\text{He},n)^{15}\text{O}$ Reaction	59
9.	Parameters used for the $^{13}\text{C}(^3\text{He},n)^{15}\text{O}$ HF Calculations	60
10.	Ground State Q Values	91

Two-nucleon-transfer reactions have been extensively investigated both experimentally and theoretically in recent years. Due to the complexity of the reaction mechanism a quantitative theoretical understanding is not as reliable as for the case of the single-nucleon-transfer reactions. Despite this, much valuable spectroscopic information has been extracted from the experimental results.

The usefulness of the two-nucleon-transfer reactions are that nuclei and levels not easily studied by other means can be studied, that is the levels having two nucleons or two holes excited can be easily formed by two-nucleon-transfer reactions. Also, as in the case of single-nucleon-transfer reactions, the reaction is highly selective, in favor of channels which produce states having a parentage based on the target in its ground state.

Reactions of the types (t,p) , (t,n) , $({}^3\text{He},p)$ and $({}^3\text{He},n)$ and their inverses are usually considered to be most suitable for the two-nucleon-transfer reaction studies. There are also indications that in more complex reactions such as (α,d) reactions (ME 60) and $({}^6\text{Li},\alpha)$ reactions (LE 61) are interesting.

Among these reactions only (t,p) and $({}^3\text{He},n)$ reactions transfer a pair of identical particles leading to neutron rich or proton rich final nuclei respectively. Both reactions have the simplifying features that the internal spin of the

transferred pair is zero. Also, one generally gets higher reaction Q values by these two reactions than by other reactions, thus high excited states of the final nuclei can be studied. However, the health hazards associated with tritium beams have limited the studies of the tritium induced reactions. On the other hand the difficulties of fast neutron detection have delayed the ($^3\text{He},n$) studies.

For the ($^3\text{He},n$) reactions, not only most of the sd shell and heavier nuclei remain unstudied, but also many of the lp shell nuclei are still not fully investigated to date. It is the purpose of this work to initiate a systematic study of ($^3\text{He},n$) reactions in order to obtain a better understanding of two-nucleon-transfer reaction mechanism and to deduce spectroscopic information for the nuclei ^{15}O , ^{14}O , and ^{13}N , which lie near the closed lp shell.

CHAPTER ONE

THE REACTION MECHANISM1. Direct Interaction (DI) and Compound Nucleus (CN) Formation

Thomas (TH 55) has written the differential cross section for a reaction as

$$\frac{d\sigma}{d\Omega} = \left(\frac{d\sigma}{d\Omega}\right)_D + \left(\frac{d\sigma}{d\Omega}\right)_C + \left(\frac{d\sigma}{d\Omega}\right)_I$$

where D, C, I indicate the contributions from the direct, the compound nucleus formation, and the interference between direct and compound formation respectively.

For the ${}^3\text{He}$ induced reactions, at ${}^3\text{He}$ energies of less than approximately 5 MeV the existing experimental data suggest that except for some particular cases, the reaction proceeds in a relatively complex fashion, and therefore the interpretation of the reaction is complex. However, as the ${}^3\text{He}$ energy is increased, due to the competition between the larger number of open channels the compound system amplitude for a given reaction channel becomes less important.

Since most of the (${}^3\text{He},n$) reactions on light nuclei (some of them can be seen in later chapters), show a prominent direct interaction pattern, and in these cases one may assume that $\left(\frac{d\sigma}{d\Omega}\right)_C$ and $\left(\frac{d\sigma}{d\Omega}\right)_I$ play much less important roles than $\left(\frac{d\sigma}{d\Omega}\right)_D$. Only the reaction mechanism based on DI and CN formation will be dealt with in present work. A resume of various models which could be applied to the results of the present work will be given in this chapter.

Tobocman (TO 56) and Butler (BU 57) treated the plane wave approximation on two particle stripping reactions, by simply considering the stripped particles as a two "lumps" of nuclear matter. The angular distributions of the double stripping were predicted to have the form

$$g(\theta) [j_L(kr_0)]^2$$

where L is the orbital angular momentum transferred by the captured nucleon, k is the linear momentum transfer at the scattering angle θ , and r_0 is a parameter related to the nuclear radius. $g(\theta)$ is a function related to the internal wave function of the projectile.

In order to interpret the complex experimental results, it is obvious that the structure of the nuclei involved should also be taken into consideration. The first attempt to do this was made by El Nadi (EL 57), and was followed by News (NE 60) & Glendenning (GL 62, GL 63, GL 65). Later theoretical approaches also included the more complex distorted wave Born approximation (HE 64A, RO 64A, LI 64, GL 67, FL 68).

2. The Plane Wave Born Approximation (News' approach)

There are two approaches to stripping theory in Born's approximation. The Butler approach takes the perturbation in the initial channel while the Bhatia and Huang approach takes the perturbation in the final channel. The distorted wave formalism of Rook and Mitra takes the former approach while News' formalism takes the latter approach.

In analogy to the single nucleon transfer reaction one may write the transition matrix for reaction $A(^3\text{He}, n)B$ as

$$T = \langle f | V | i \rangle$$

where $V = V_{1A}(\underline{r}_1, \underline{\xi}) + V_{2A}(\underline{r}_2, \underline{\xi})$,

$$|i\rangle = |J_A, M_A, 3\rangle$$

$$\langle f | = \langle J_B, M_B, n |$$

1 and 2 : are nucleons stripped from the projectile and captured in the nucleus.

n : the outgoing neutron

3 : the incident ^3He

ξ : the coordinate of the initial nucleus.

r_1, r_2 : the coordinates of the captured nucleons in the centre of mass system.

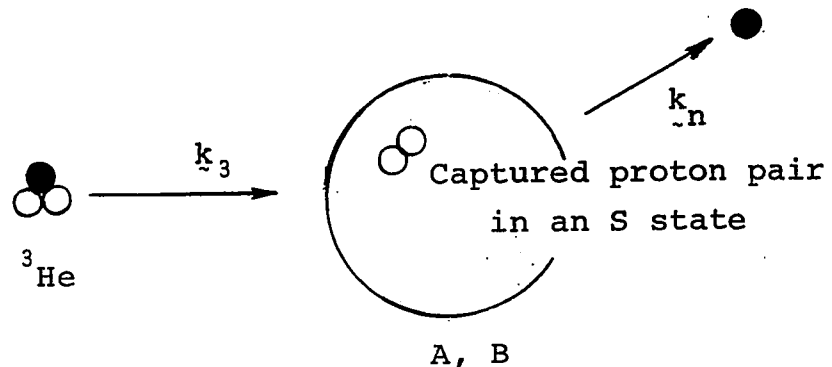


fig. 1-a

From purely shell model point of view V is a function of \underline{r}_1 and \underline{r}_2 only, thus

$$V_{1A}(\underline{r}_1, \underline{\xi}) = V_{1A}(r_1)$$

$$V_{2A}(\underline{r}_2, \underline{\xi}) = V_{2A}(r_2)$$

where $r_1 = |\underline{r}_1|$, and $r_2 = |\underline{r}_2|$.

After Huby (HU 53), the differential cross section was written by News as

$$\frac{d\sigma(\theta)}{d\Omega} = \frac{m_n^* m_3^*}{4\pi^2 \bar{n}^4} \frac{k_n}{k_3} \frac{1}{2(2J_A + 1)} \sum_{M_A, M_B, \mu_n, \mu_3} |T|^2 \quad (1-1)$$

$$\text{with } T = \langle J_B, M_B, n | V_{1A}(r_1) + V_{2A}(r_2) | J_A, M_A, 3 \rangle \quad (1-2)$$

m_n^*, μ_n , and m_3^*, μ_3 being the reduced masses and the spin components of the emerging neutron and ^3He projectile respectively. If the following assumptions are made

i) that the main contribution to the matrix element comes from $r_1 = r_2 = r_0$, where r_0 is the length of order of magnitude of the nuclear radius

ii) a Gaussian wave function such as

$$\chi_3 = \left(\frac{2\gamma^2}{\sqrt{\pi}}\right)^3 \exp\{-\gamma^2(|\underline{r}_1 - \underline{r}_2|^2 + |\underline{r}_2 - \underline{r}_n|^2 + |\underline{r}_n - \underline{r}_1|^2)\} \quad (1-3)$$

can be used to describe the ^3He nucleus,

then (1-1) leads to

$$\frac{d\sigma(\theta)}{d\Omega} \sim \exp\left\{-\frac{K^2}{4\gamma^2}\right\} \sum_L \frac{C_L}{2L+1} |B(\ell_1, \ell_2, L; kr_0)|^2 \quad (1-4)$$

where L is the angular momentum transferred by the stripped 'diproton', B contains all the angle-dependence and is weighted by C_L . C is the jj to LS coupling transformation coefficient. $\underline{K} = \underline{K}_n - \frac{1}{3}\underline{k}_3$ is the momentum transferred to the outgoing neutron and $\underline{k} = \underline{k}_3 - \frac{m_A}{m_B}\underline{k}_n$ is the momentum transferred by the 'diproton'. The differential cross section (1-4) can be simplified by assuming, firstly the projectile is a comparatively small particle, but still retains its structure, and secondly that the nucleons move as a 'lump' in the final

nucleus. The angular dependence can then be written as

$$\frac{d\sigma(\theta)}{d\Omega} \sim \exp\left\{-\frac{K^2 \mu^2}{4}\right\} \sum_L |A(JLS) j_L(kr_0)|^2 \quad (1-5)$$

where A is the weighting factor to the possible L transferred (which contains possible nuclear structure information), and $\mu = \gamma^{-1}$.

Finally if the structure of the projectile is completely neglected (1-5) yields the results of Tobocman and Butler (TO 56, BU 57).

The selection rules: The total orbital angular momentum transferred by the two protons is

$$\underline{L} = \underline{l}_1 + \underline{l}_2. \quad (1-6)$$

The angular momentum \underline{L} can be broken into two parts λ , the angular momentum of the stripped pair in their own centre of mass system and Λ , the angular momentum of their centre of mass in the nuclear system.

$$\underline{L} = \underline{\lambda} + \underline{\Lambda} = \underline{l}_1 + \underline{l}_2$$

In the ${}^3\text{He}$ system there is a high probability that the two nucleons are in an S state, thus $\lambda = 0$ and $\Lambda = L$. The parity rule gives

$$\Pi_i \Pi_f = (-)^{l_1+l_2} = (-)^{\Lambda} = (-)^L \quad (1-7)$$

The transferred total spin is

$$\underline{S} = \underline{s}_1 + \underline{s}_2.$$

Conservation of angular momentum yields

$$\underline{J}_B = \underline{J}_A + \underline{L} + \underline{S}. \quad (1-8)$$

For (${}^3\text{He}, n$) reactions, the Pauli principle allows $\underline{S} = 0$ only. Thus one has the selection rule

$$\underline{J}_B = \underline{J}_A + \underline{L}. \quad (1-8')$$

Equation (1-8') implies that if the target nucleus has zero spin, the orbital angular momentum transfer determines uniquely the spin and parity of the final state. However, in reaction mechanisms other than double stripping such as a two stage process (SH 65, BA 67) or a knock-out process (RO 64A), the Pauli principle no longer rules out the possibility of $S = 1$.

3. The Distorted Wave Born Approximation.

The use of the more realistic distorted wave theory has considerably improved the explanation of the experimental results. The PWBA as applied to single nuclear stripping is a simple but very crude theory for low energies, the 'good fit' is usually a fortuitous cancellation of the Coulomb and nuclear distortions (HO 63). Obviously a theory which will describe more than the PWBA is also needed for double stripping reactions.

In the DWBA the matrix element of (1-2) is written as

$$T = \langle \psi_n(r_n) \psi_c^Y(r_1, r_2, \xi) | V | \psi_3(r_3) \phi_3 \psi_a^\alpha(\xi) \rangle \quad (1-9)$$

$\phi_3, \psi_n(r_n)$ and $\psi_3(r_3)$ denote the ^3He wave function, the distorted waves describing the motion of the neutron and the ^3He respectively. These distorted waves are usually generated by those optical model potentials that can satisfactorily explain the appropriate elastic scattering data. $\psi_a^\alpha(\xi)$ and $\psi_c^Y(r_1, r_2, \xi)$ represent the initial and final nuclear states of spins a and c and their projections α and γ respectively.

In order to perform the integration of (1-9) in a reasonable time there are two schools of approximation.

They are:

a) Zero-range-interaction approximation by Glendenning (GL 65, GL 67), Lin and Yoshida (LI 64, LI 66), Henley and Yu (HE 64A), and by Abul-Magd and El Nadi (AB 66). This approximation physically means that the neutron is emitted from the point at which the ^3He was absorbed.

The finite range effects in double stripping reactions were treated by means of the 'local energy approximations' by Bencze and Zimányi (BE 66). They found that the inclusion of finite range forces reduces the contribution of the nuclear interior and changes the shape of the reaction form factor. This implies that it is desirable to include the finite range effects in double stripping reactions.

b) Point- ^3He approximation of Rook and Mitra (RO 64A), who in addition to zero range wrote $r_n = r_1 = r_2 = r$.

The practical calculation of DWBA usually involves very complicated computer codes. Unfortunately the Glendenning code, TSally or Julie code of Oak-Ridge, Yoshida code and Henley code were not available and only Yates code, which was written after the Rook and Mitra formation, was available for the present analysis.

By neglecting the spin orbit coupling in the distorting potentials Rook and Mitra have written

$$\frac{d\sigma(\theta)}{d\Omega} \approx \frac{k_n}{k_3} \frac{\hat{c}^2}{\hat{a}^2} \sum_{LM} \left| \sum_{\ell i} B_{\ell i}^M(L) Y_{\ell i}^M(\theta_0) \right|^2 \quad (1-10)$$

In order to perform the integration of (1-9) in a reasonable time there are two schools of approximation.

They are:

a) Zero-range-interaction approximation by Glendenning (GL 65, GL 67), Lin and Yoshida (LI 64, LI 66), Henley and Yu (HE 64A), and by Abul-Magd and El Nadi (AB 66). This approximation physically means that the neutron is emitted from the point at which the ^3He was absorbed.

The finite range effects in double stripping reactions were treated by means of the 'local energy approximations' by Bencze and Zimányi (BE 66). They found that the inclusion of finite range forces reduces the contribution of the nuclear interior and changes the shape of the reaction form factor. This implies that it is desirable to include the finite range effects in double stripping reactions.

b) Point- ^3He approximation of Rock and Mitra (RO 64A), who in addition to zero range wrote $r_n = r_1 = r_2 = r$.

The practical calculation of DWBA usually involves very complicated computer codes. Unfortunately the Glendenning code, TSally or Julie code of Oak-Ridge, Yoshida code and Henley code were not available and only Yates code, which was written after the Rock and Mitra formulation, was available for the present analysis.

By neglecting the spin orbit coupling in the distorting potentials Rock and Mitra have written

$$\frac{d\sigma(\theta)}{d\Omega} \propto \frac{k_n}{k_3} \frac{\hat{c}^2}{\hat{a}^2} \sum_{LM} \left| \sum_{\ell_i} B_{\ell_i}^M(L) Y_{\ell_i}^M(\theta_0) \right|^2 \quad (1-10)$$

where $\hat{c} = \sqrt{(2c+1)}$, $\hat{a} = \sqrt{(2a+1)}$

and $B_{\ell_i}^M(L)$ is given by

$$B_{\ell_i}^M(L) = \sum_{\ell_1 \ell_2 \ell_f} i^{\ell_1 - \ell_f - \ell_2} \frac{\hat{\ell}_1 \hat{\ell}_2 \hat{\ell}_f}{\hat{L} \hat{\ell}_i} (\ell_1 0 \ell_2 0 | L 0) \\ \times (L 0 \ell_f 0 | \ell_i 0) (L M \ell_f 0 | \ell_i M) I(\ell_i \ell_f \ell_1 \ell_2) \theta_L(\ell_1 \ell_2) \quad (1-11)$$

$I(\ell_i \ell_f \ell_1 \ell_2)$ being the space integral, and $\theta_L(\ell_1 \ell_2)$ represents the contribution of the individual states of the transferred nucleons and thus contains the nuclear structure information.

4. The Diffraction Model

The DWBA analysis certainly yields the most information about the nuclear structure, angular momentum effects and even the type of reaction involved. However, the complexity and ambiguity of the optical model parameters, especially for the ${}^3\text{He}$ (for example see reference BR 68), make the DWBA theory very difficult to apply. What parameters must be free in the search? What form must be given to the absorptive part of the potential (surface, volume, a mixture of both) etc.? These are the common questions which have arisen in the use of the DWBA code (DE 64A). In view of these difficulties a more simple model, the diffraction model for direct nuclear reactions, has been presented by Dar (DA 64) and separately by Henley and Yu (HE 64B). In Dar's model only one parameter is needed for the calculations.

The generalization of the diffraction model can be found in reference BL 57. The model is based on the assump-

where $\hat{c} = \sqrt{(2c+1)}$, $\hat{a} = \sqrt{(2a+1)}$

and $B_{\ell_i}^M(L)$ is given by

$$B_{\ell_i}^M(L) = \sum_{\ell_1 \ell_2 \ell_f} i^{\ell_1 - \ell_f - \ell_2} \frac{\hat{\ell}_1 \hat{\ell}_2 \hat{\ell}_f}{\hat{L} \hat{\ell}_i} (\ell_1 0 \ell_2 0 | L 0) \times (L 0 \ell_f 0 | \ell_i 0) (L M \ell_f 0 | \ell_i M) I(\ell_i \ell_f \ell_1 \ell_2) \theta_L(\ell_1 \ell_2) \quad (1-11)$$

$I(\ell_i \ell_f \ell_1 \ell_2)$ being the space integral, and $\theta_L(\ell_1 \ell_2)$ represents the contribution of the individual states of the transferred nucleons and thus contains the nuclear structure information.

4. The Diffraction Model

The DWBA analysis certainly yields the most information about the nuclear structure, angular momentum effects and even the type of reaction involved. However, the complexity and ambiguity of the optical model parameters, especially for the ${}^3\text{He}$ (for example see reference BR 68), make the DWBA theory very difficult to apply. What parameters must be free in the search? What form must be given to the absorptive part of the potential (surface, volume, a mixture of both) etc.? These are the common questions which have arisen in the use of the DWBA code (DE 64A). In view of these difficulties a more simple model, the diffraction model for direct nuclear reactions, has been presented by Dar (DA 64) and separately by Henley and Yu (HE 64B). In Dar's model only one parameter is needed for the calculations.

The generalization of the diffraction model can be found in reference BL 57. The model is based on the assump-

tion that for nuclear projectiles with 'medium' incident energies the mean free path within nuclear matter is small compared with the nuclear radius. Since the direct nuclear reactions at 'medium' energy involve incoming and outgoing particles which are localized at the nuclear surface and because of the strong absorption within nuclear matter, a particle has to originate from the vicinity of the 'shadow line' of the target in order to be emitted in a forward direction.

By assuming that all the particles emitted from the reaction are produced in an annular region, which is located in the periphery of the strong absorption plane, Dar wrote the differential cross section for the reaction as

$$\frac{d\sigma(\theta)}{d\Omega} \propto F(\theta) (2\pi R\Delta R) \sum_{m=-L, -L+2, \dots, L}^{L} \left(\frac{2L+1}{4\pi}\right) \frac{(L-m)!(L+m)!}{[(L-m)!!(L+m)!!]^2} \times J_{|m|} \left(\frac{k}{R}\right)^2 \quad (1-12)$$

where R is a length of the order of magnitude of the nuclear radius L is the angular momentum being transferred and $F(\theta)$ is given by

$$F(\theta) = \left(1 + \frac{k}{K} \cos\theta\right)^2$$

k , K being defined in Section 2.

The main deviation of equation (1-12) from the News' theory occurs for $L > 1$, where the News' theory predicts a sum of two spherical Bessel function terms with a known coefficient $A(J, L, S)$, the diffraction model predicts a linear combination of the cylindrical Bessel functions.

Surprisingly, in view of its simplicity, the predictions of the latter model fit most of the experimental data rather well.

5. Other Considerations on the DI Mechanism

It was pointed out by Bang et al. (BA 67) that in general the reaction has to be treated as a four-point Feynman graph as shown in fig. 1-b. Only if the energies E_1 and E_2 of the first and second captured nucleons are nearly equal can the capture of a two-nucleon association occur and fig. 1-b may then be replaced by a pole diagram. Here E_1 is

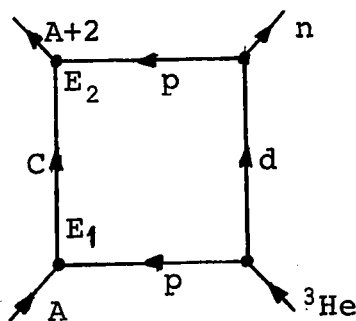


fig. 1-b

the energy for the dissociation of the nucleus $A+1$ in state C into the nucleus A in the ground state and a proton; E_2 is the energy for dissociation of the nucleus $A+2$ in the fixed final state into the nucleus $A+1$ in the state C and a proton. A table containing $\Delta E = E_1 - E_2$ for some $1p$ shell nuclei was given by Bang et al. The table indicates clearly that ΔE is greatest for the nuclei in the middle of the shell. This concept has only been applied using plane wave formulism. Some success was obtained in explaining the forward peaked distributions for higher L value transfer in the $^{10}\text{B}(t,p)^{12}\text{B}$ reaction.

Even in the crude plane wave approach the calculations are very lengthy. Unless the theory can be simplified, it will be difficult to apply in a practical case and probably very difficult to use in conjunction with the distorted wave theory.

An approach applying the general methods of the theory of strong interactions was attempted by Shapiro and Timashev (SH 65). In their calculations four-ray vertices were considered for both double stripping and knockout processes. Many excellent fits to experimental data have been obtained and it is possible that this theory may yield more insight into the reaction mechanism of double stripping reactions.

6. Compound Nucleus Formation

Because of their high Q values ($^3\text{He},n$) reactions usually result in high excitation energies in the compound nucleus, typically 20 \sim 30 MeV where many overlapping states occur. To estimate how much contribution is from compound nucleus (CN) formation the statistical CN process was considered.

A general theory of the CN process is available (BL 52). Developments of the theory along statistical lines are due to Wolfenstein (WO 51), and Hauser and Feshbach (HA 52). In the present work a code written by Smith (SM 65) and modified by Davison (DA 68) was used for all Hauser-Feshbach (HF) calculations. The detailed discussion of the theory and codes can be found in references SM 65, DA 68, FR 68.

Consider for a CN formation reaction $A(a,b)B, J, \pi$

be the spin and parity of the compound nucleus. One may write the statistical CN differential cross section as follows:

$$\frac{D\sigma(\theta)}{d\Omega} = \frac{1}{4k^2} \sum_{\nu} A_{\nu} P_{\nu}(\cos \theta) \quad (1-13)$$

where P_{ν} are Legendre polynomials and

$$A_{\nu} = \sum_{J, \pi} \frac{2J+1}{D} \cdot D_A \cdot D_B \quad (1-14)$$

where D_A, D_B are factors depend on incoming and outgoing channels transmission coefficients and the statistical properties of level densities. D is the corresponding similar factor for all open outgoing channels. The transmission coefficients are usually calculated from the optical model potentials by matching the wave functions at the nuclear boundary. In case the level densities are not known, especially at higher excitation energies, say above E_{beg} , Newton's formula (NE 56) can be used for estimation.

$$\log N(E_x) = a + b \sqrt{E_x}$$

where $N(E_x)$ is the number of levels below E_x . Therefore in the present HF calculations beside the normal kinematical and spin and parity parameters, one needs for each open channel a set of optical model parameters, and for each residual nucleus a set of level density constants, a , b , and E_{beg} . Also a parameter k is needed to determine the spin cut-off parameter when level densities are used.

CHAPTER TWO

THE EXPERIMENTAL METHODS1. The Neutron Time-of-Flight System

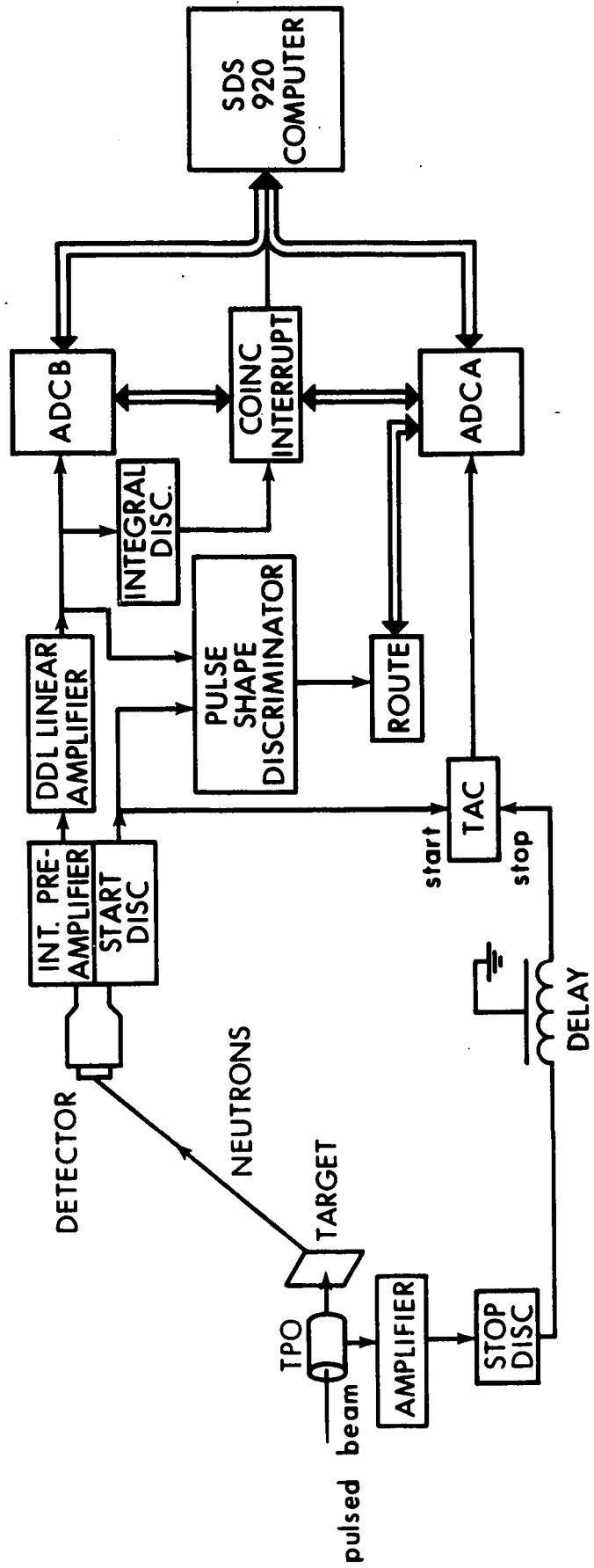
The neutron time-of-flight system employed in the present experiments was similar to that which has been described previously by many other authors (FI 67, GR 67, MC 67A). Only particulars will be described here.

Throughout the lengthy measurement periods, many changes were made to the entire system. The major changes can be classified into two categories.

In system I a small ion source extraction channel was used. A wider channel was used in system II. It is believed that the ion source channel sizes are vital in the time spread of the final bunched beam pulses. The narrower channel (.076" orifice) gives much more well-defined beam pulses before bunching in the Mobley magnet, while the wider channel (.083 orifice) seems to give pulses with longer wings. The shapes of the pre-bunched pulses were found to have considerable effect on the final time resolutions as can be seen in fig. 3 and fig. 30. The data of fig. 3 was obtained using the narrow channel system and illustrates a time resolution less than 0.9 nsec. FWHM. However, as seen in fig. 30 a time resolution of 1.2 nsec. was obtained using the wider channel.

A general block diagram of the electronics system used is shown in fig. 1, where TAC is a time-to-amplitude

Figure 1. A general block diagram of the electronics system used for the measurements.



converter and ADCA and ADCB are two separate TMC* Model 217A analog-to-digital converters.

System I: Timing circuits designed by D. L. Wieber (WI 63) were used for start and stop discriminators and also for the TAC. The outputs of ADCA and ADCB were fed to an SDS-920** on-line computer where the 'walk' (amplitude dependent timing error) corrections were made as described in the reference MC 67A. Many 'shift tables' were made just prior to the measurements, the tables were generated by means of two-dimensional displays of the neutron peaks of $T(d,n)^4\text{He}$ reaction and the similar displays of γ -ray peaks of $^{11}\text{B}(^3\text{He},n)^{13}\text{N}$ reactions. The former tables were used in $^{13}\text{C}(^3\text{He},n)^{15}\text{O}$ runs. For $^{11}\text{B}(^3\text{He},n)^{13}\text{N}$ measurements the latter tables were employed.

A Reid and Hummel (RE 66) type γ eliminator circuit was also included in this system. The eliminator generates signals to command the routing circuit to route the genuine neutron events to be stored in the last two bins (2048-4095 channels out of 4096 total channels), while other events, mostly background neutrons and multiscattered captured γ rays events were stored in the first two bins (0-2047 channels).

System II: In this latter system the TAC was replaced by an ORTEC Model 437 time converter***, and the discriminators were replaced by 'Constant Fraction of Pulse

*Technical Measurement Corporation, 441 Washington Avenue, North Haven, Connecticut, U. S. A.

**Scientific Data Systems, Sanata Monica, California.

***ORTEC, 102 Midland Road, P. O. Box C, Oak Ridge, Tennessee, U.S.A.

Height Trigger Circuits' (GE 67). This circuit was added in order to improve the dynamic range and time resolutions of the neutron detectors, and in addition to eliminate the 'walk' problem. Hence ADCB and the 'walk' table were excluded from the system. A different type n- γ discriminator circuit after Roush et al. (RO 64B) was included in this system to replace that of Reid and Hummel.

2. The Neutron Detectors

Three different types of detectors and photomultipliers were also used in the experiments. Detector I was made from cylindrical ($3\frac{1}{2}$ diameter X $3/4$ " height) NE 218* liquid scintillator and an RCA C70133 photomultiplier. A similar shape but slightly small diameter (3.45") Ne 213 liquid scintillator was coupled to a Philips XP 1040 photomultiplier to make Detector II.

Detector III normally served as the monitor detector and was constructed from a small Naton** disc phosphor and an RCA 8575 photomultiplier. The electronics system for the monitor detector was a straight forward neutron time-of-flight system of the conventional design, the n- γ discriminator was not included. The data were analyzed and stored in a separated TMC Model CN 1024 multichannel analyzer.

The individual detector efficiencies for Detector I and Detector II were calculated by using a code written by Grandy (GR 67). In this code Grandy has taken into account

*Nuclear Enterprise Ltd., Winnipeg, Manitoba, Canada.

**Nash and Thompson Ltd., Hookrise South, Tolworth, Surrey England.

the double scattering from the hydrogen, single scattering from carbon together with the detector resolution. By neglecting the surface losses and the second order effects, the detector efficiency is also given by the expression:

$$\epsilon = [1 - \exp(-n\sigma t)] \left[1 - \frac{E_0}{E}\right]$$

where t is the thickness of the scintillator, E the neutron energy, E_0 the cut-off energy, n the number of hydrogen atoms, and σ the n-p cross section at energy E .

The calculated results from Grandy's code were compared with that from this simple formula. Disagreements were found at lower and higher neutron energies. However, the calculated efficiencies were within 5% (except the region of cut-off, where it has no great concern to present work). Grandy's efficiency calculations were used throughout this experiment.

The overall errata in the absolute efficiency curves were estimated to be within 10%.

Table 1 lists the experimental set ups used for the individual measurements.

3. Target Assembly

Since the studies of angular distribution of neutrons are the primary concern of the present works, the target chamber is made from a thin-walled cylindrical shaped stainless steel pot.

The target holder is made from 1/16 inch copper sheet located at the centre of the chamber and can be slid

TABLE 1, Systems Used for Measurements.

Reactions	Type of Measurements	System	Detector	Detector III Location
-	Survey works	I	I, II	
$^{11}\text{B}(^3\text{He},n)^{13}\text{N}$	Yield Curves	I	I	0° , 2m
	4.7 MeV Angular Distributions	I	I	-10° , 2.25m
	6.1 MeV Angular Distributions	I	I	-10° , 2.25m
	6.5 MeV Angular	II	II	-10° , 2.25m
$^{13}\text{C}(^3\text{He},n)^{15}\text{O}$	Yield Curves	I	I	90° , 2.25m
	5.0 MeV Angular Distributions	II	II	-10° , 2.25m
	6.2 MeV Angular Distributions	I	I	-10° , 2.25m

and rotated with respect to the direction of the incident beam from outside of the chamber by means of double Wilson seals. The rotation of the target enables the selection of different target angles and thus severe neutron scattering at glancing angles due to the target backing can be avoided.

The target holder was insulated to facilitate charge integration and also was biased to +300 volts D.C. with respect to the ground in order to reduce secondary electron emission. The entrance slits of the target chamber were biased to +300 volts. The target cooling was dependent on good thermal contact of the target backings to the air cooled copper holder. After several hours of 2μ amp. continuous ^3He bombardment on this target assembly the temperature rise at the holder was less than 11°C , and thus the problem of the target deterioration due to evaporation was minimized.

Both the ^{11}B and ^{13}C targets (on .202" and .010" gold backings) were made by the separator group of AERE at Harwell, England.* There was no information supplied as to their thickness. However, the ^{13}C target thickness was measured by various methods (see Appendix I), and was determined to be $42.5 \mu\text{g}/\text{cm}^2$. A fresh, approximately $200 \mu\text{g}/\text{cm}^2$ ^{11}B target, also from AERE, was used for accurate thickness measurements and for the absolute cross section normalization of the $^{11}\text{B}(^3\text{He},n)^{13}\text{N}$ data. The thickness was measured to be $323 \mu\text{g}/\text{cm}^2$ (see appendix I).

* The targets had been existant in this laboratory since 1960 and were bombarded previously. Some traces of carbon deposits were found on the surfaces.

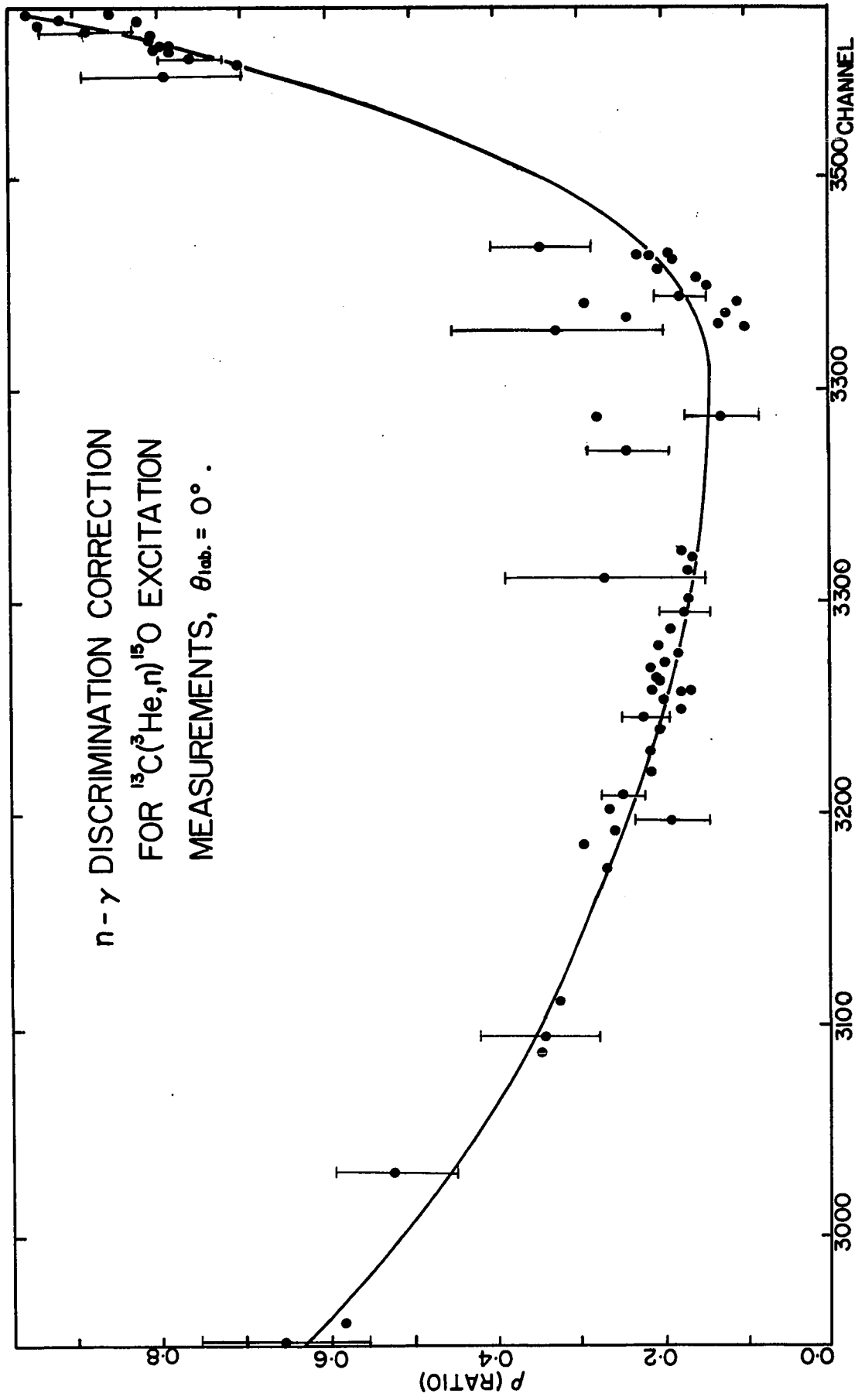
4. The Data Extractions

The peak fitting code originally written by Tepel (TE 66) was used for finding the area under the peaks and the peak positions. The code subtracts from the main spectrum with the fitted background, and then finds and fits peaks to a given shaped standard peak.

Neutron events were stored in bins 3 and 4 (see page 15), whereas the rejected events were stored in bins 1 and 2. Due to the imperfection of the $n - \gamma$ discriminator, some neutron events were rejected as γ -ray events which appear as peaks in bins 1 and 2. The rejected peaks in bins 1 and 2 were also fitted by the same code. In the rejected peak fitting process some difficulties were encountered. In general, due to the large background and poor statistics, some peaks failed to be fitted under the criterion of the fitting process. For those which fit, the ratios of the area under the false peak to that of the corresponding genuine neutron peak were calculated, and these ratios were plotted against channel numbers (equivalent to neutron flight time). A typical curve is shown in figure 2. This curve was used to get a resultant total area under the peak. Figure 2 also indicates the quality and the stability of the $n - \gamma$ discriminator circuits. This type of curve has not been published for the various $n - \gamma$ discriminator circuits (FI 65). The author strongly recommends that all $n - \gamma$ discriminator circuits to be published in the future should present curves of a similar kind to that of figure 2.

Figure 2. A typical curve used for summing the area under the peak. ρ is the ratio of the area under the peak in bins 1 and 2 (rejected spectrum) to the area of the corresponding peak in bins 3 and 4 (neutron spectrum).

n- γ DISCRIMINATION CORRECTION
FOR $^{13}\text{C}(^3\text{He},n)^{15}\text{O}$ EXCITATION
MEASUREMENTS, $\theta_{\text{lab.}} = 0^\circ$.



Since the reactions studied have a strong forward yield, in order to ensure good statistics the monitor detector (Detector III) was placed at 10° and at a distance of 2.25m. The areas under the monitor peaks were also determined using the Tepel code. For a check some of the angular distributions were extracted completely by hand calculations. The two methods gave results which were consistent.

A computer code was used to calculate the Q values (see Appendix II) corresponding to peaks of the main detector spectrum. The results were listed separately in Table 3 and Table 9 in Chapter 3 and Chapter 4 respectively.

In order to find the scale for the absolute cross section, for the $^{11}\text{B}(^3\text{He},n)^{13}\text{N}$ reactions, a separate set of runs were carried out. In these measurements, at bombarding energies of 6.1 MeV and 4.7 MeV spectra at 0° and 90° were taken immediately after the target thickness was measured. The absolute cross section normalization factor for the 4.7 MeV and 6.1 MeV angular distributions was found by averaging these results. The 6.5 MeV data were normalized by using the 6.1 MeV data and the 90° excitation curves.

For the $^{13}\text{C}(^3\text{He},n)^{15}\text{O}$ reactions, the target thickness was measured by using (p,n) threshold measurement before taking the 6.2 MeV angular distributions. After the 5.0 MeV angular distributions were taken the target thickness was again checked using (α ,n) and (p, γ) resonances. The extraction of absolute cross sections was therefore direct with no

excitation curves involved.

The sources of cross section error and their magnitudes are listed in Table 2.

TABLE 2, Source of Cross Section Error

Detector efficiency		5 - 10%
Peak area fitting error (absolute)		3 - 5%
Detector geometry		1%
Current integration		1%
³ He charge state		2%
Target thickness	¹¹ B	9%
	¹³ C	5%

RESULTS (I) $^{11}\text{B}(^3\text{He},n)^{13}\text{N}$ Reaction1. General Background

The energy levels of ^{13}N have been studied by elastic and inelastic scattering of protons on ^{12}C by many authors during the past two decades (BA 63A, SH 62, AD 61, RE 56, JA 53A). Because of the strong binding of ^{12}C , most of the excited states of ^{13}N can be observed through this process. The single nucleon pick-up reactions such as $^{14}\text{N}(p,d)^{13}\text{N}$ and $^{14}\text{N}(^3\text{He},d)^{13}\text{N}$ were also studied recently by various groups (FL 68, KO 67, BA 66, MA 66C, GA 63).

The single nucleon stripping reaction $^{12}\text{C}(d,n)^{13}\text{N}$ is a potential tool also, however the low ground state Q value has limited the applicability of this reaction to the low-lying levels. Also, the single nucleon transfer reactions can only strongly excite states having configurations of addition or subtraction of a single nucleon from the target nucleus.

Alternative methods of reaching ^{13}N are two-nucleon-transfer reactions, which, as yet, have received very little attention. Recently a comprehensive study of $^{15}\text{N}(p,t)^{13}\text{N}$ by Fleming et al. has been published (FL 68). This double pick-up reaction is mainly limited to the $(lp)^9$ configuration states as is $^{14}\text{N}(^3\text{He},\alpha)^{13}\text{N}$ reaction.

The double stripping reaction, $^{11}\text{B}(^3\text{He},n)^{13}\text{N}$ is not restricted by the above mentioned limitations, that is, this reaction has a high ground state Q value of 10.18 MeV, and levels having configurations other than $(lp)^9$ can be easily

excited. Previous work on this reaction was carried out using a proton recoil technique, but only those neutrons leading to the ground state of ^{13}N were studied (DI 66).

2. The Energy Levels and Their Excitation Curves

Figure 3 presents the neutron energy spectrum of the reaction $^{11}\text{B}(^3\text{He},n)^{13}\text{N}$, taken at $\theta_{\text{lab}} = 0^\circ$ and at a bombarding energy of 6.1 MeV. An overall time resolution of approximately 0.9 nsec was obtained. For the flight path of 6 meters used this corresponds to a 250 keV FWHM for a neutron energy of 16.2 MeV or approximately 1.5% energy resolution. The energy resolution improves as neutron energy decreases. The excitation energies shown were calculated using peaks observed throughout 34 spectra measured at different angles (see Appendix II for details).

An interesting feature of the spectrum is the even parity states have been observed throughout the spectrum. This is expected since one of the protons can be easily transferred to the d-shell to form the even parity states. The strong population of the odd parity states is mainly by addition of two protons to a $(1p)^7$ core target nucleus. Shown in Table 3 are the calculated excitation energies and their estimated errors together with previously reported values, also the probable spin and parity assignments for each level. For the most part the results of the present measurements agree with previously known values (FL 68, KO 67, BA 63A, SH 62, AJ 62).

Figure 3. A neutron time-of-flight spectrum for the
 $^{11}\text{B}(^3\text{He},n)^{13}\text{N}$ reaction at $E_{^3\text{He}} = 6.1$ MeV.

$^{11}\text{B}(^3\text{He},n)^{13}\text{N}$

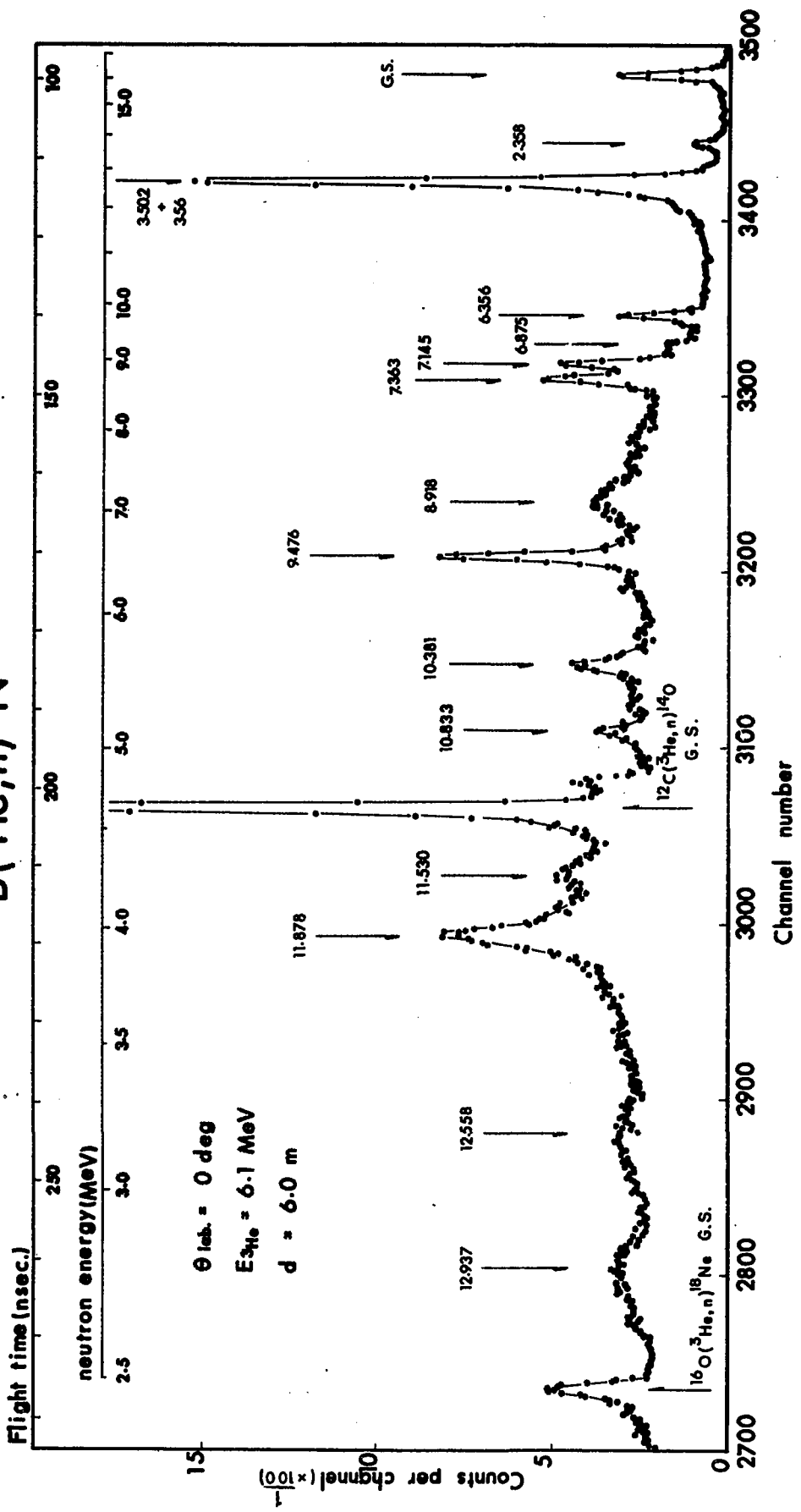


Table 3. Energy Levels of ^{13}N

J^π	Q (MeV) $^{11}\text{B}(^3\text{He},n)^{13}\text{N}$	Error (keV)		Excitation (MeV \pm keV)	Ajzenberg ^{a)}	Fleming ^{b)}
$\frac{1}{2}^-$	10.183	2*	11 [†]	0.0	0.0	0.0 \pm 25
$\frac{1}{2}^+$	7.825	2	10	2.358 \pm 10 ^{††}	2.367	2.36 \pm 30
$\frac{3}{2}^-$	6.681	2	10	3.502 \pm 10	3.510	3.51 \pm 30
$\frac{5}{2}^+$	6.64	10	9	3.55 \pm 18	3.56	
$\frac{5}{2}^+$	3.829	1	8	6.353 \pm 9	6.382	6.38 \pm 30
$\frac{3}{2}^+$	3.308	2	8	6.875 \pm 10	6.91	
$\frac{7}{2}^+$	3.038	2	8	7.145 \pm 9	7.18	
$\frac{5}{2}^-$	2.820	1	8	7.363 \pm 8	7.385	7.38 \pm 20
$\frac{3}{2}^+$	2.0	14	40	8.2 \pm 22	8.1	
$\frac{1}{2}^-$	1.265	3	8	8.918 \pm 11	8.9	8.93 \pm 50
$\frac{3}{2}^-$	0.707	1	7	9.476 \pm 8	9.48	
$\frac{7}{2}^-$	-0.198	1	7	10.381 \pm 8	10.36	
$\frac{1}{2}^-$	-0.651	2	7	10.833 \pm 9		10.78 \pm 60
	-1.347	5	8	11.530 \pm 12	11.64	
$\frac{3}{2}^-$	-1.695	5	7	11.878 \pm 12	11.85	11.88 \pm 40
	-2.375	15	19	12.558 \pm 23	12.08	
	-2.754	16	20	12.937 \pm 24		

* errors are the weighted standard deviations from the mean.
[†] overall uncertainty. ^{††} errors include uncertainty in estimation of the thickness of ^{12}C contaminants.
a) AJ 62. b) FL 68.

A broad state at about 8.1 MeV which has been reported previously (AJ 62) was very weakly populated at all angles in the present measurements. Judging from the shapes of the peak, especially from the backward angle spectra, one would conclude that this is a complex peak due to the presence of more than one level in ^{13}N . Shute et al. (SH 62) have reached a similar conclusion concerning a very broad resonance (1400 keV width) at equivalent excitation energy 8.0 MeV of ^{13}N .

The excitation curves for bombarding energies from 5.4 MeV to 6.5 MeV were measured at 90° laboratory angle with the detector 4.5 meters from the target. Figure 4 shows the yield of the ground state, 2.358 MeV, 7.145 MeV, 7.363 MeV and unresolved 3.502 MeV + 3.55 MeV states. The smooth curves show the trend. It can be seen for the low lying states the yield curves are flatter beyond $E_{3\text{He}} \sim 6$ MeV than are those for the higher states. Angular distributions were studied at bombarding energies of 4.7, 6.1 and 6.5 MeV. The 4.7 MeV measurement allowed a comparison with the ground state angular distribution at 4.75 of Din et al. (DI 66). All angular distributions are presented in Figures 5 to 29, which will be fully discussed in later sections.

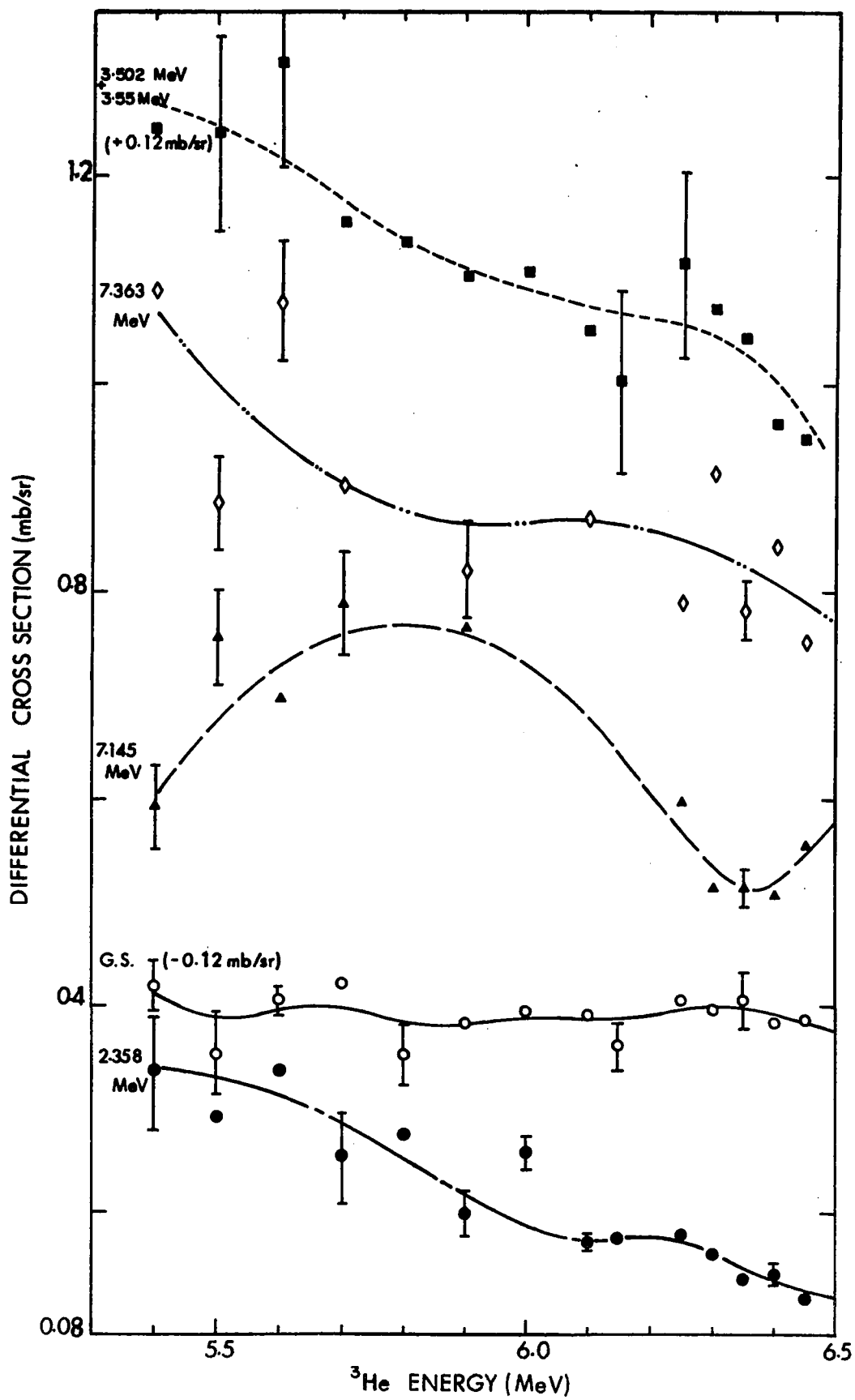
3. The Analysis

(i) The Plane-Wave-Born-Approximation (PWBA)

The simplified Newns' formula (1-5) was used throughout the calculations. Since the size of ^3He is not negligible compared to that of the target nucleus, it was considered to

Figure 4. The neutron yield of $^{11}\text{B}(^3\text{He},n)^{13}\text{N}$ at $\theta_{\text{lab}} = 90^\circ$, leading to 0.0, 2.358, 7.145, 7.363 MeV levels, and to an unresolved 3.502 + 3.55 MeV levels.

$^{11}\text{B}(^3\text{He},n)^{13}\text{N}$ 90° YIELD



be improper to neglect the contributing term due to the ^3He form factor. Thus a ^3He form factor term was included in all PWBA calculations. Examination of expression (1-5) shows the correlation in μ and r_0 to the calculated cross sections. Some minor adjustments of these parameters were made in order to obtain a good fit to the first excited state data. Values $\mu = 5.0$ fermis, comparable to that of Gunn and Irving (GU 51), and $r_0 = 4.5$ fermis were found to give the best fit to the data. The same μ and r_0 values were used for all other calculations for this reaction.

The selection rules (1-7) and (1-8) permit only two values of L , either both odd or both even (except for $J_B = \frac{1}{2}$, when only one L value is permitted). 1-5 can therefore be written as following

$$\frac{d\sigma(\theta)}{d\Omega} \sim \exp\left(-\frac{k^2\mu^2}{4}\right) [j_L^2(kr_0) + \alpha^2 j_{L+2}^2(kr_0)] \quad (3-1)$$

where α is a constant to replace the ratio $A(J,L+2,S)/A(J,L,S)$.

Since the magnitude of the second Bessel function is small except at large angles α must be large number (>10) in order to get a significant change in the calculated angular distribution for small angles. In the present calculations α was set equal to zero for simplicity. The calculated PWBA results are presented in Figures 5 to 29.

(ii) The Simple Diffraction Model Calculations (SDM)

Formula (1-12) of Dar was used for this calculation. In his original calculations (DA 64) Dar neglected the factor $F(\theta)$ of (1-12). However the angular distribution dependence on this factor is not negligible when one is interested in

more than the forward angle approximation. Although little effect was found from the $F(\theta)$ factor for small L transfer reactions, for larger L values it was found that including the factor $F(\theta)$ did improve the fit to the data. It was then decided to include the factor $F(\theta)$ in all calculations. Expression (1-12) was rewritten as:

$$\begin{aligned}
 \text{for } L = 0, \quad \frac{d\sigma(\theta)}{d\Omega} &\propto F(\theta) J_0^2(kR) \\
 L = 1, \quad &\propto F(\theta) J_1^2(kR) \\
 L = 2, \quad &\propto F(\theta) \left[\frac{1}{4} J_0^2(kR) + \frac{3}{4} J_2^2(kR) \right] \\
 L = 3, \quad &\propto F(\theta) \left[\frac{3}{8} J_1^2(kR) + \frac{5}{8} J_3^2(kR) \right] \\
 L = 4, \quad &\propto F(\theta) \left[\frac{9}{64} J_0^2(kR) + \frac{20}{64} J_2^2(kR) \right. \\
 &\quad \left. + \frac{35}{64} J_4^2(kR) \right] \quad (3-2)
 \end{aligned}$$

Although the physical meaning of R is not necessarily the same as that of r_0 in News' theory. A similar value, $R = 4.5$ fms, was found to give the most satisfactory results. Some of the calculated results are also presented together with the experimental data through Figures 5 to 29.

(iii) The Distorted-Wave-Born-Approximation (DWBA)

As mentioned in a previous chapter the DWBA code of Yates was used for the DWBA calculations. Since the appropriate two-nucleon coefficients of fractional parentage were not available, no attempts were made to estimate $\theta_L(l_1 l_2)$ of equation (1-11). This also implies that no absolute cross sections are obtainable from the present calculations (RO 67). All calcu-

lated results shown from Figures 5 to 29 are arbitrarily normalized to the maximum of the experimental results.

Due to difficulties in the fabrication of pure ^{11}B targets, the appropriate ^3He elastic-scattering data are not available to date. Shown in Table 4 are some of the parameters obtained from the existing ^3He elastic-scattering data on some light nuclei. All potentials listed were assumed to have the form

$$U(r) = V_c(r) - V_g(r, r_v, \alpha_v) - i W g'(r, r_w, \alpha_w) \quad (3-3)$$

where V_c is the Coulomb potential resulting from a uniform charge distribution of radius $1.3 A^{1/3}$. A has the ordinary meaning of mass number of the target nucleus. V and W are the real and imaginary parts of the 'central' potential, g and g' are the Woods-Saxon form factors, $1 + \exp \{ (r - r_{v,w}) A^{1/3} / \alpha_{v,w} \}$. For the four-parameter potentials $r_v = r_w$ and $\alpha_v = \alpha_w$ were assumed.

As can be seen from Table 4 realistic potentials can be classified into two categories, either the so called 'deep well' or 'shallow well' potentials. It was found by Glover et al. (GL 66) that on applying the Rook and Mitra theory better agreements can be obtained if the 'deep well' potentials are used. It was also suggested by Rook (RO 65) that a deep real well depth is consistent with the real optical potential being given by the sum of the potentials of the constituent nucleons.

Table 4. Some Optical Model Potentials for the Entrance Channel

Set	V	W	α_V	α_W	r_V	r_W	$E_{^3\text{He}}$ (MeV)	^3He on
I	83	56	0.7			1.6	(5.5)	^{12}C
II	66.7	52.4	0.588			1.6	(29)	^{12}C
III	61.9	60.0	0.57			1.62	(29)	^{14}N
IV	64.8	65.6	0.58			1.60	(29)	^{16}O
V	169	32.1	0.675	0.566	1.14	1.82	(29)	^{14}N
VI	170	20.0	0.893	0.510	1.03	2.06	(10.5)	^{16}O
VII	140.9	28.1	0.78	0.61	1.14	1.88	(6-8)	^9Be

I(HO61); II(GA62); III,IV(SE62A) V,VI(HI67); VII(EA67)

All potentials were tried and the results were as follows: The 'shallow potentials' sets I, II, III, and IV failed to fit our ground state data at all three energies. On the other hand, reasonable fits in shape were obtained from the 'deep potentials'. The potential set VII, which was obtained from the elastic scattering of 6 to 8 MeV ^3He on ^9Be , gave the best results.

Slight improvement to fit the ground state data were obtained by adjusting the parameters of set VII. Since the transition to the ground state of ^{13}N can be considered as a pure (lp, lp) transition, the adjusted potential parameters were considered to represent the optical model potential of ^3He to ^{11}B nucleus more realistically. Listed in Table 5 are the adjusted parameters used as incident channel parameters

for all subsequent calculations.

Table 5. Optical Model Parameters Used in the DWBA Calculations for $^{11}\text{B}(^3\text{He},n)^{13}\text{N}$.

$E_{^3\text{He}}$ (MeV)	V (MeV)	W (MeV)	α_V (fm)	α_W (fm)	r_V (fm)	r_W (fm)
6.5	145	28.5	0.78	0.61	1.30	1.80
6.1	148	28	0.78	0.61	1.30	1.71
4.7	160	24	0.78	0.61	1.30	1.79

For the exit channel parameters the following average neutron optical model parameters, taken from Rosen (RO 66), were used for all calculations:

$$V = 49.3 - 0.33 E, \quad W = 5.75, \quad r_{V,W} = 1.25,$$

$$\alpha_V = 0.65, \quad \alpha_W = 0.70.$$

It was found that the calculations were not too sensitive to the choice of exit channel parameters, except in cases where neutron energies are high. In order to avoid the confusion arising from parameter fitting, no attempts were made to get a set of best fit potentials for the exit channel.

(iv) The Hauser-Feshbach Calculations (HF)

To estimate the amount of compound nucleus formation, $\left(\frac{d\sigma}{d\Omega}\right)_c$ is given by Hauser-Feshbach theory.

In the present calculations the HF cross-sections were calculated by means of the Smith code. All possible open macrochannels ($^3\text{He}, ^3\text{He}$), ($^3\text{He}, p$), ($^3\text{He}, d$), ($^3\text{He}, \alpha$) and

for all subsequent calculations.

Table 5. Optical Model Parameters Used in the DWBA Calculations for $^{11}\text{B}(^3\text{He},n)^{13}\text{N}$.

$E_{^3\text{He}}$ (MeV)	V (MeV)	W (MeV)	α_V (fm)	α_W (fm)	r_V (fm)	r_W (fm)
6.5	145	28.5	0.78	0.61	1.30	1.80
6.1	148	28	0.78	0.61	1.30	1.71
4.7	160	24	0.78	0.61	1.30	1.79

For the exit channel parameters the following average neutron optical model parameters, taken from Rosen (RO 66), were used for all calculations:

$$V = 49.3 - 0.33 E, \quad W = 5.75, \quad r_{V,W} = 1.25,$$

$$\alpha_V = 0.65, \quad \alpha_W = 0.70.$$

It was found that the calculations were not too sensitive to the choice of exit channel parameters, except in cases where neutron energies are high. In order to avoid the confusion arising from parameter fitting, no attempts were made to get a set of best fit potentials for the exit channel.

(iv) The Hauser-Feshbach Calculations (HF)

To estimate the amount of compound nucleus formation, $\left(\frac{d\sigma}{d\Omega}\right)_c$ is given by Hauser-Feshbach theory.

In the present calculations the HF cross-sections were calculated by means of the Smith code. All possible open macrochannels ($^3\text{He}, ^3\text{He}$), ($^3\text{He}, p$), ($^3\text{He}, d$), ($^3\text{He}, \alpha$) and

($^3\text{He}, t$) were taken into account for the calculation. Listed in Table 6 are those parameters used for $^{11}\text{B}(^3\text{He}, n)^{13}\text{N}$ calculations.

Table 6. Parameters used for $^{11}\text{B}(^3\text{He}, n)^{13}\text{N}$ HF Calculations.

Channel	V	W	α_V	α_W	r_O	r_W	E_{beg}	a	b	γ
p - $^{13}\text{C}^*$	45	10	0.5	0.5	1.2	1.2	3.8	-0.702	0.597	0.9
d - $^{12}\text{C}^{**}$	50	16	0.79	0.79	1.5	1.5	8.0	-0.933	0.518	0.9
t - $^{11}\text{C}^\dagger$	140.9	28.1	0.78	0.61	1.14	1.88	4.8	-0.758	0.606	0.9
α - $^{10}\text{B}^{\dagger\dagger}$	50	5.3	0.58	0.58	1.99	1.99	4.8	-1.212	0.882	0.9
^{11}B							5.0	-0.906	0.625	0.9
^{13}N							5.0	-1.651	0.930	0.9

* (RO61); ** (HO63); † (EA67); †† (HU62)

Those parameters for proton, deuteron and triton channels were taken from references RO 61, HO 63, and EA 67 respectively. For α -channels potentials of Huizena and Igo (HU 62) were used. For the elastic and neutron channels parameters used for $E_{^3\text{He}} = 6.49$ MeV DWBA calculations were employed. The calculated cross sections were not too sensitive to the optical model parameters and spin cut-off parameters. However, the magnitude of the calculated cross sections are very sensitive to the choosing of level density parameters. All a, b shown in Table 6 are taken from the presently known level schemes. It is known that the HF calculation may overestimate the compound formation cross section (KU 60, LA 67A, LA 67B). However,

no adjustments to the calculated results were made. All HF cross sections are shown together with experimental cross sections in Figures 5 to 29.

4. Levels of ^{13}N .

(i) The 0.0 MeV level.

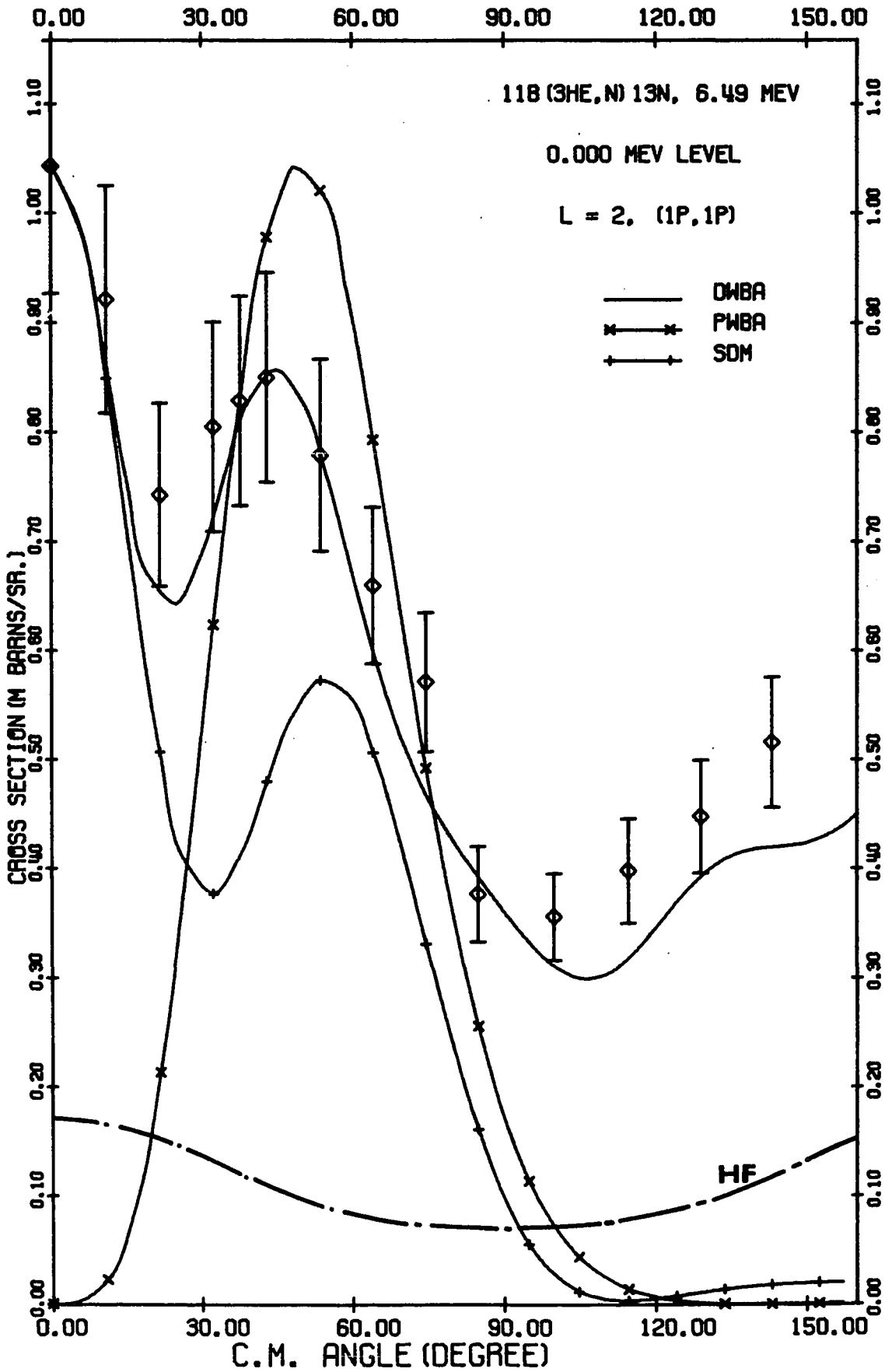
This ground state is the only level of ^{13}N that had been observed by the $(^3\text{He},n)$ reaction prior to this work (DI 66). Figures 5, 6, 7 represent angular distributions of $E_{3\text{He}} = 6.49, 6.10,$ and 4.70 MeV. The $E_{3\text{He}} = 4.7$ MeV result of the present measurements agrees with that of Din et al. at $E_{3\text{He}} = 4.76$ MeV.

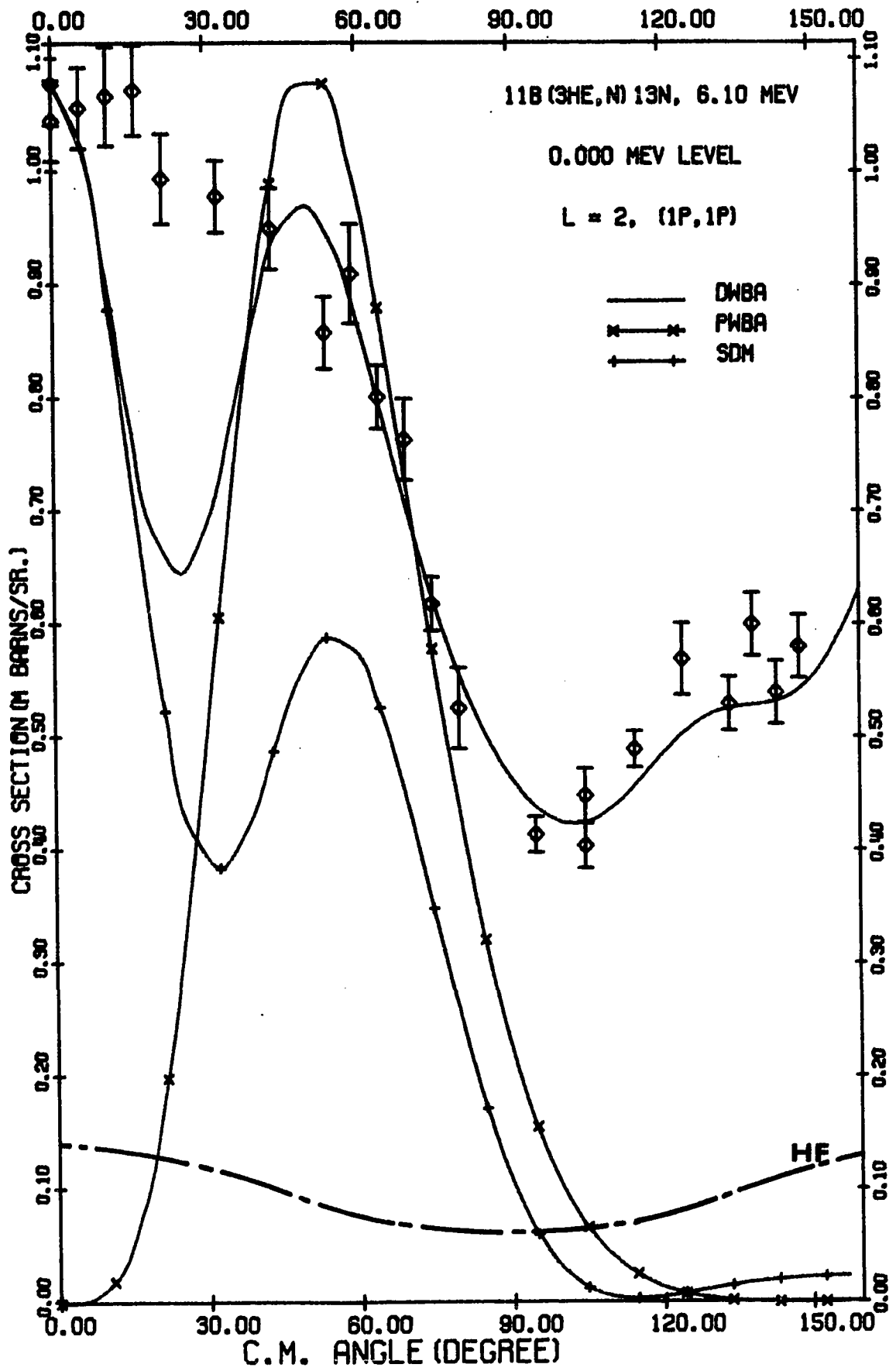
The ground states of nuclei ^{11}B and ^{13}N have spin and parity of $\frac{3}{2}^-$ and $\frac{1}{2}^-$ respectively. The selection rules restrict the total orbital angular momentum transfer to $L = 2$. As can be seen in Figures 5, 6, 7, with $L = 2$ the PWBA calculations fail to explain the forward peaked distributions. However, with $L = 2$ and $R = 4.5$ fms, the simple diffraction model calculations do give a prediction of forward peak together with a second peak near $50 - 60$ degrees, (Fig. 5, 6 and 7). Assuming the ground state of ^{11}B and ^{13}N have $(1p)^7$ and $(1p)^9$ configurations respectively, then both protons have to be transferred to $1p$ shells of ^{13}N . Reasonable fits were obtained for DWBA calculations with $L = 2$ and $(1p, 1p)$ transition. Results of the SDM and DWBA calculations coupled with the fact that the HF prediction for the cross section is small lead one to conclude that the direct process predominates in populating this level especially at energies above 5 MeV.

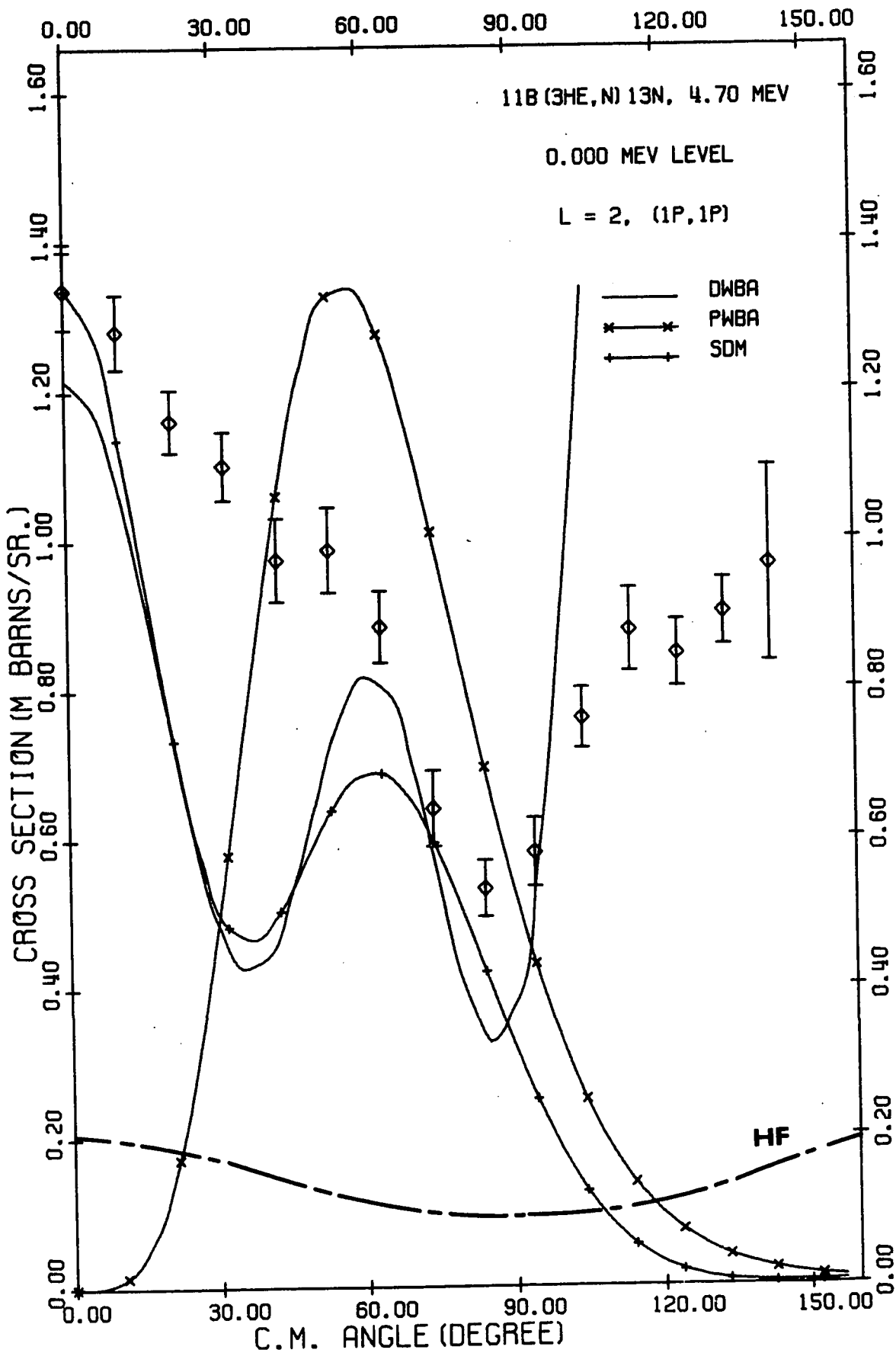
Figure 5. Angular distribution of the neutrons leading to the ground state of ^{13}N for $E_{3\text{He}} = 6.49$ MeV. $r_0 = 4.5$ fms and $\mu = 5.0$ fms were used for PWBA calculation. $R = 4.5$ fms was used for SDW calculation. See text for parameters used for DWBA calculation. Dash and dot line indicates the Hauser-Feshbach calculation.

Figure 6. Angular distribution of the neutrons leading to the ground state of ^{13}N for $E_{3\text{He}} = 6.1$ MeV (see also caption under figure 5).

Figure 7. Angular distribution of the neutrons leading to the ground state of ^{13}N for $E_{3\text{He}} = 4.7$ MeV (see also caption under figure 5).







(ii) The 2.358 MeV Level.

This level is known to have spin and parity of $\frac{1}{2}^+$ (AJ 62) consistent with a single particle configuration of $(1p)^8 2s$ (TA 60, LA 55, LA 54). The sharpness of the resonance observed in the elastic scattering of protons on ^{12}C (JA 53A), the strong excitation by the $^{12}\text{C}(d,n)^{13}\text{N}$ reaction (OB 66), and the weak excitation by both (p,d) and (p,t) reactions (FL 68, KO 67) indicate that this is a good $2s_{\frac{1}{2}}$ single particle state. The selection rules for the $(^3\text{He},n)$ reaction restrict this transition to a pure $L = 1$ transfer. All three calculations for this level (of Figures 8, 9, 10) confirmed that this is the case. The present DWBA calculations over-estimate the forward-angle cross sections for the $E_{^3\text{He}} = 6.1$ and 6.49 MeV distributions.

It was pointed out by Kozub et al. (KO 67), that there may exist some $1d_{\frac{3}{2}}$ components in this level. A pure $(1p,1d)$ transition was also tried for calculation but produced only small differences in the shape of the distributions.

When the HF cross sections are taken into account it can be seen that reaction leading to this level is predominantly direct, and the cross section agrees well with prediction of both plane wave and diffraction model theories.

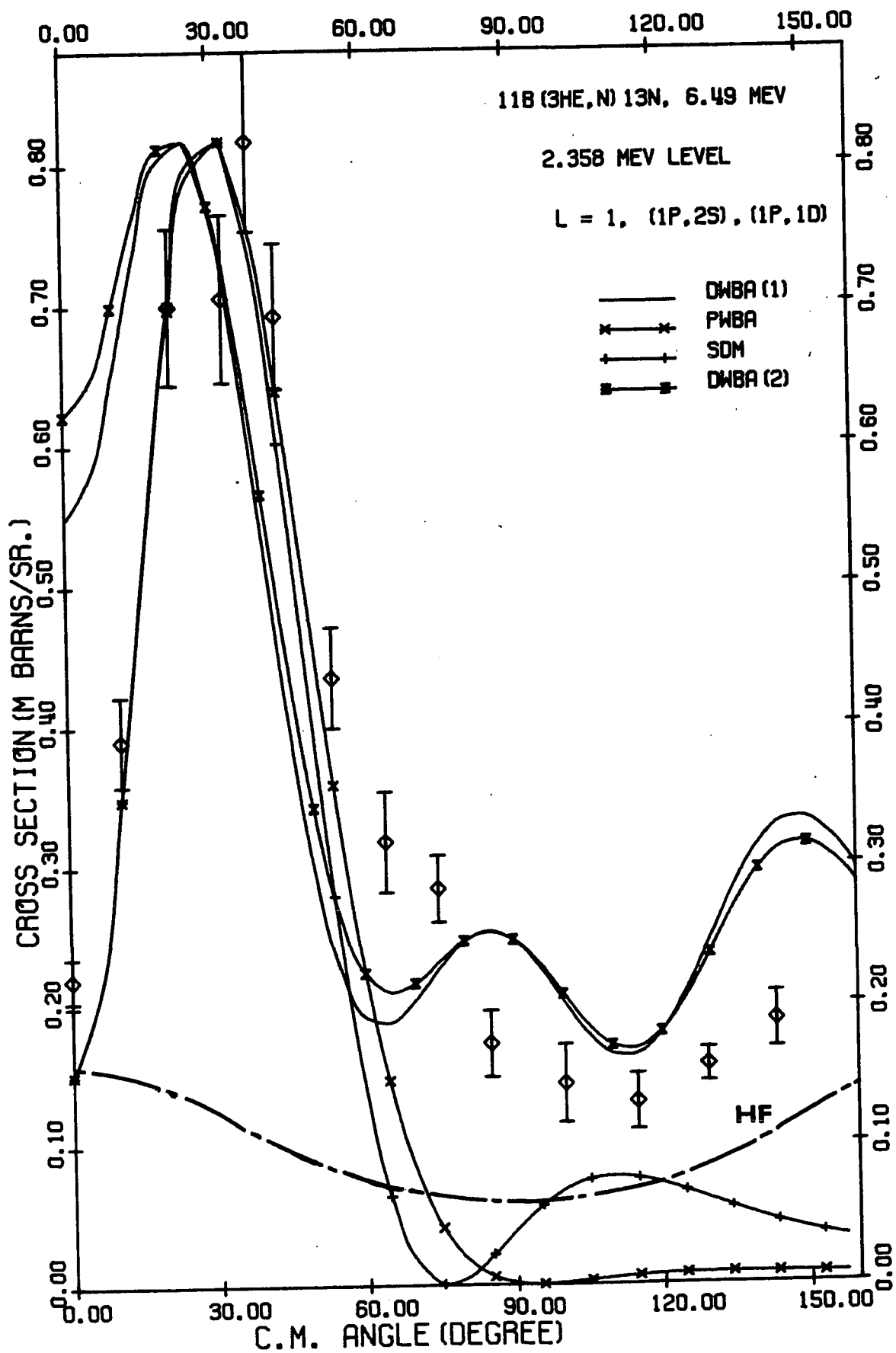
(iii) The 3.502 and 3.55 MeV levels.

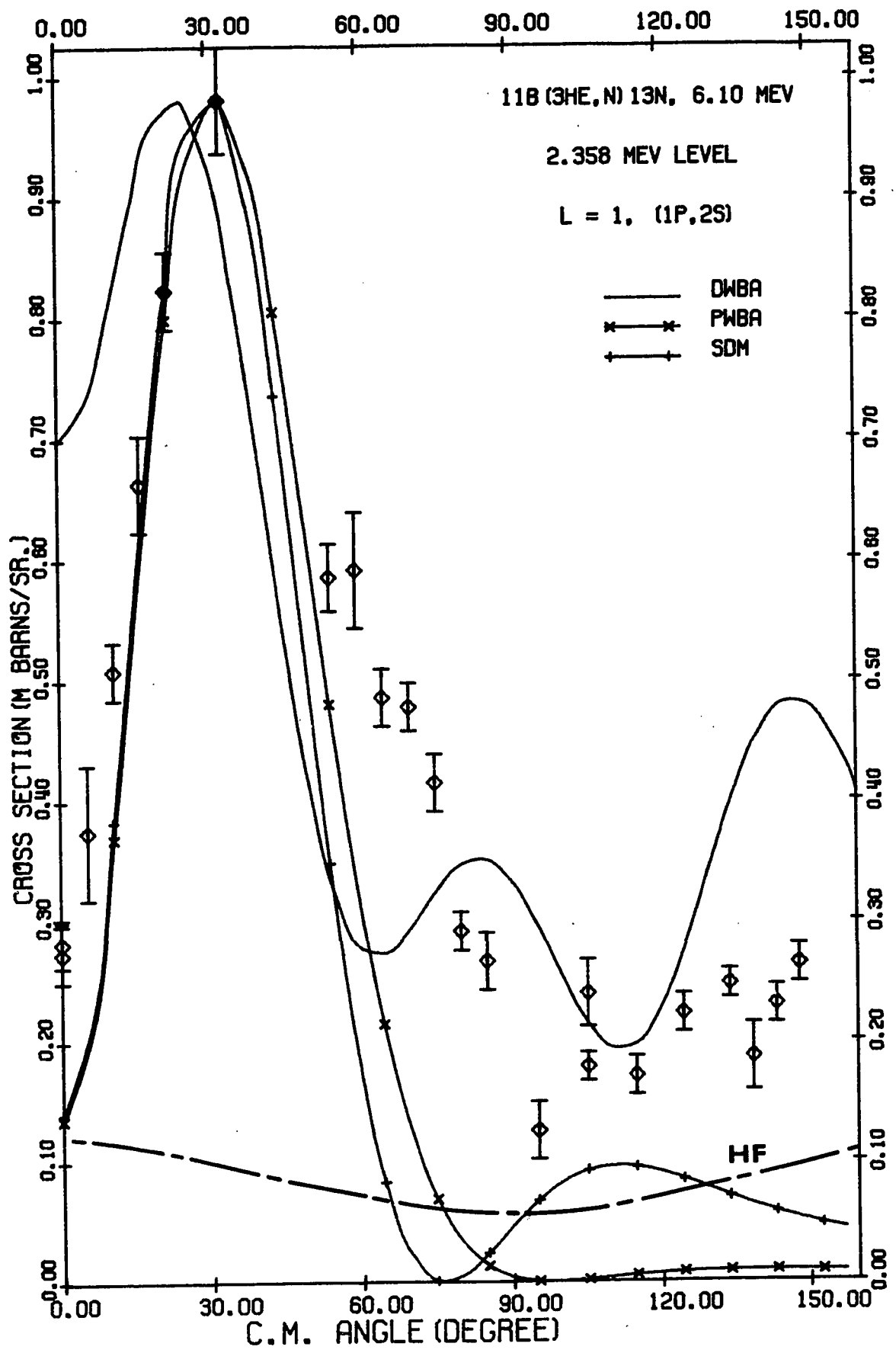
The neutron groups leading to these two states remained unresolved in these measurements. Shell model calculations predict that the 3.502 MeV level should be predominantly a $1p_{\frac{3}{2}}$ level, and that the 3.55 MeV state is predominantly a $d_{\frac{5}{2}}$ single particle level (LA 55). Measurements of Jackson

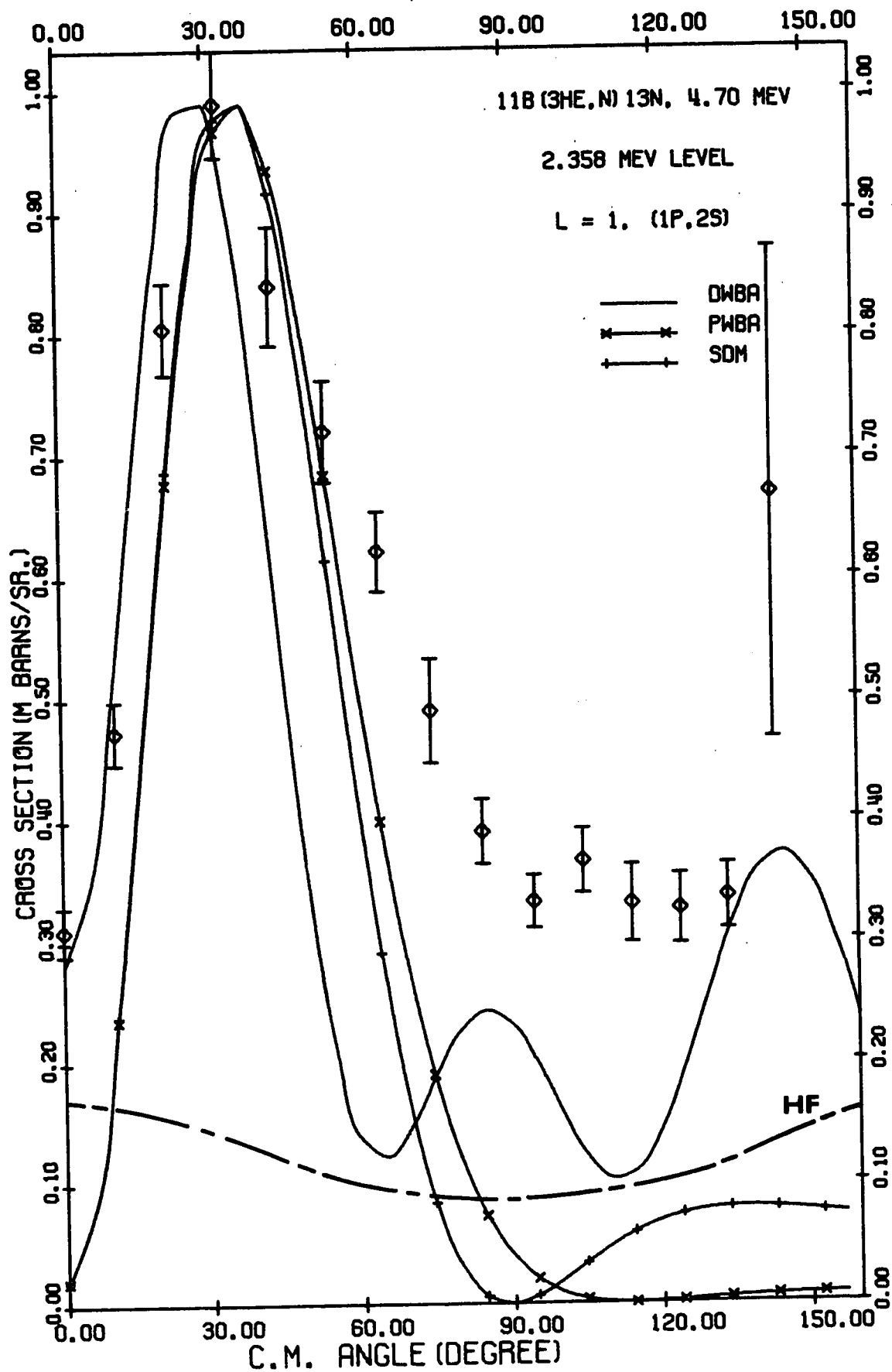
Figure 8. Angular distribution of neutrons leading to the 2.358 MeV level of ^{13}N for $E_{3\text{He}} = 6.49$ MeV. DWBA(1) and DWBA(2) represent results of (1p,2s) and (1p,1d) respectively. (See also caption under figure 5).

Figure 9. Angular distribution of neutrons leading to the 2.358 MeV level of ^{13}N for $E_{3\text{He}} = 6.1$ MeV. (See also caption under figure 5).

Figure 10. Angular distribution of neutrons leading to the 2.358 MeV level of ^{13}N for $E_{3\text{He}} = 4.7$ MeV. (See also caption under figure 5).







and Galonsky (JA 53A, JA 53B) gave some confirmation to the above statements. In agreement with the $1p_{3/2}$ assignment, the 3.502 MeV level proved to be strongly excited by the $^{15}\text{N}(p,t)^{13}\text{N}$ reaction (FL 68). On the other hand small yields were seen in both the $^{14}\text{N}(^3\text{He},\alpha)^{13}\text{N}$ and $^{14}\text{N}(p,d)^{13}\text{N}$ reactions for both levels. This created some difficulty in describing the single particle pick-up reaction for the 3.502 MeV level. However, the strong $L = 0$ transition in the present measurements is an additional evidence for a $1p_{3/2}$ configuration for the 3.502 MeV level (fig. 11, 12, and 13).

Since the transitions to the positive parity states of ^{13}N are not negligible for the $(^3\text{He},n)$ reaction, one would expect a fair transition strength for the 3.55 MeV level. The angular distributions shown in Figures 11 to 13 indicate that there could have been some contributions (L greater than 1) from the transition to the $1d_{5/2}$ state (3.55 MeV).

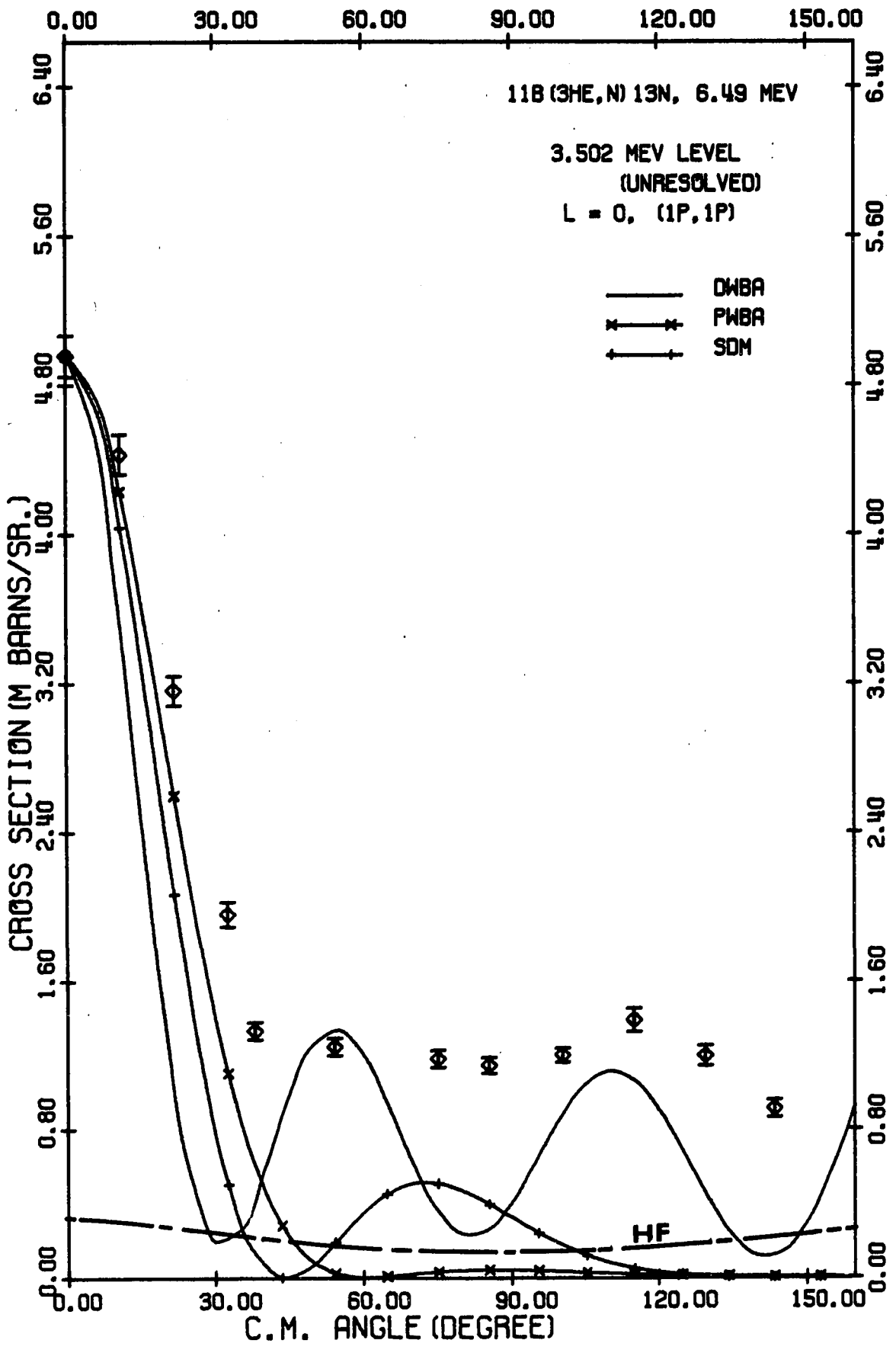
(iv) The 6.353, 6.875, and 7.145 MeV levels.

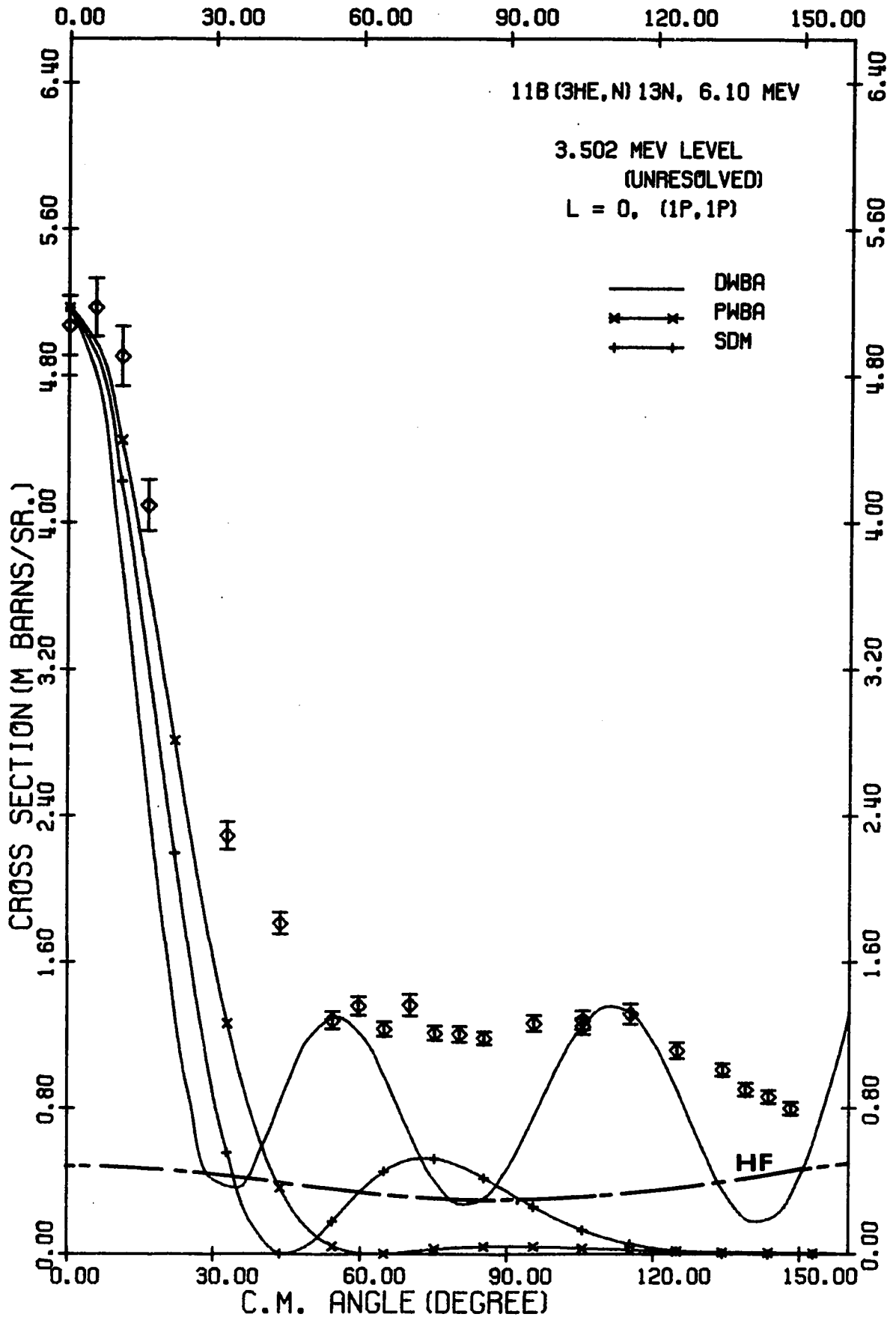
The 6.353, 6.875 and 7.145 MeV levels are known to have positive parity. The 6.353 MeV level was previously studied by proton scattering on ^{12}C , and was interpreted as a $2s_{1/2}$ state (RE 56). Kozub et al. (KO 67) have shown that there is some $1d_{5/2}$ admixture in the $2s_{1/2}$ configuration. Present calculations for $L = 1$ transitions are shown in figures 14 and 15. Very little difference was found in the calculated results using either the $(1p,1d)$ or $(1p,2s)$ configuration. The Hauser-Feshbach calculations predicted a comparatively large cross-section for this level. As it is shown in figure 14, for $E_{^3\text{He}} = 6.1$ MeV, the predicted HF

Figure 11. Angular distribution of the neutrons leading to the unresolved levels 3.502 and 3.55 MeV for $E_{3\text{He}} = 6.49$ MeV. (See also caption under figure 5). The HF cross sections are the sum of cross sections contributed from both 3.502 and 3.55 MeV levels.

Figure 12. Angular distribution of the neutrons leading to the unresolved levels 3.502 and 3.55 MeV for $E_{3\text{He}} = 6.1$ MeV. (See also captions under figure 5 and 11).

Figure 13. Angular distribution of the neutrons leading to the unresolved levels 3.502 and 3.55 MeV for $E_{3\text{He}} = 4.7$ MeV. (See also captions under figure 5 and 11).





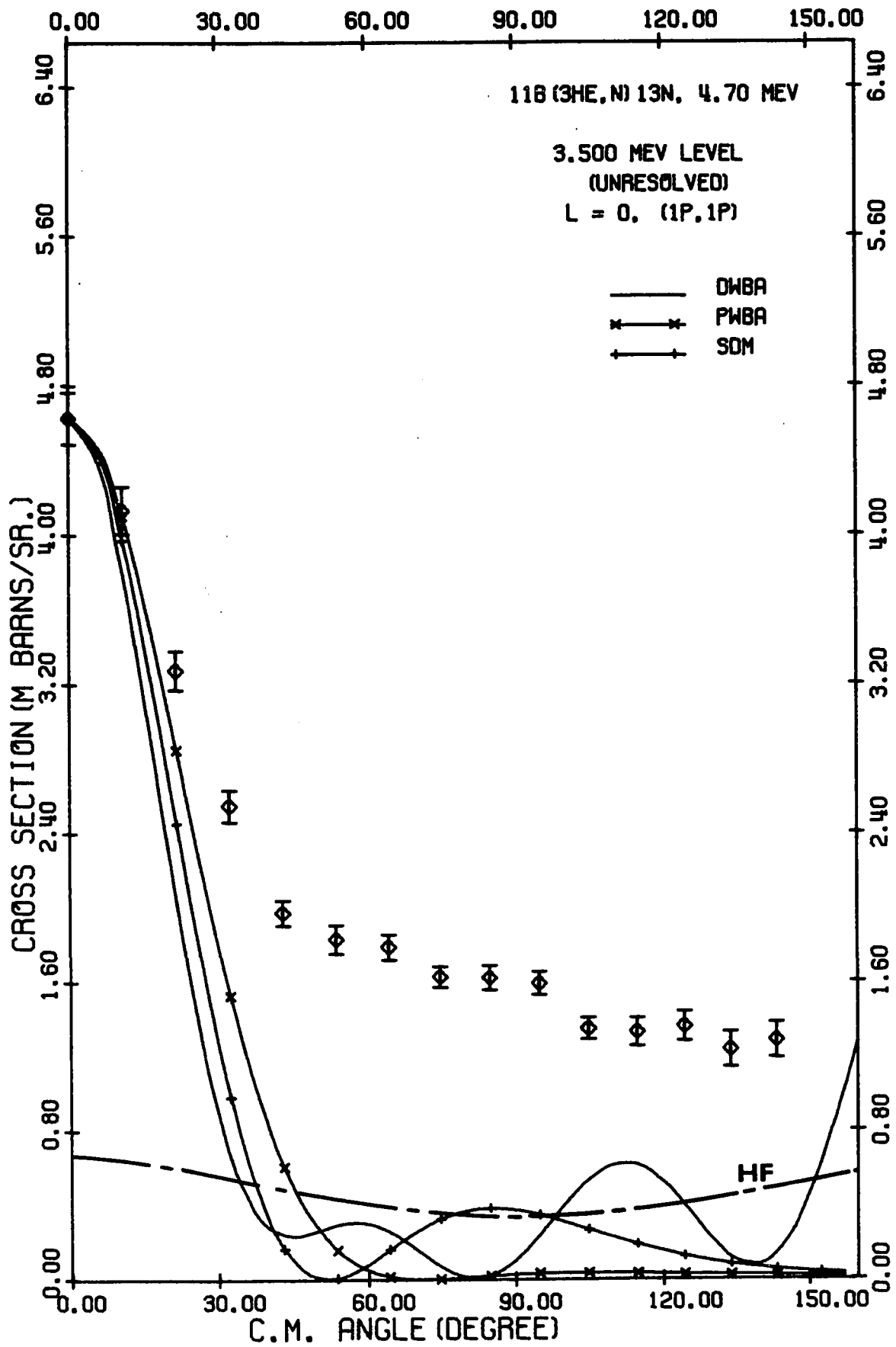


Figure 14. Angular distribution of neutrons leading to the 6.353 MeV level of ^{13}N for $E_{3\text{He}} = 6.1$ MeV. $L = 1$ was used for all calculations. Configurations (1p, 1d) and (1p, 2s) were used for DWBA(1) and DWBA(2) respectively. (See also caption under figure 5).

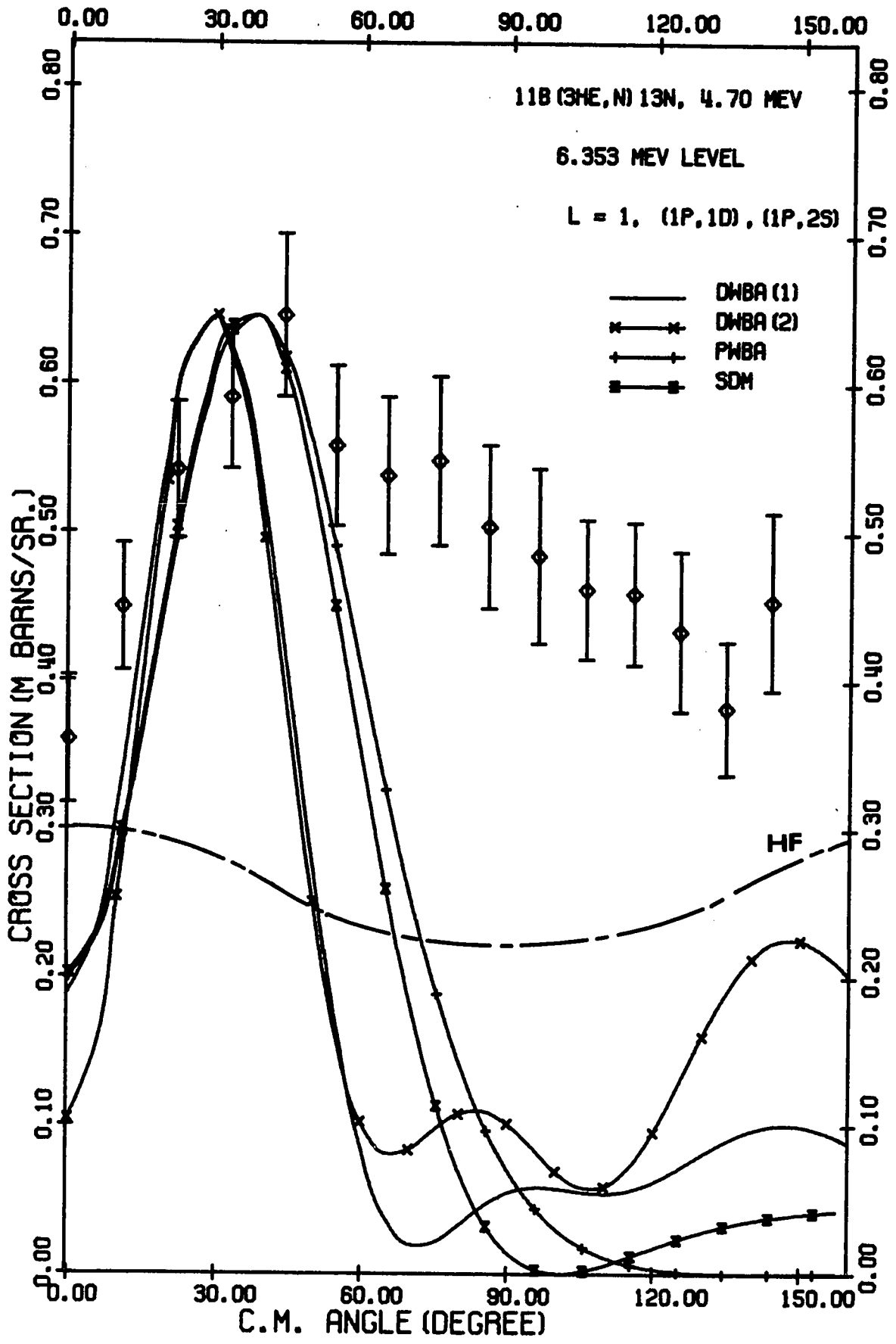
Figure 15. Angular distribution of neutrons leading to the 6.353 MeV level of ^{13}N for $E_{3\text{He}} = 4.7$ MeV. (See also caption under figure 5 and figure 14).

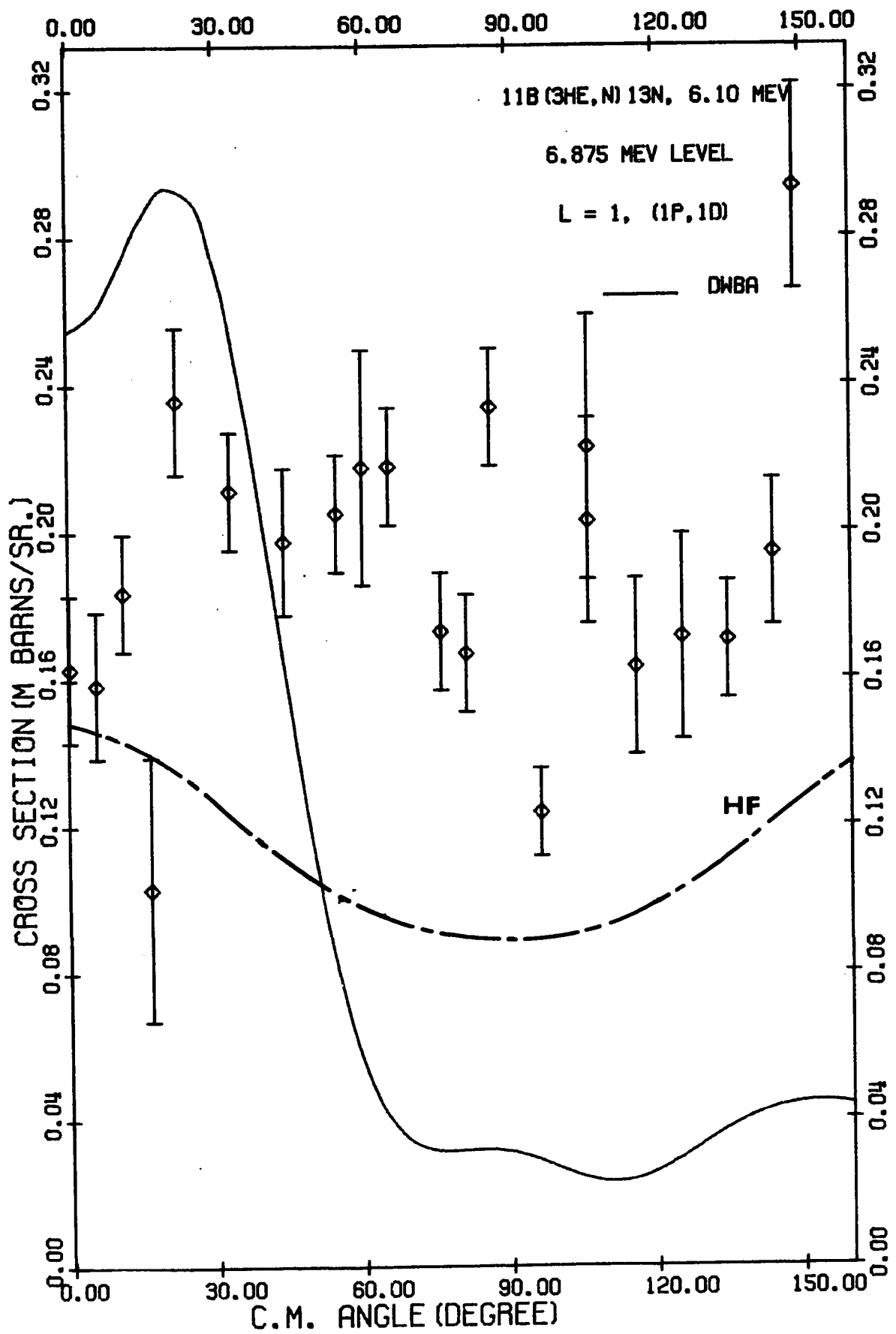
Figure 16. Angular distribution of neutrons leading to the 6.875 MeV level of ^{13}N for $E_{3\text{He}} = 6.1$ MeV.

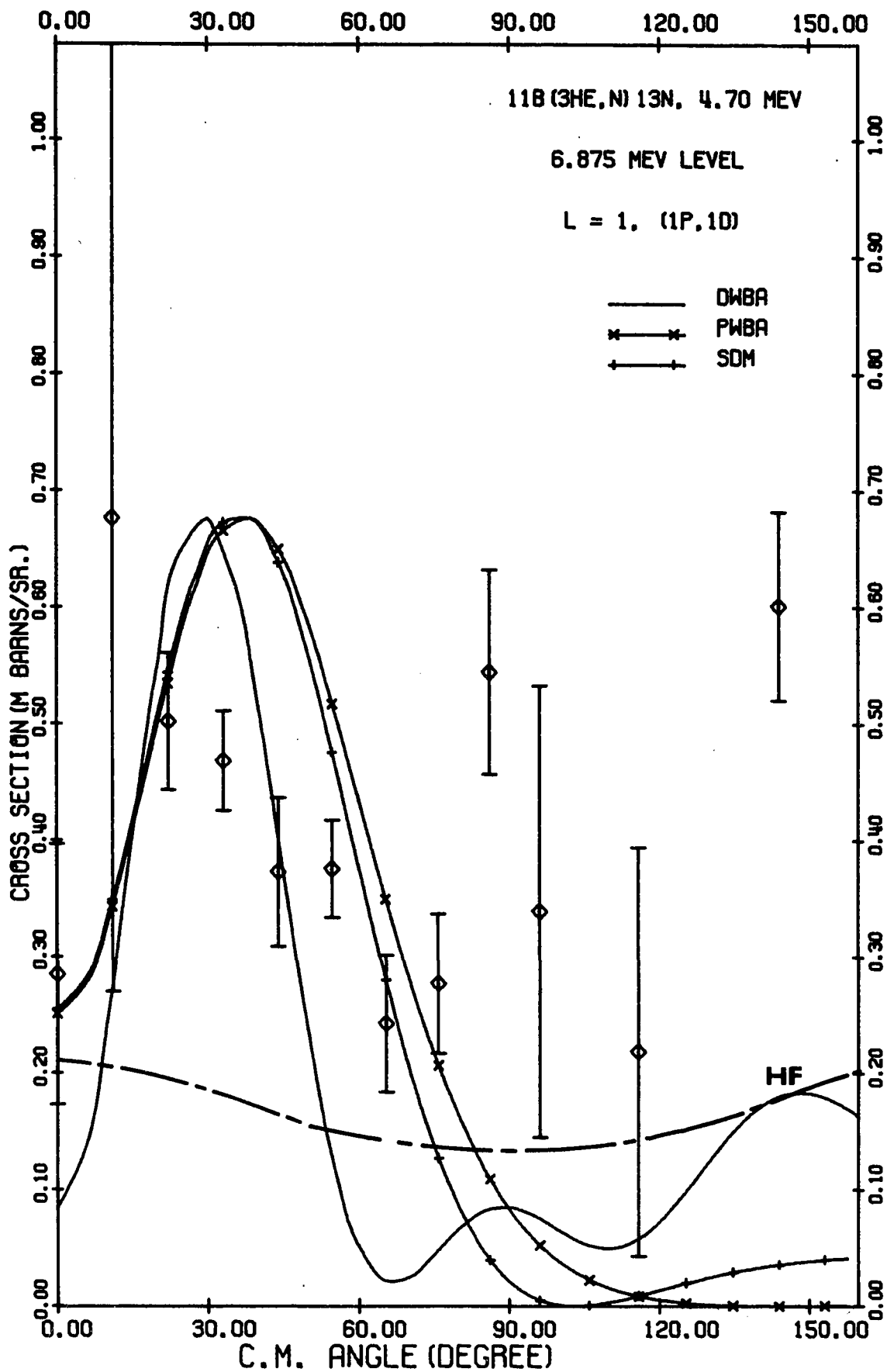
Figure 17. Angular distribution of neutrons leading to the 6.875 MeV level at $E_{3\text{He}} = 4.7$ MeV. (See also caption under figure 5).

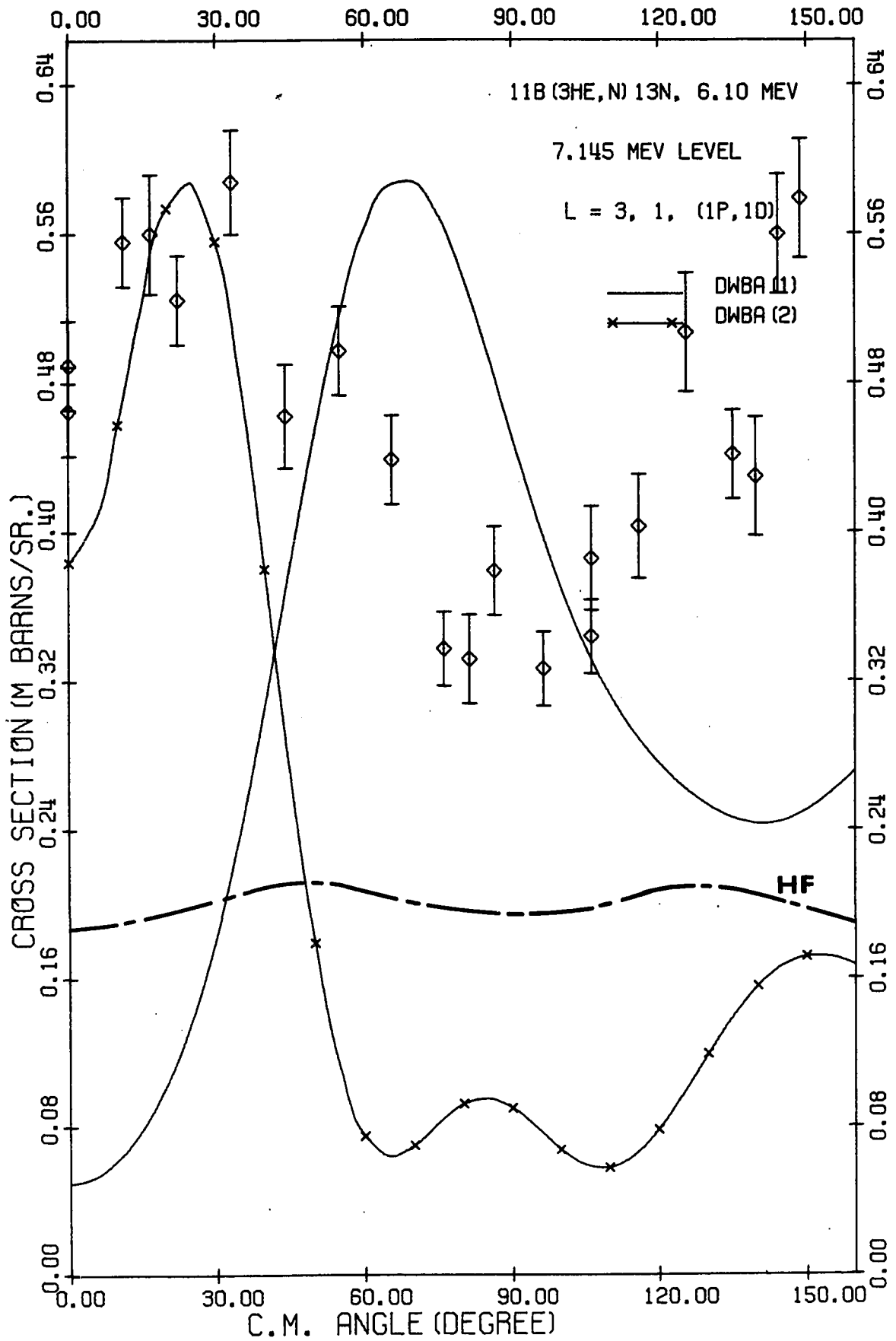
Figure 18. Angular distribution of neutrons leading to the 7.145 MeV level of ^{13}N for $E_{3\text{He}} = 6.1$ MeV. $L = 3$ and 1 were used for DWBA(1) and DWBA(2) respectively where (1p, 1d) configuration was used for both calculations.

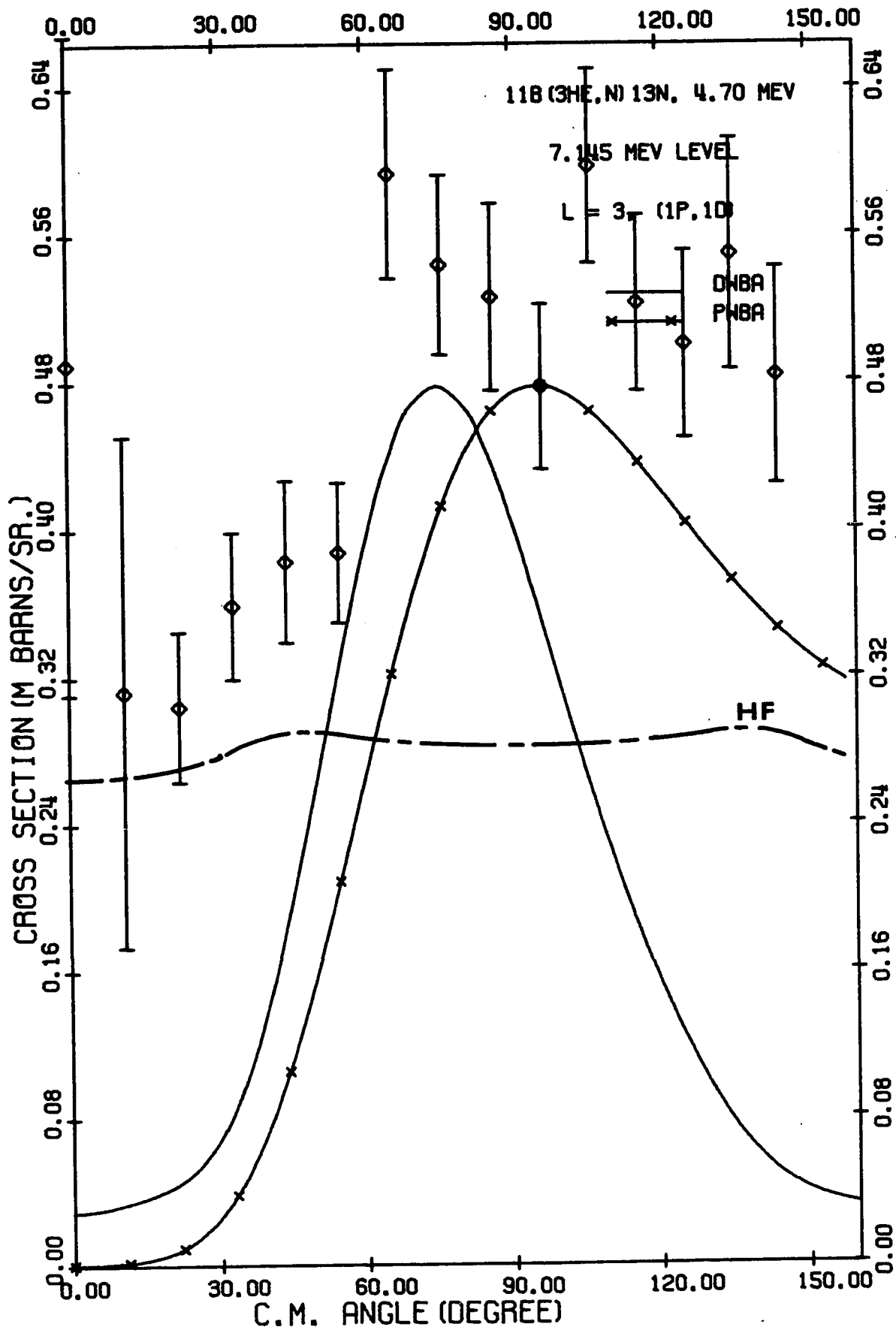
Figure 19. Angular distribution of neutrons leading to the 7.145 MeV level for $E_{3\text{He}} = 4.7$ MeV. (See caption under figure 5).











cross sections are obviously too large for the experimental data. This is evidence that the HF calculation has overestimated the compound formation cross sections. By taking into account the compound nucleus cross sections given by HF calculations, it was noted that calculations of direct interaction part agree reasonably well with the present results (figure 14 and 15).

The 6.875 MeV level is located just above the threshold for proton inelastic scattering from the first excited state of ^{12}C . This level with width of 115 keV has been assumed to a $1d_{3/2}$ configuration from the $(p,p'\gamma)$ measurements (RE 56, SH 62, BA 63B,C). Previous measurements for $^{15}\text{N}(p,t)^{13}\text{N}$, $^{14}\text{N}(^3\text{He},\alpha)^{13}\text{N}$ and $^{14}\text{N}(p,d)^{13}\text{N}$ (FL 68, KO 67) indicated that the double stripping strength for this level is weak. This result was also observed in the present study as the CN formation cross section predicted by the HF calculation was able to account for much of the observed cross section. Any direct component was too small to be fitted using the DF predictions. It is likely that this level is more complicated than a $1d_{3/2}$ configuration.

The 7.145 MeV level was first reported by Nikolic et al. (NI 61, YO 60). From the γ -ray angular distributions the spin of this level was assigned as $\frac{1}{2}$. However, from the analysis of inelastic scattering data Barker et al. (BA 63B, BA 63C) reassigned this level as $\frac{7}{2}^+$. The calculations of Barker also predicted that the lowest $\frac{7}{2}^+$ level of ^{13}N should consist mainly of the ^{12}C 2^+ excited state plus a $1d_{5/2}$ proton. The reactions $^{15}\text{N}(p,t)^{13}\text{N}$, $^{14}\text{N}(^3\text{He},\alpha)^{13}\text{N}$ and $^{14}\text{N}(p,d)^{13}\text{N}$ (FL 68, KO 67) showed no evidence for the existence of this

level. The reason was due to low resolution, perhaps coupled with a small yield. The present ($^3\text{He},n$) results showed a moderate transition strength to this level, however, the angular distributions shown in figures 18 and 19 indicate a strong dependency on ^3He energies. This suggests that at these moderate bombarding energies the reaction mechanism for formation of this state is more complex than the simple DI or CN formations.

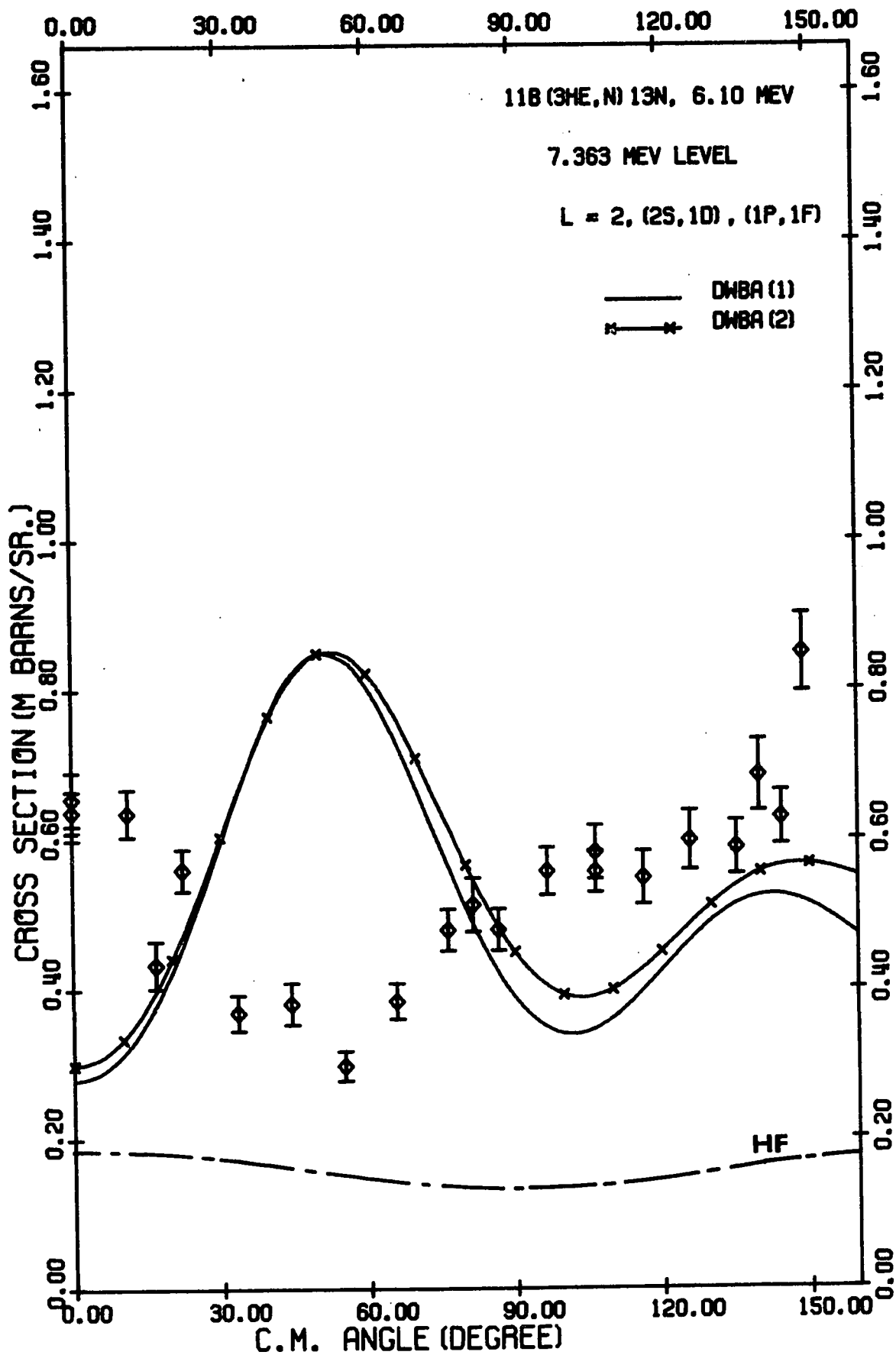
(v) The 7.363 MeV level.

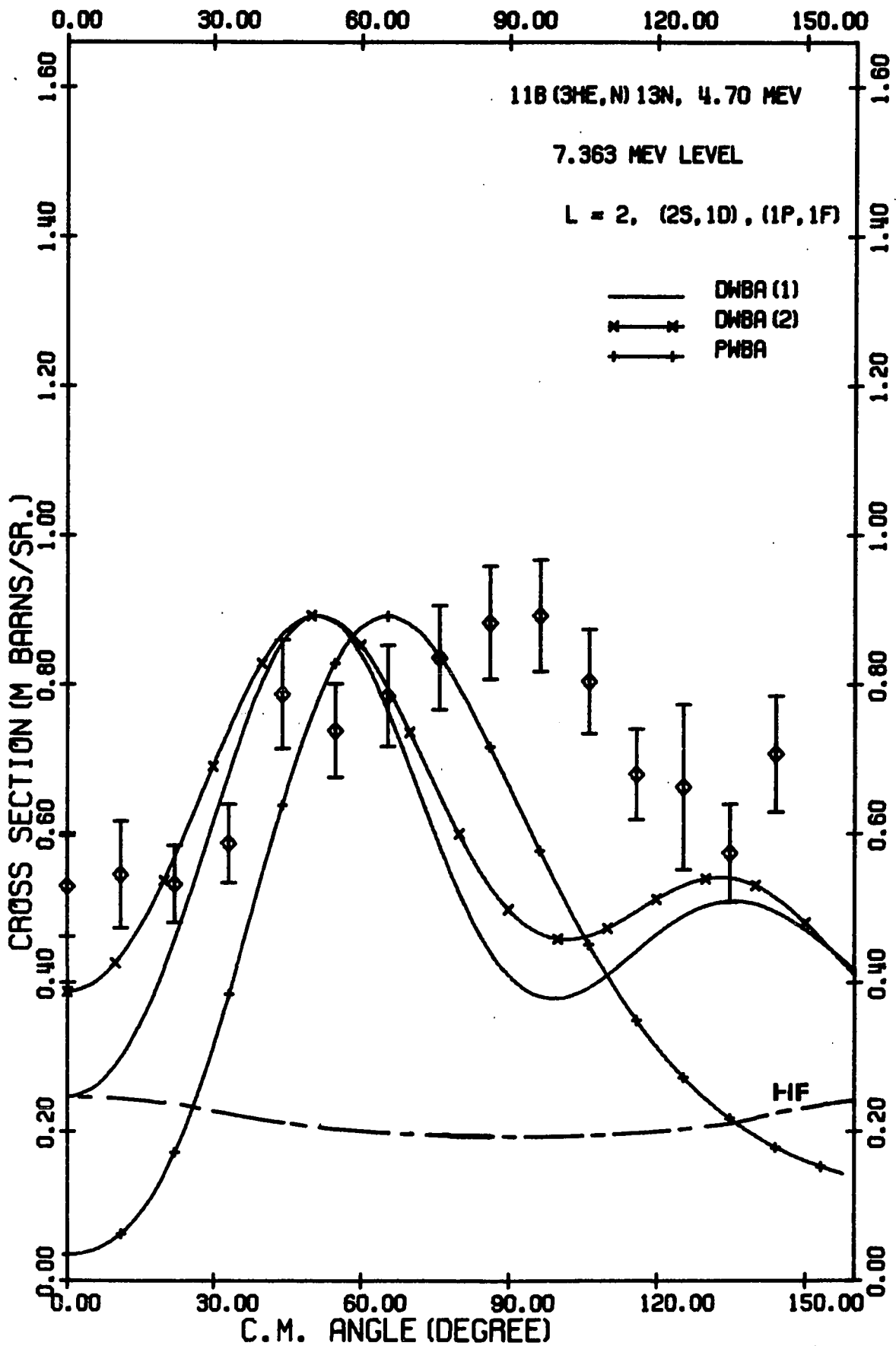
Prior to the work of Barker et al. (Ba 63A,B) many groups have suggested a $\frac{5+}{2}$ assignment for this level (SH 62, NO 62, AD 61). This assignment presented difficulties for the shell model calculations for ^{13}N (BA 61A, KU 61, KU 56). The intermediate coupling calculations predicted two $\frac{5+}{2}$ levels in ^{13}N at 3.5 MeV and 6.38 MeV. No other $\frac{5+}{2}$ level was expected to lie below 10 MeV. Furthermore, a $\frac{5-}{2}$ level, predicted by the same calculations to lie near 5 MeV, was missing in this region. In view of these difficulties, many experiments were carried out in a search for this missing level (GA 63).

The Shell model calculations and the analysis of the inelastic proton scattering data of Barker et al. (BA 63B, BA 63C) indicates that this is a $\frac{5-}{2}$ level. This ended the long search for the $\frac{5-}{2}$ level predicted by the intermediate coupling calculation. All later measurements, the (p,d) work (KO 67, MA 66C) and the (p,t) results (FL 68) indicated that the $\frac{5-}{2}$ assignment is the correct one. The present ($^3\text{He},n$) results as can be seen in figures 20 and 21 show energy dependence. Calculations with $L = 2$ and various configurations were made but none of them

Figure 20. Angular distribution of neutrons leading to the 7.363 MeV level of ^{13}N for $E_{3\text{He}} = 6.1$ MeV. Configurations (2s,1d) and (1p,1f) were used for DWBA(1) and DWBA(2) respectively. For both calculations $L = 2$ was assumed. (See also caption under figure 5).

Figure 21. Angular distribution of neutrons leading to the 7.363 MeV level for $E_{3\text{He}} = 4.7$ MeV. (See also captions under figure 5 and figure 20).





were able to fit the $E_{3\text{He}} = 6.1$ MeV distribution.

(vi) The 9.476 MeV and 11.878 MeV levels

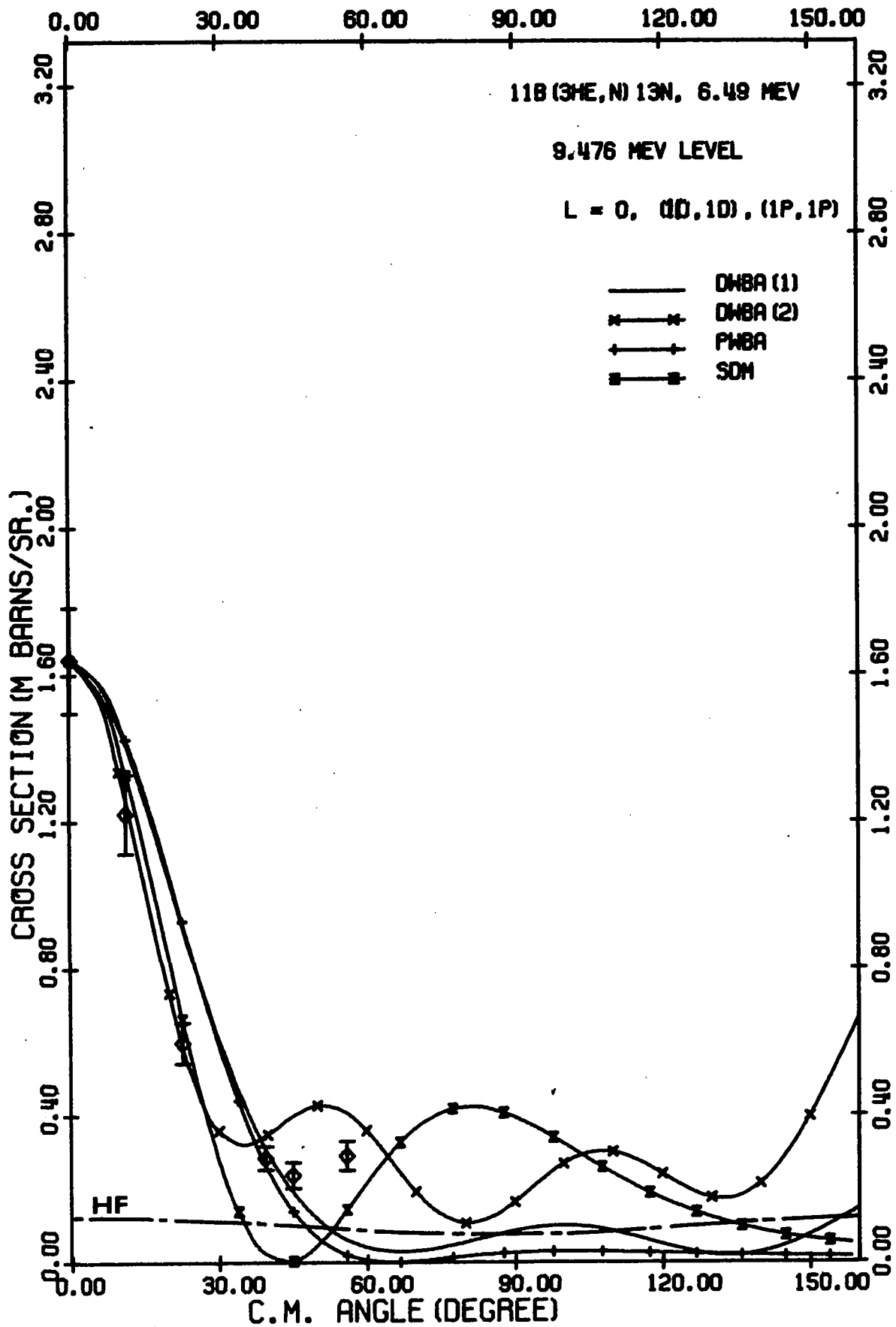
The 9.476 MeV level was originally assigned as the second $\frac{3}{2}^-$ level of the intermediate coupling calculation by the proton scattering work (NO 62, AD 61). However, weak transitions from both single particle pick-up (KO 67, BA 66), and also from the (p,t) reaction results led Fleming et al. to conclude that this level is not a simple $(1p)^9$ configuration level. Instead, this level was expected to contain appreciable $(2s,1d)^2$ admixtures. Thus the second $\frac{3}{2}^-$ state of the intermediate coupling calculation was assigned to a level at excitation 11.878 MeV.

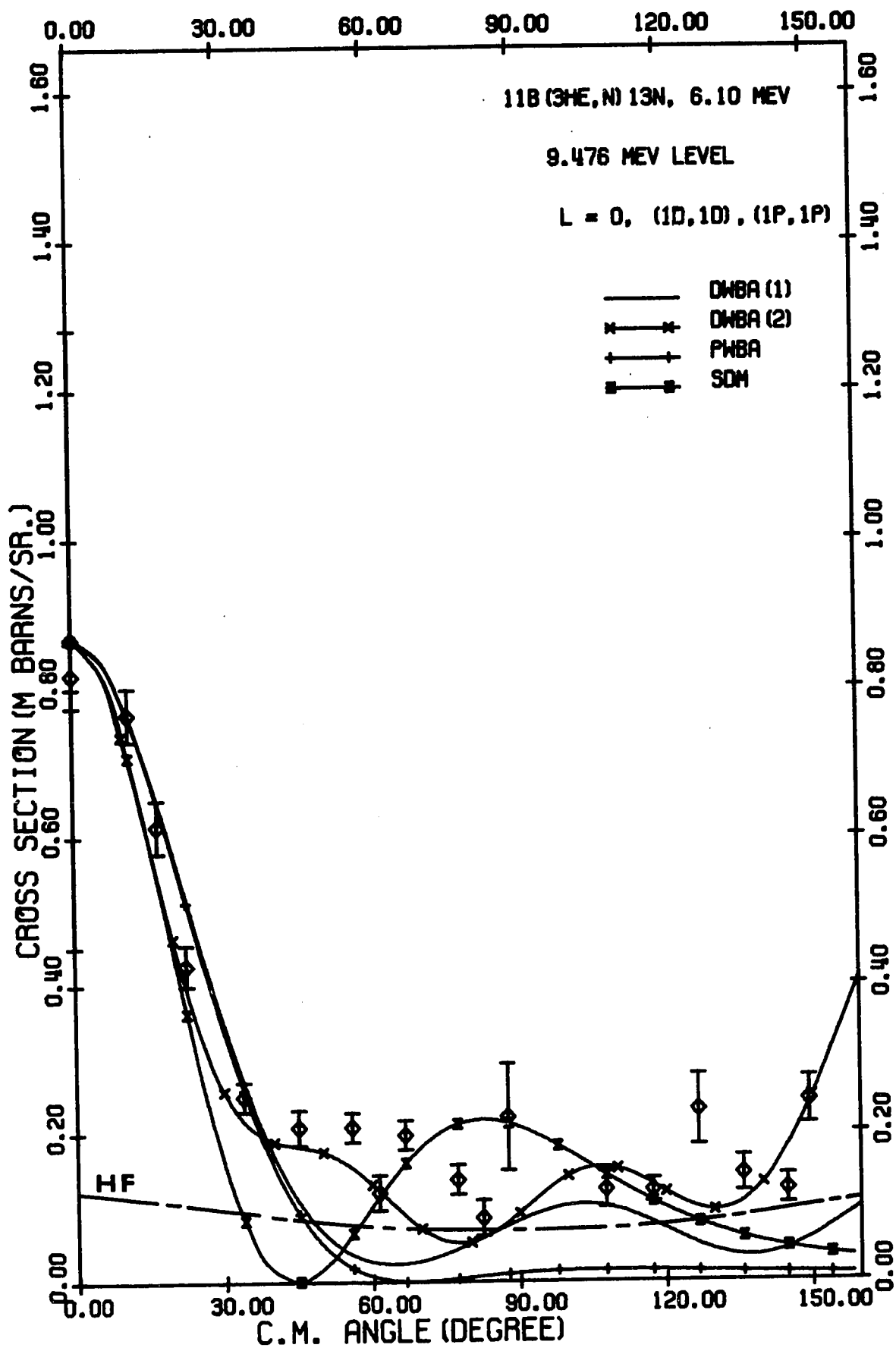
The 11.878 MeV level has been reported recently by many authors (FL 68, KO 68, BA 66), and has been assigned a $\frac{3}{2}^-$ character with the dominant configuration being $(p_{\frac{1}{2}})^2 (p_{\frac{3}{2}})^{-1}$. In figures 22, 23 and 24 comparison of the data and results of the DWBA for the transition to the 9.476 MeV level are shown. Angular distributions for 11.878 MeV are presented in figures 25 and 26. These results are also consistent with the previous spin assignments. HF cross section for neutrons leading to these two levels are small compared with observed cross sections. All evidences have indicated that transition to these two levels are mainly from DI.

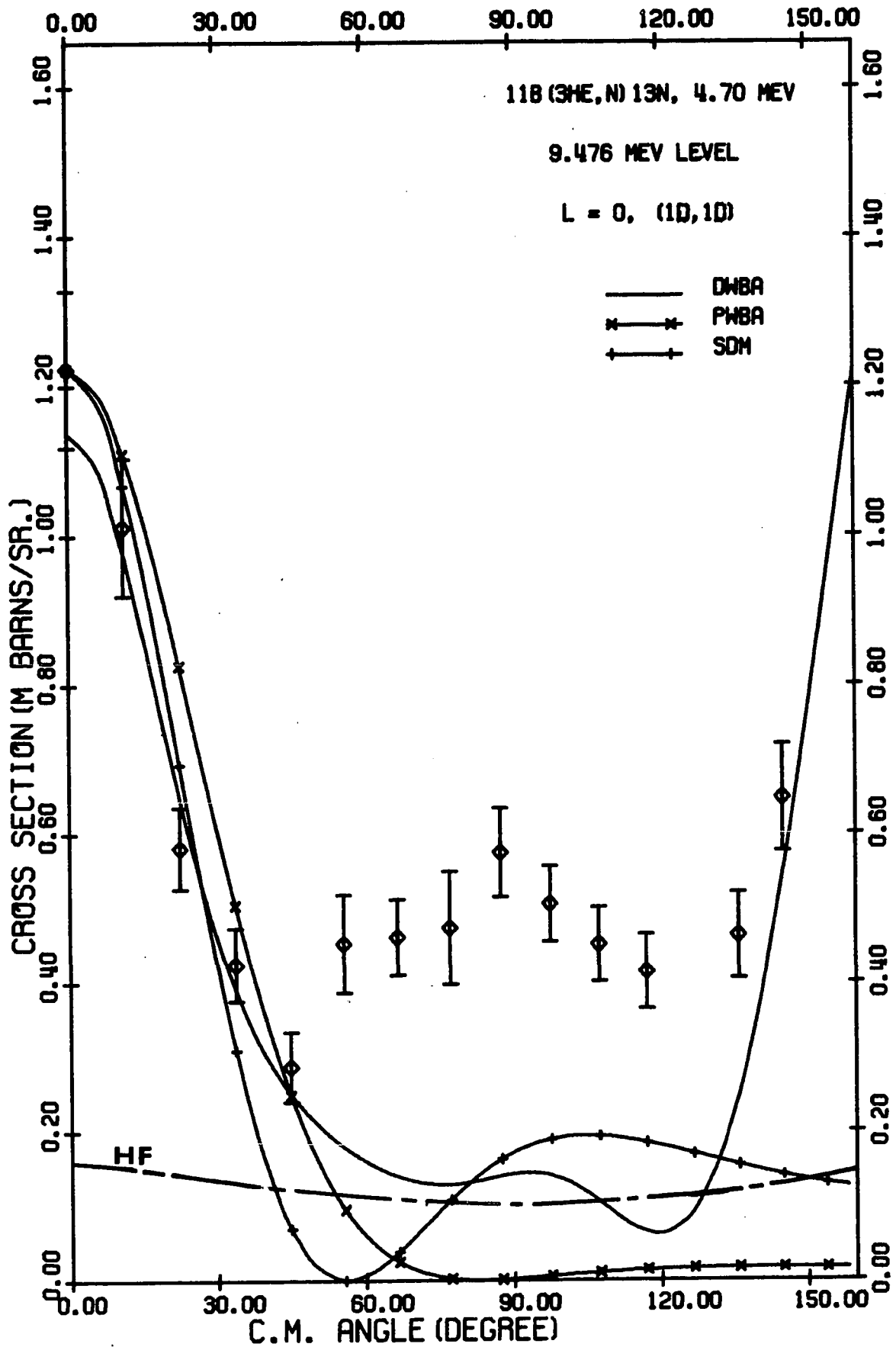
(vii) The 10.381 MeV level.

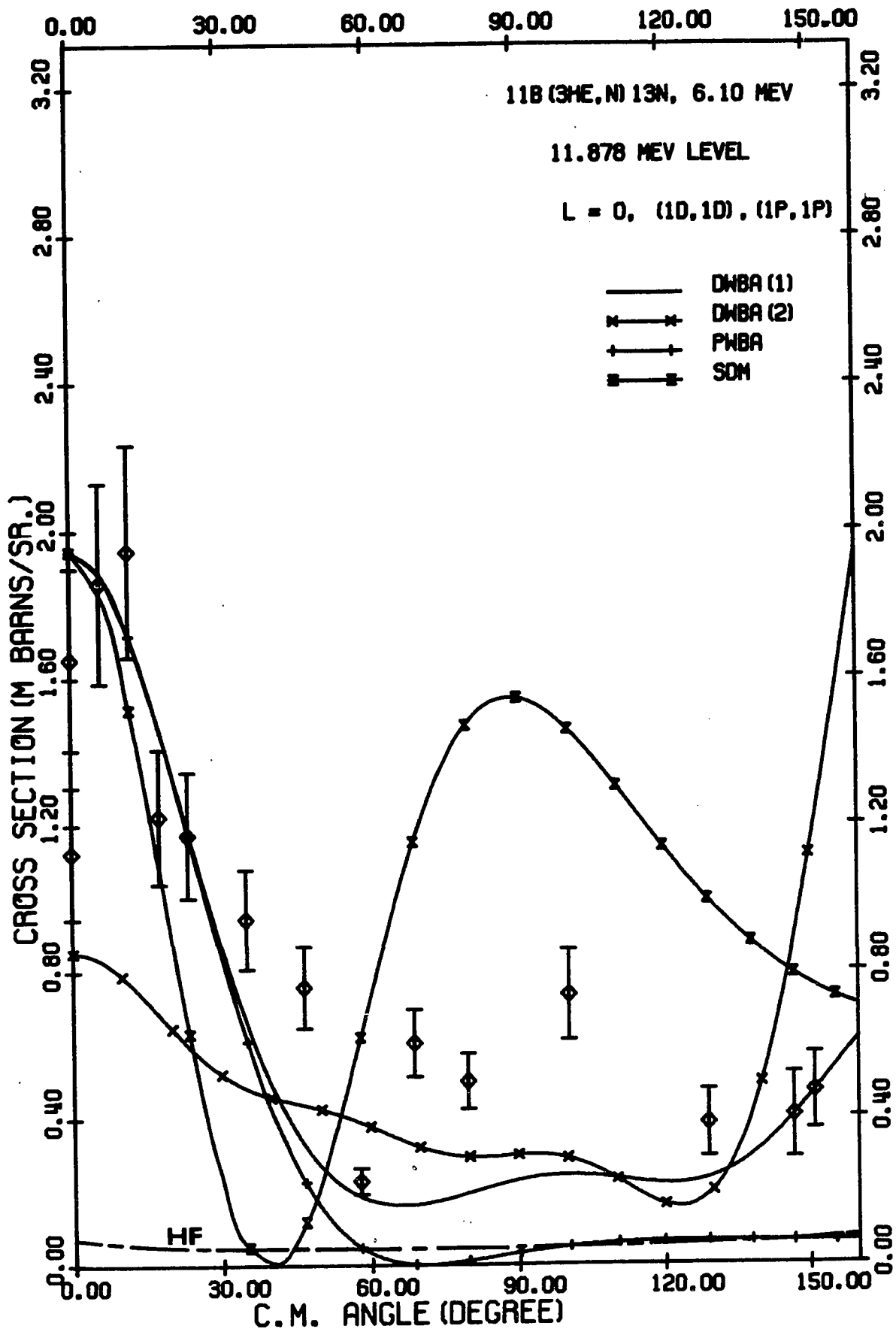
At a proton bombarding energy of 9.14 MeV Shute et al. observed a very strong resonance at all angles (SH 62). Their analysis suggested an f-wave formation for this level which

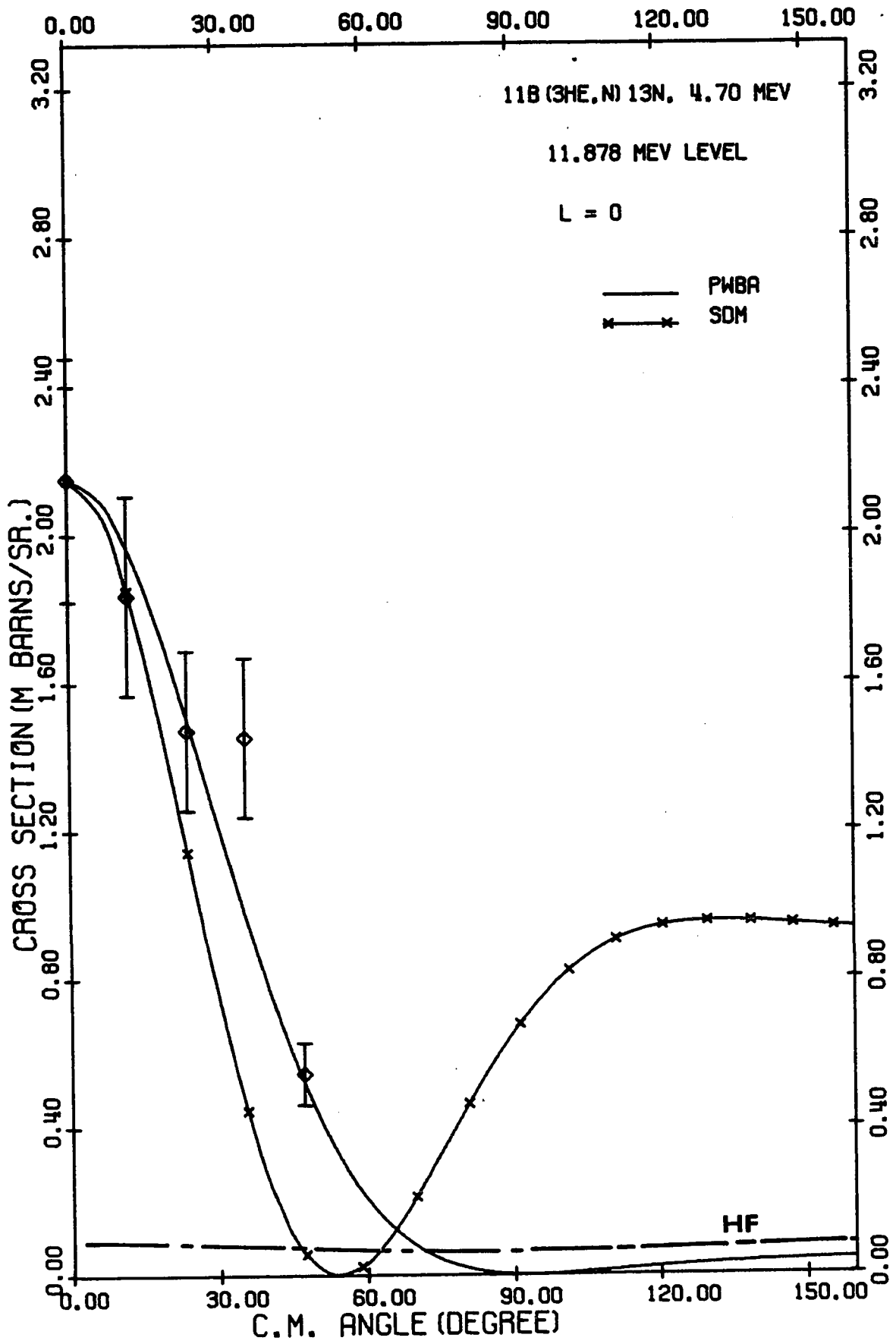
- Figure 22. Angular distribution of neutrons leading to the 9.476 MeV level of ^{13}N for $E_{3\text{He}} = 6.49$ MeV. Configurations (ld,ld) and (lp,lp) were used for DWBA(1) and DWBA(2) respectively. (See also caption under figure 5).
- Figure 23. Angular distribution of neutrons leading to the 9.476 MeV level of ^{13}N for $E_{3\text{He}} = 6.1$ MeV. Configurations (ld,ld) and (lp,lp) were used for DWBA(1) and DWBA (2) respectively. (See also caption under figure 5).
- Figure 24. Angular distribution of neutrons leading to the 9.476 MeV level of ^{13}N for $E_{3\text{He}} = 4.7$ MeV. (See also caption under figure 5).
- Figure 25. Angular distribution of neutrons leading to the 11.878 MeV level of ^{13}N for $E_{3\text{He}} = 6.1$ MeV. Configurations (ld,ld), (lp,lp) were used for DWBA(1) and DWBA(2) respectively. $L = 0$ was assumed for both calculations. (See also caption under figure 5).
- Figure 26. Angular distribution of neutrons leading to the 11.878 MeV of ^{13}N for $E_{3\text{He}} = 4.7$ MeV. $L = 0$ was assumed for both DWBA and SDM. (See also caption under figure 5).









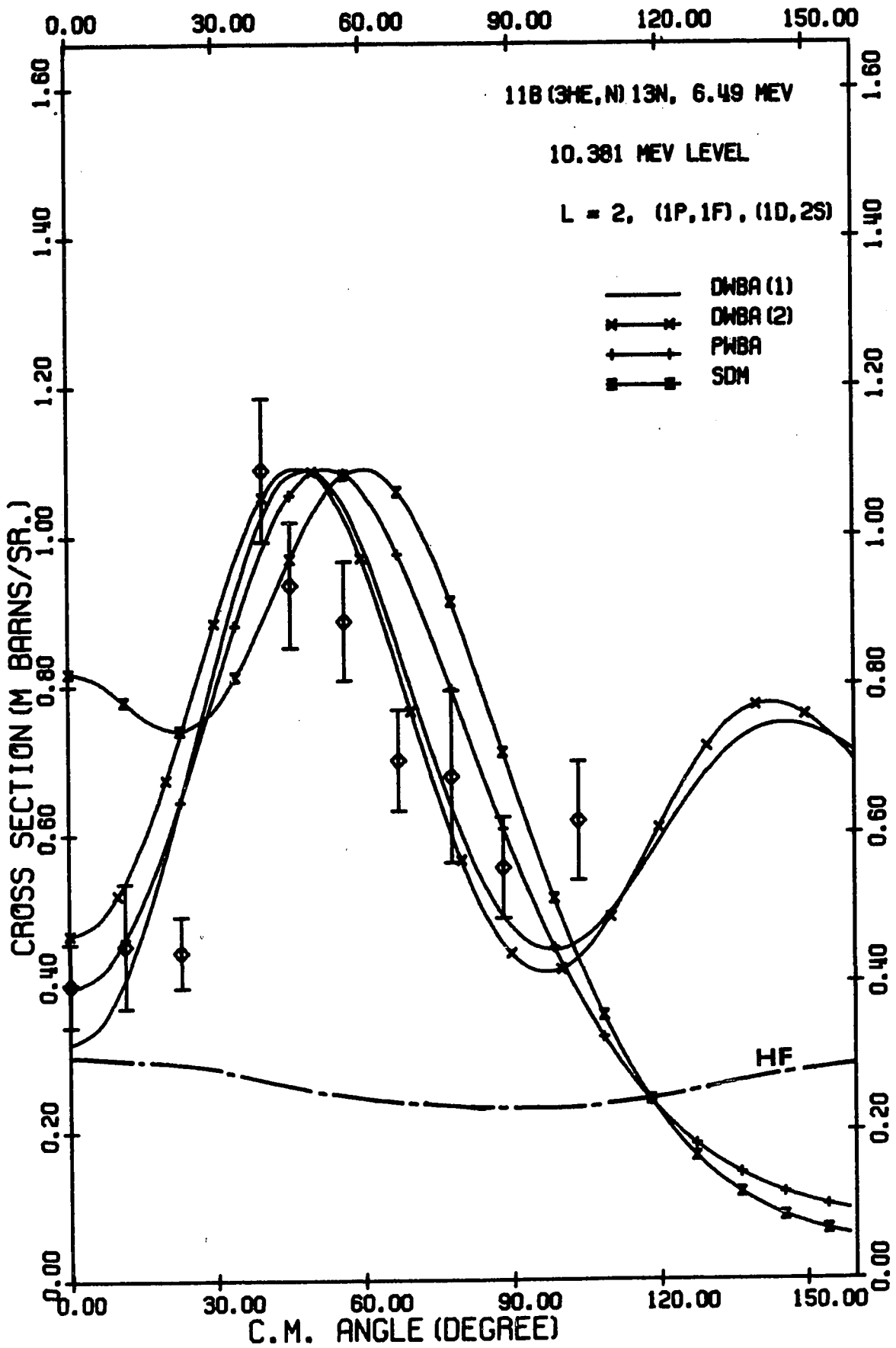


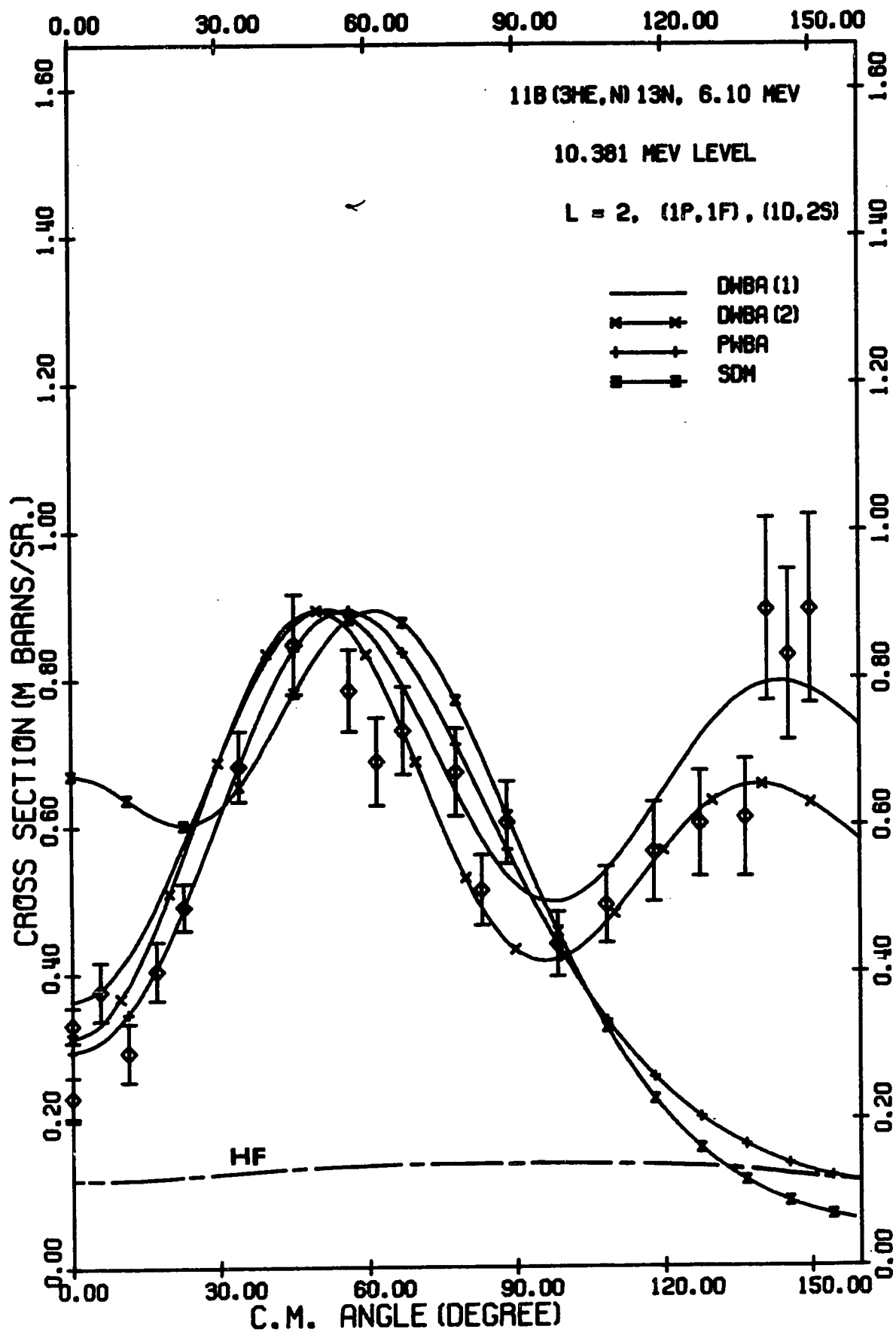
was assigned to have $J^\pi = \frac{7}{2}^-$. Compared with other single or two particles transfer reactions, the present (${}^3\text{He},n$) excitation of this level is strong. The strong $L = 2$ angular distribution patterns of figures 27, 28, 29 suggest this is a negative parity state with the possible spin of $\frac{1}{2}$, $\frac{3}{2}$, $\frac{5}{2}$ or $\frac{7}{2}$. The DWBA calculations using (lp,lf) or (ld,2s) configurations did not show significant differences in the distribution shapes. Various configurations including (lp,lp) were also used in the DWBA calculations, however only the (lp,lf) and the (2s,ld) configurations gave good fits to the data. This is in agreement with the assignment of Shute et al. (SH 62).

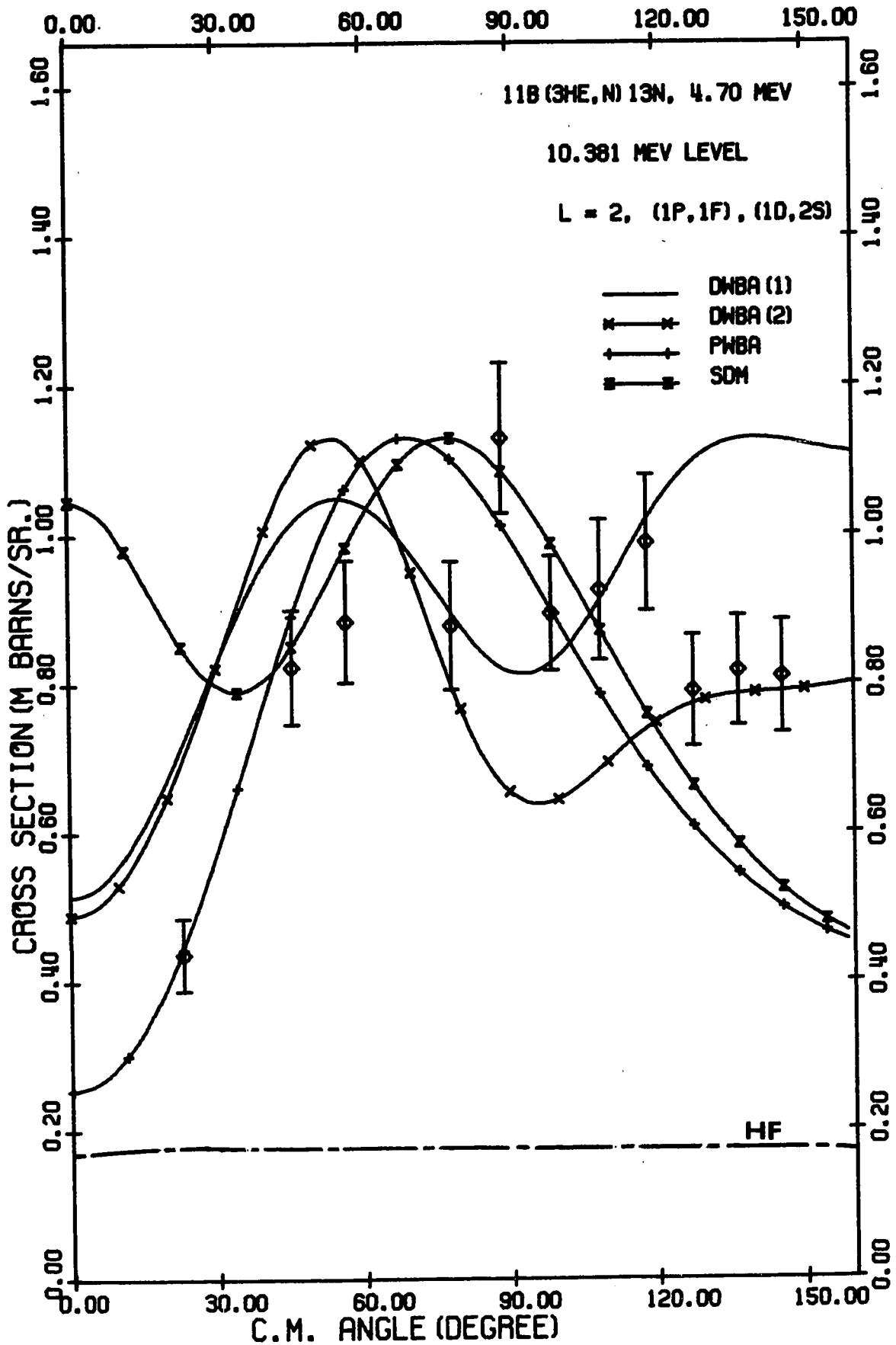
Figure 27. Angular distribution of neutrons leading to 10.381 MeV level of ^{13}N for $E_{3\text{He}} = 6.49$ MeV. Configuration (1p,1f) and (1d,2s) were used for DWBA(1) and DWBA(2) respectively. (See also caption under figure 5).

Figure 28. Angular distribution of neutrons leading to 10.381 MeV level of ^{13}N for $E_{3\text{He}} = 6.1$ MeV. (See also caption under Figure 27).

Figure 29. Angular distribution of neutrons leading to 10.381 MeV level of ^{13}N for $E_{3\text{He}} = 4.7$ MeV. (See also caption under figure 27).







CHAPTER FOUR

RESULTS (II), $^{13}\text{C}(^3\text{He},n)^{15}\text{O}$ and $^{12}\text{C}(^3\text{He},n)^{14}\text{O}$ 1. The General Background.

Due to simplicity in fabrication of the targets, ^{12}C has been one of the earliest and most frequently bombarded isotopes. The reaction $^{12}\text{C}(^3\text{He},n)^{14}\text{O}$ and $^{13}\text{C}(^3\text{He},n)^{15}\text{O}$ were among the first $(^3\text{He},n)$ reactions studied. The former reaction is of more than ordinary interest because it transfers two protons to a stable core of ^{12}C and leads to the unfamiliar proton rich nucleus ^{14}O . However, due to the negative Q values, not very much information on the higher excited states of ^{14}O has been obtained. Most of the earlier work was restricted to a study of the neutron group leading to the ground state (FU 65, MA 63, DI 61, TO 61, GA 60, BR 57).

The nucleus ^{15}O lacks only one neutron to complete the $1p$ shell. With this special status this nucleus has attracted both theoretical and experimental interest. There are available, shell model calculations of English (IN 53), of Halbert and French (HA 57B), of Lane and Radicati (LA 54, LA 60), of Ripka (RI 64), and strong coupling rotational model calculations by El-Batanoni and Kresnin (El 66). As in the case of ^{13}N , the experimental information on this particular nucleus comes mostly from studies of the elastic and the inelastic scattering of protons by ^{14}N . However, the binding energy of $^{14}\text{N} + p$ is known to be 7.291 MeV above the ground state of ^{15}O , thus the direct scattering measure-

ments are restricted to the studies of the levels above 7.55 MeV. The lower levels could only be measured indirectly by γ -ray decays. A detailed summary of the previous experiments, especially an account of the proton scattering and (p, γ) measurements, can be found in Reference EV 66.

The low-lying states of the nucleus ^{15}O can be studied by various nuclear reactions, such as $^{14}\text{N}(d, n)^{15}\text{O}$, $Q = 5.07$ MeV; $^{14}\text{N}(p, n)^{15}\text{O}$, $Q = -3.543$ MeV; $^{16}\text{O}(^3\text{He}, \alpha)^{15}\text{O}$, $Q = 4.908$ MeV; $^{14}\text{N}(^3\text{He}, d)^{15}\text{O}$, $Q = 1.798$ MeV and $^{13}\text{C}(^3\text{He}, n)^{15}\text{O}$; $Q = 7.123$ MeV (AJ 62). A summary of the previous measurements can be found in Reference WA 65A.

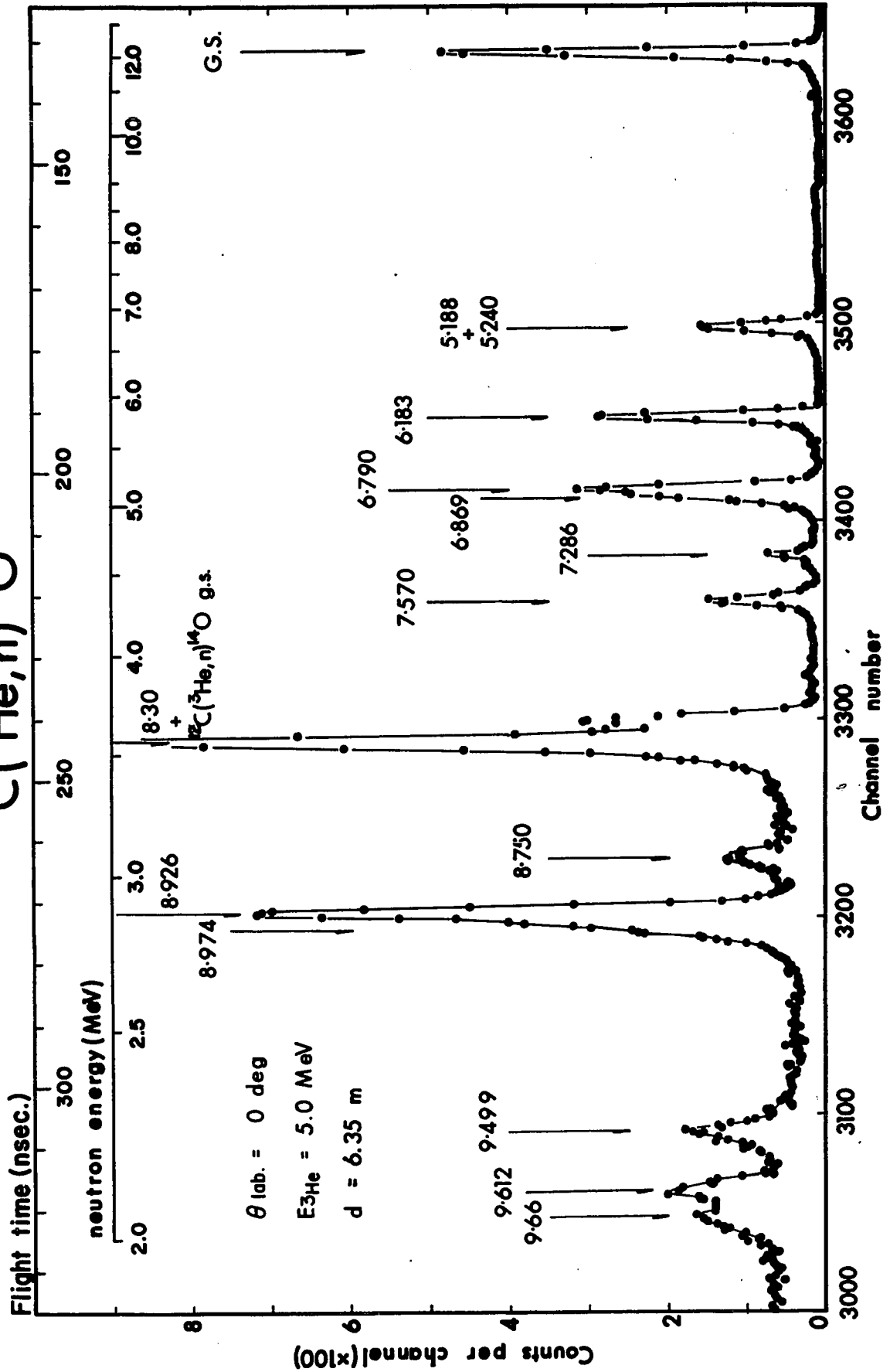
Among these reactions the $(^3\text{He}, n)$ reaction has the highest ground state Q value. With the accuracy of today's low energy machines, this implies more information can be obtained for the higher excited states of ^{15}O through this reaction. However, compared with other reactions detailed studies on this reaction are rather scarce (DI 65, DE 64B, DU 63, JO 61). The levels studied by these previous authors were restricted to those neutron groups leading to the ground and 6.18 MeV states only. In the present work excited states up to 9.611 MeV in ^{15}O were observed, and for most of the states observed angular distributions were also studied.

2. The Energy Levels and Their Excitation Curves

A typical neutron time-of-flight spectrum is shown in Figure 30. This spectrum was obtained at $\theta_{\text{lab}} = 0^\circ$ with a neutron flight path of 6.35 meters, and a ^3He bombarding

Figure 30. A neutron time-of-flight spectrum for the $^{13}\text{C}(^3\text{He},n)^{15}\text{O}$ reaction at $E_{^3\text{He}} = 5.0$ MeV.

$^{13}\text{C}(^3\text{He},n)^{15}\text{O}$



energy of 5.0 MeV. The overall time resolution was ~ 1.2 nsec. For the $E_{3\text{He}} = 6.2$ MeV, the resolution was 0.9 nsec. Excitation energies were extracted from the measured Q values (Appendix II). Excitation energies for the observed states of ^{15}O together with the previously reported excitation energies are given in Table 7.

Table 7. Energy Levels of ^{15}O

$^{13}\text{C}(^3\text{He},n)^{15}\text{O}$	Q(MeV)	Error (KeV)	Excitation (MeV)	Ajzenberg ^{a)} (MeV)	Warburton ^{b)} (MeV)	Evans ^{c)} (MeV)		
	7.123	3* 7†	0.0		0.0	0.0		
(1.891)	3	7	5.232	8	5.18	5.188 ± 6.0		
					5.24	5.240 ± 1.3		
	0.940	2	6	6.183	7	6.16	6.180 ± 4.0	
	0.333	2	6	6.790	7	6.79	6.789 ± 6.5	
	0.254	2	6	6.869	7	6.85	6.857 ± 3.2	
	-0.163	1	6	7.286	6	7.16	7.284 ± 7.0	
	-0.447	3	6	7.570	8	7.55	7.550 ± 2.2	
	-1.187	7	8	8.310	12	8.28	8.283 ± 3.0	8.283
	-1.628	2	5	8.750	7	8.74	8.735 ± 6.0	8.75
	-1.804	1	5	8.926	6	8.92	8.915 ± 3.0	8.915
	-1.851	3	6	8.974	8	8.98	8.980 ± 3.0	8.972
	-2.376	2	5	9.498	7	9.49		
	-2.489	1	5	9.612	6	9.53		
	-2.543	1	5	9.665	6	9.60		

a) AJ 62,

b) WA 65A,

c) EV 66.

* The weighted standard deviations from the mean.

† Overall uncertainty.

Disagreements with the tabulation of Warburton et al. (WA 65A) in excitation energies were found for some levels. The present work unlike the γ -ray measurements, includes internal errors such as uncertainties in the target thickness, bombarding energies, and especially the surface condition of the target. However, the good agreement with the Q-value calculated from the mass tables to the ground state Q-value of the present measurements has indicated that this is not the reason for the disagreement. Examination of all spectra obtained for this reaction shows no evidence of the previously reported level at 7.17 MeV (HE 59). Instead, in agreement with the result of Warburton et al. (WA 65A) a level at 7.286 MeV was observed. The 8.283 MeV level was obscured in most spectra by a peak corresponding to neutrons leading to the ^{14}O ground state, from the reaction $^{12}\text{C}(^3\text{He},n)^{14}\text{O}$. An interesting feature of the spectrum is that all the known levels of ^{15}O are almost equally populated by this reaction.

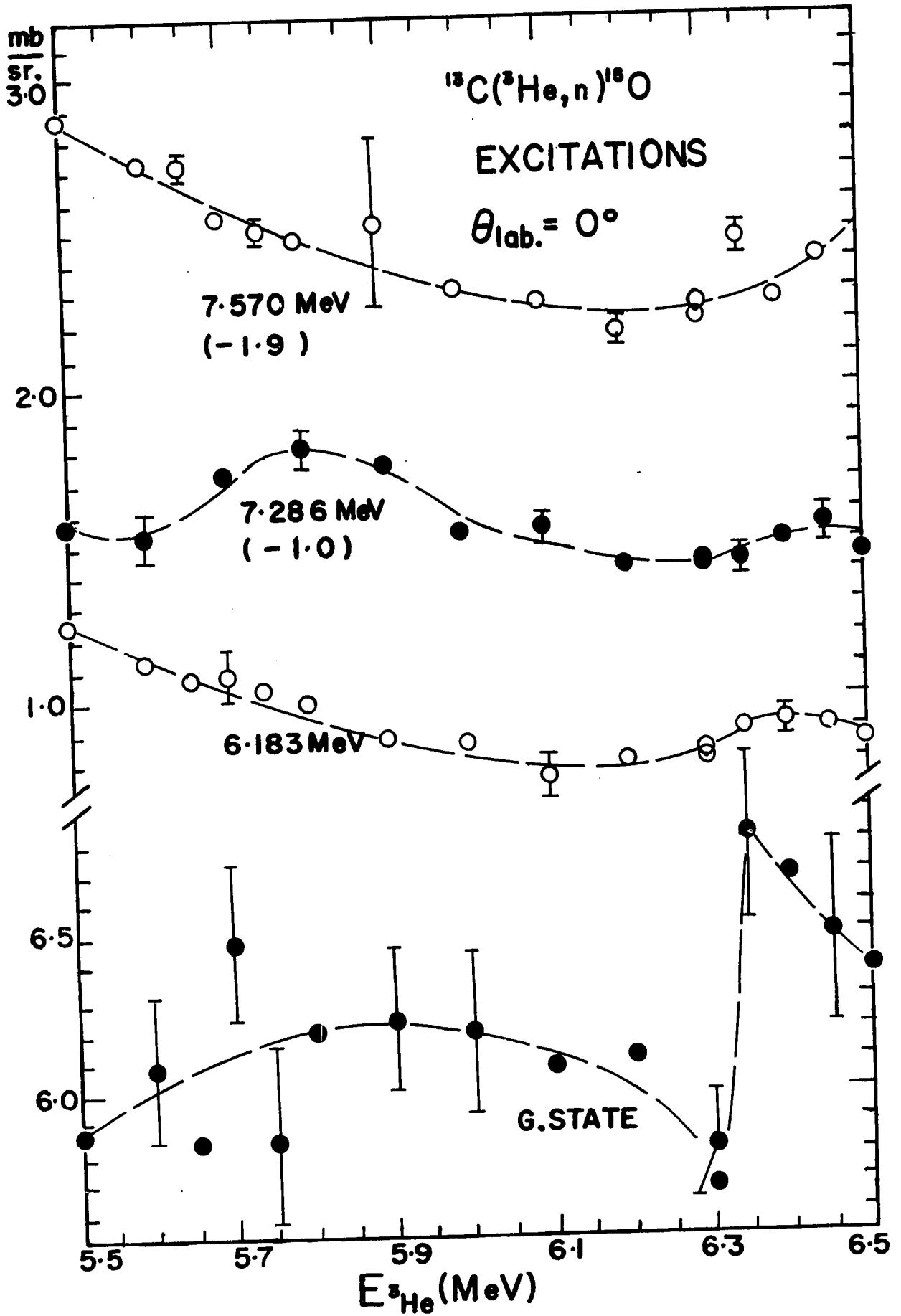
Excitation curves were measured at 0 degrees with respect to the ^3He beam, for ^3He bombarding energies between 5.5 and 6.5 MeV. The excitation curves including the ground state, 6.183, 7.286, 7.570, 8.750, 9.498, 9.612 and 9.665 MeV are presented in figures 31 and 32.

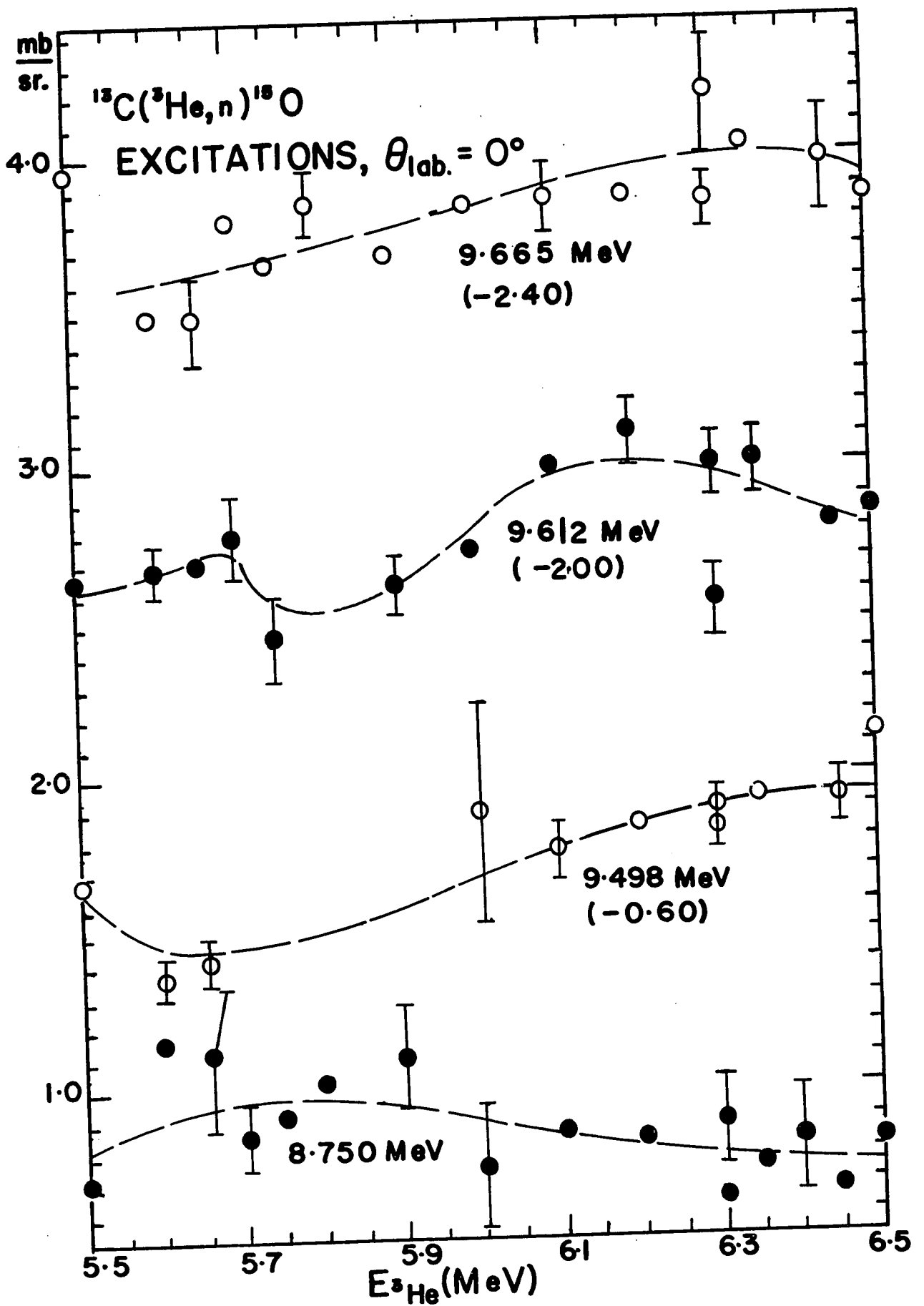
The excitation curves of the unresolved states 5.188 MeV + 5.240 MeV, 6.79 + 6.87 MeV and 8.926 MeV + 8.974 MeV are presented in figure 33. The curves in figures 31, 32 and 33 were drawn for reading convenience. Obviously the excitation curves have some structure. The present excitation curves

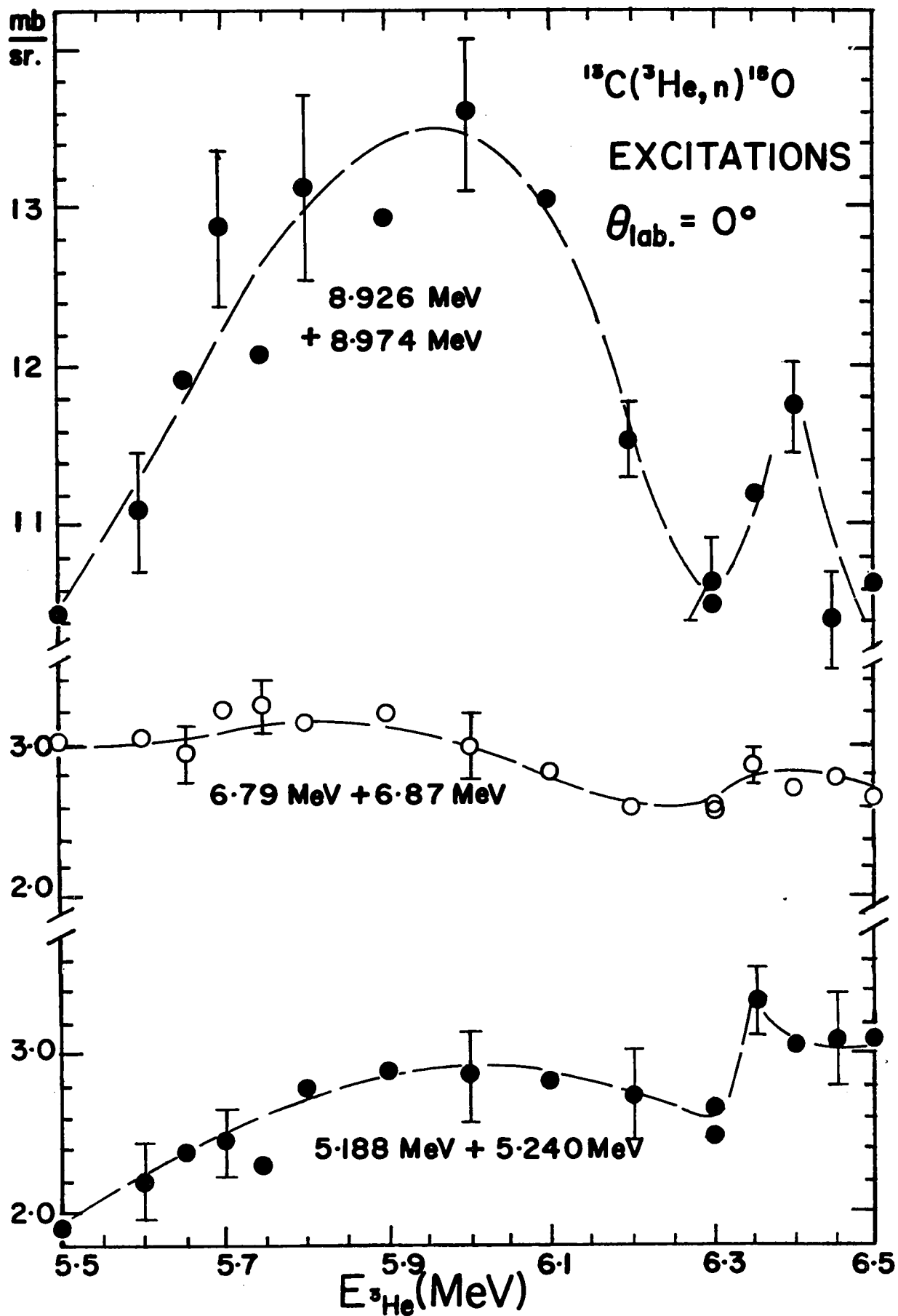
Figure 31. The neutron yield of $^{13}\text{C}(^3\text{He},n)^{15}\text{O}$ at $\theta_{\text{lab}} = 0^\circ$ leading to 0.0, 6.183, 7.286 and 7.570 MeV levels.

Figure 32. The neutron yield of $^{13}\text{C}(^3\text{He},n)^{15}\text{O}$ at $\theta_{\text{lab}} = 0^\circ$ leading to 8.75, 9.498, 9.612, and 9.665 MeV levels.

Figure 33. The neutron yield of $^{13}\text{C}(^3\text{He},n)^{15}\text{O}$ at $\theta_{\text{lab}} = 0^\circ$ leading to unresolved levels (8.926 + 8.974, 6.79 + 6.87 and 5.188 + 5.240 MeV).







and the ground state excitation curve of Din et al. (DI 65) were used to select the ^3He energies of 5.0 and 6.2 MeV at which the angular distributions were to be studied.

3. Analysis of the $^{13}\text{C}(^3\text{He},n)^{15}\text{O}$ and $^{12}\text{C}(^3\text{He},n)^{14}\text{O}$ Results

The fact that the spin and parity of the ^{12}C ground state is $\frac{1}{2}^-$ means that only one L value can play a role in the cross section for the $^{13}\text{C}(^3\text{He},n)^{15}\text{O}$ reaction. Formula (3-1) of the simplified PWBA is therefore reduced further to

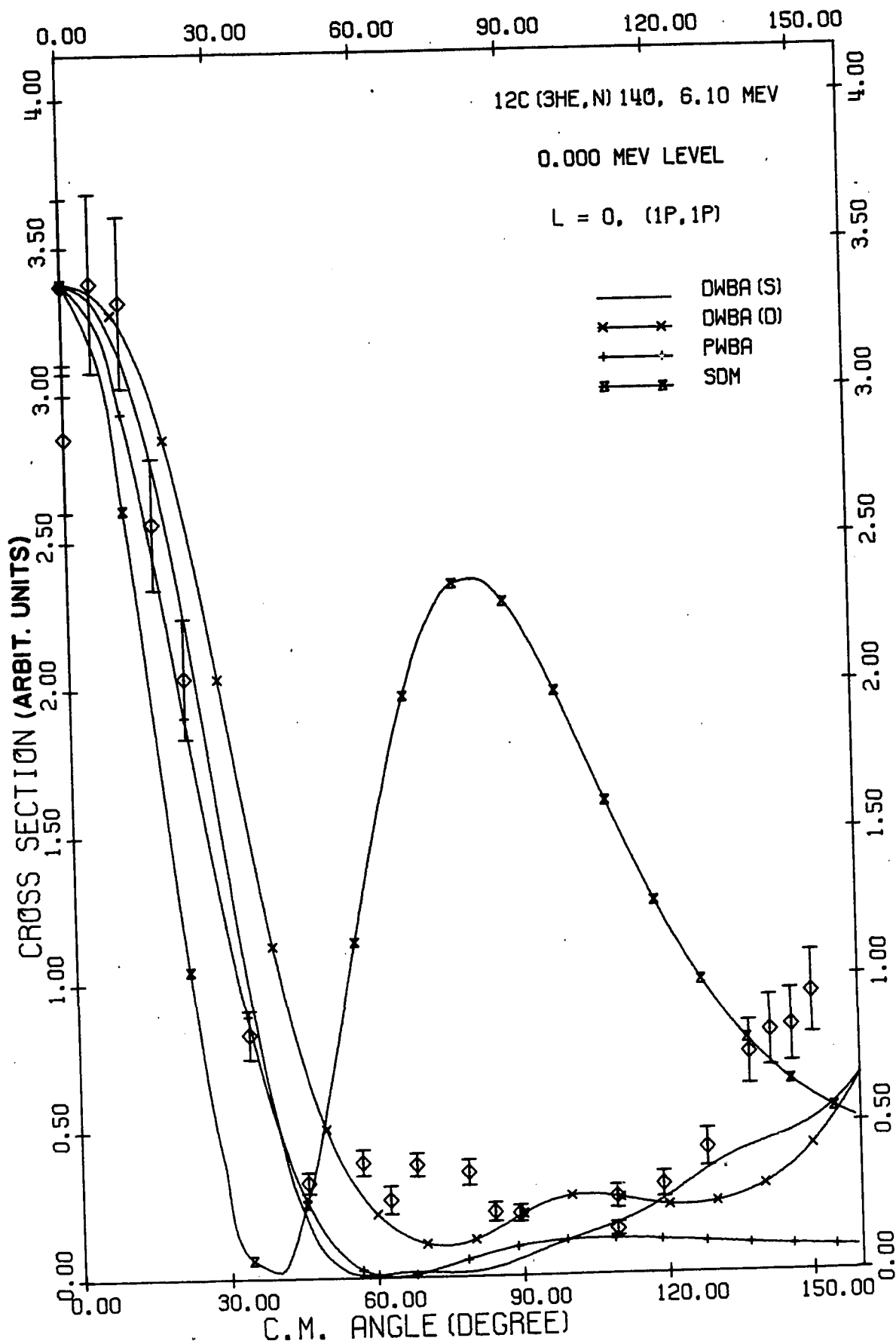
$$\frac{d\sigma(\theta)}{d\Omega} \sim \exp\left(-\frac{K^2\mu^2}{4}\right) j_L^2(kr_0) \quad (4-1).$$

This simplification is also true for the $^{12}\text{C}(^3\text{He},n)^{14}\text{O}$ ground state transition, where both ground state of ^{12}C and ^{14}O have $J^\pi = 0^+$, and thus only a pure $L = 0$ transfer is possible. A value $\mu = 5.0$ fms was used for all calculations (similar to that used for $^{11}\text{B}(^3\text{He},n)^{13}\text{N}$) involving the $^{13}\text{C}(^3\text{He},n)^{15}\text{O}$ reactions and also for the $^{12}\text{C}(^3\text{He},n)^{14}\text{O}$ reaction leading to the ground state of ^{14}O . A value of $r_0 = 5.0$ fms was used for the $^{13}\text{C}(^3\text{He},n)^{15}\text{O}$ calculations, and a value $r_0 = 4.7$ fms was used for the $^{12}\text{C}(^3\text{He},n)^{14}\text{O}$ calculations.

Diffraction model calculations were carried out for the $^{12}\text{C}(^3\text{He},n)^{14}\text{O}$ and the $^{13}\text{C}(^3\text{He},n)^{15}\text{O}$ reactions (cf. Chapter 3 for details). Similar radii to those used in PWBA calculations were also used for the simple diffraction model calculations.

For the DWBA calculations, all incident channel parameters listed in Table 4 were tried in the calculations. Rosen's parameters (RO 66) were used for exit channel parameters. It can be seen from figure 34 that for the

Figure 34. Angular distribution of the neutrons leading to the ground state of ^{14}O for $E_{^3\text{He}} = 6.1$ MeV. $L = 0$ was assumed for all calculations. DWBA(S) and DWBA(D) indicate results of shallow well potentials and deep well potentials respectively. PWBA and SDM indicate calculations of plane wave and diffraction model respectively. (See text for detail of parameters used)



$^{12}\text{C}(^3\text{He},n)^{14}\text{O}$ reaction, better agreement to the experimental data was obtained with the 'shallow potential' (set I of Table 4) than with the 'deep potential' (set VII of Table 4). This was true also for the $^{13}\text{C}(^3\text{He},n)^{15}\text{O}$ cases.

A slight adjustment to the parameters was made and the following parameters were finally adapted for both the 6.2 MeV and the 5.0 MeV $^{13}\text{C}(^3\text{He},n)^{15}\text{O}$ calculations. The final parameters were then,

$$V = 69.0 \text{ MeV}, W = 56.0 \text{ MeV}, \alpha = 0.7 \text{ fm}, \text{ and } r_0 = 1.61 \text{ fm}.$$

All calculated results together with the experimental results are presented in figures 35 to 57.

Shown in Table 8 is a summary of the L values from the present DWBA calculations and the possible spin and parity assignments to the corresponding levels. Also shown is the previous known assignments (WA 65A, EV 66).

Listed in Table 9 are parameters used in HF calculations. Calculated results are shown together with the measured cross sections in figures 35 to 57. As in the case of the $^{11}\text{B}(^3\text{He},n)^{13}\text{N}$ the HF calculation shows a tendency to overestimate the CN cross sections for $^{13}\text{C}(^3\text{He},n)^{15}\text{O}$. The overestimations were enhanced especially in $E_{^3\text{He}} = 5 \text{ MeV}$ cases.

Table 8. L values for $^{13}\text{C}(^3\text{He},n)^{15}\text{O}$

Excitation	L	J^π	
		Present	Warburton* Evans [†]
0.0	0	$\frac{1}{2}^-$	$\frac{1}{2}^-$
5.188	1	$\frac{1}{2}^+, \frac{3}{2}^+$	$\frac{1}{2}^+$
5.240			$\frac{5}{2}$ $\frac{5}{2}^+$
6.183	(2)	$(\frac{3}{2}^-, \frac{5}{2}^-)$	$\frac{3}{2}^-$
6.790	1	$\frac{3}{2}^+, \frac{1}{2}^+$	$\frac{3}{2}^+$
6.869	(2)	$(\frac{3}{2}^-, \frac{5}{2}^-)$	$\frac{3}{2}, \frac{5}{2}$
7.286	3	$\frac{7}{2}^+, \frac{5}{2}^+$	$\frac{9}{2}$ $\frac{7}{2}^+$
7.570	1	$\frac{1}{2}^+, \frac{3}{2}^+$	$\frac{1}{2}^+$
8.310			$\frac{3}{2}^+$
8.750	1	$\frac{1}{2}^+, \frac{3}{2}^+$	$\frac{1}{2}^+$
8.926	0	$\frac{1}{2}^-$	$\frac{3}{2}^+$
8.974	0	$\frac{1}{2}^-$	$\frac{3}{2}^-$ $\frac{3}{2}^-, \frac{1}{2}^-$
9.498	2	$\frac{3}{2}^-, \frac{5}{2}^-$	$\frac{1}{2}^+$
9.612	2	$\frac{3}{2}^-, \frac{5}{2}^-$	
9.665	(0)	$(\frac{1}{2}^-)$	

*WA 65A, †EV 66.

Table 9. Parameters used for $^{13}\text{C}(^3\text{He},n)^{15}\text{O}$ HF calculations.

Channel	V	W	α_V	α_W	r_O	r_W	E_{beg}	a	b	γ
p- $^{15}\text{N}^*$	34	22	0.65	0.50	1.25	1.25	5.3	-1.188	0.781	1.0
d- $^{14}\text{N}^{**}$	76.7	20	0.73	0.73	1.3	1.3	4.9	-3.404	1.754	1.0
t- $^{13}\text{N}^{*\dagger}$	220	23.8	0.53	0.99	1.22	1.8	7.6	-1.038	0.547	1.0
α - $^{12}\text{C}^{\dagger*}$	110	5	0.68	0.68	1.4	1.3	6.0	-1.979	1.053	1.0
$^{13}\text{C}^{\dagger}$	69	56	0.7	0.7	1.61	1.61	4.3	-1.901	0.667	1.0
$^{15}\text{O}^{\dagger\dagger}$	46.7	5.75	0.65	0.7	1.25	1.25	5.3	-1.237	0.763	1.0

* (BJ 59); ** (MU 67); *† (FL 68); †* (DE 64C);
 †, †† similar potentials used for DWBA calculations.

4. The Levels of ^{15}O

1. The ground state.

The ground state of ^{15}O has been studied by means of the $(^3\text{He},n)$ reaction by many authors. Dugan et al. (DU 63) with ^3He energies from 1.6 to 2.7 MeV studied the excitation curves at $\theta_{\text{lab}} = 0^\circ$ and 90° . They also measured a neutron angular distribution at $E_{^3\text{He}} = 2.66$ MeV. Three angular distributions at ^3He energies 2.6, 2.8, and 3.1 MeV were also given by Johnson et al. (JO 61). Din et al. (DI 65) using the proton recoil technique made a most careful measurement of this state. They measured the excitation curves at 0° , 90° and 150° , with bombarding energies ranging from 1.4 to 5.8 MeV. Twelve angular distributions were taken within this region of bombarding energies.

The excitation curves for this state up to 5.8 MeV seem to consist of many resonances. This would indicate that the reaction mechanism is complicated in this energy region.

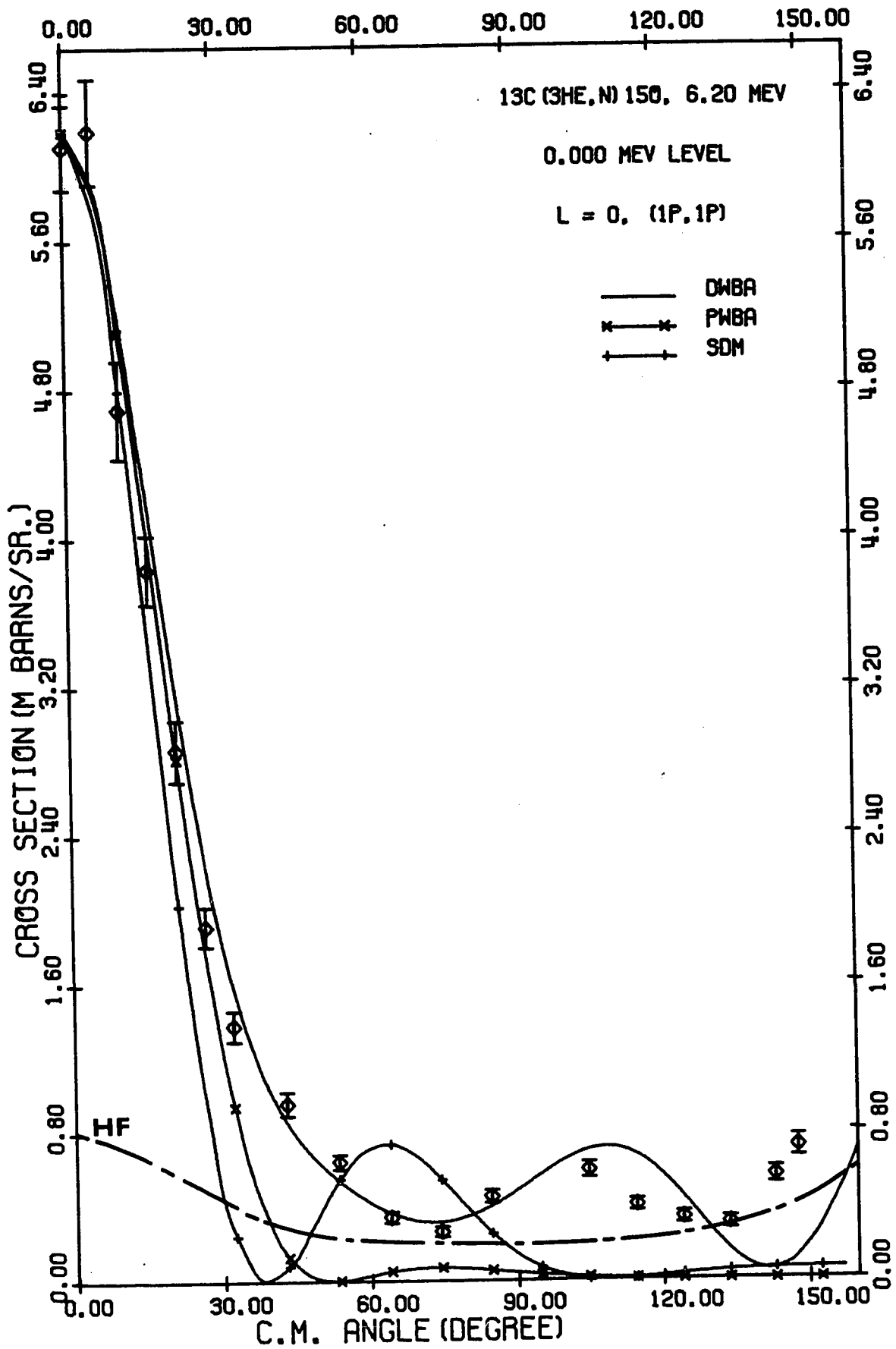
However, the excitation curve of Deshpande et al. (DE 64B) at $\theta_{\text{lab}} = 10^\circ$ indicated that there is little structure from ^3He energies 7.5 to 11.0 MeV. The excitation curve from the present work is an extension of the results of Din et al. to 6.5 MeV. The curve obtained is rather flat, however, some structures can still be seen in it. The angular distributions measured at bombarding energies at 5.0 and 6.2 MeV together with the three theoretical predictions are presented in figures 35 and 36. The (1p,1p) configuration was used for the DWBA calculations. Except for some disagreements at backward angles good agreement was obtained for the DWBA calculations. In view of the structures in the excitation curves, the good agreement to the DWBA calculations may indicate that if some of the sharp "resonances" can be avoided the reaction leading to this particular level is still predominantly direct. Although the HF calculations overestimate the CN cross sections, as shown in figures 35 and 36 the contribution from the CN formation is insignificant compared to that of DI.

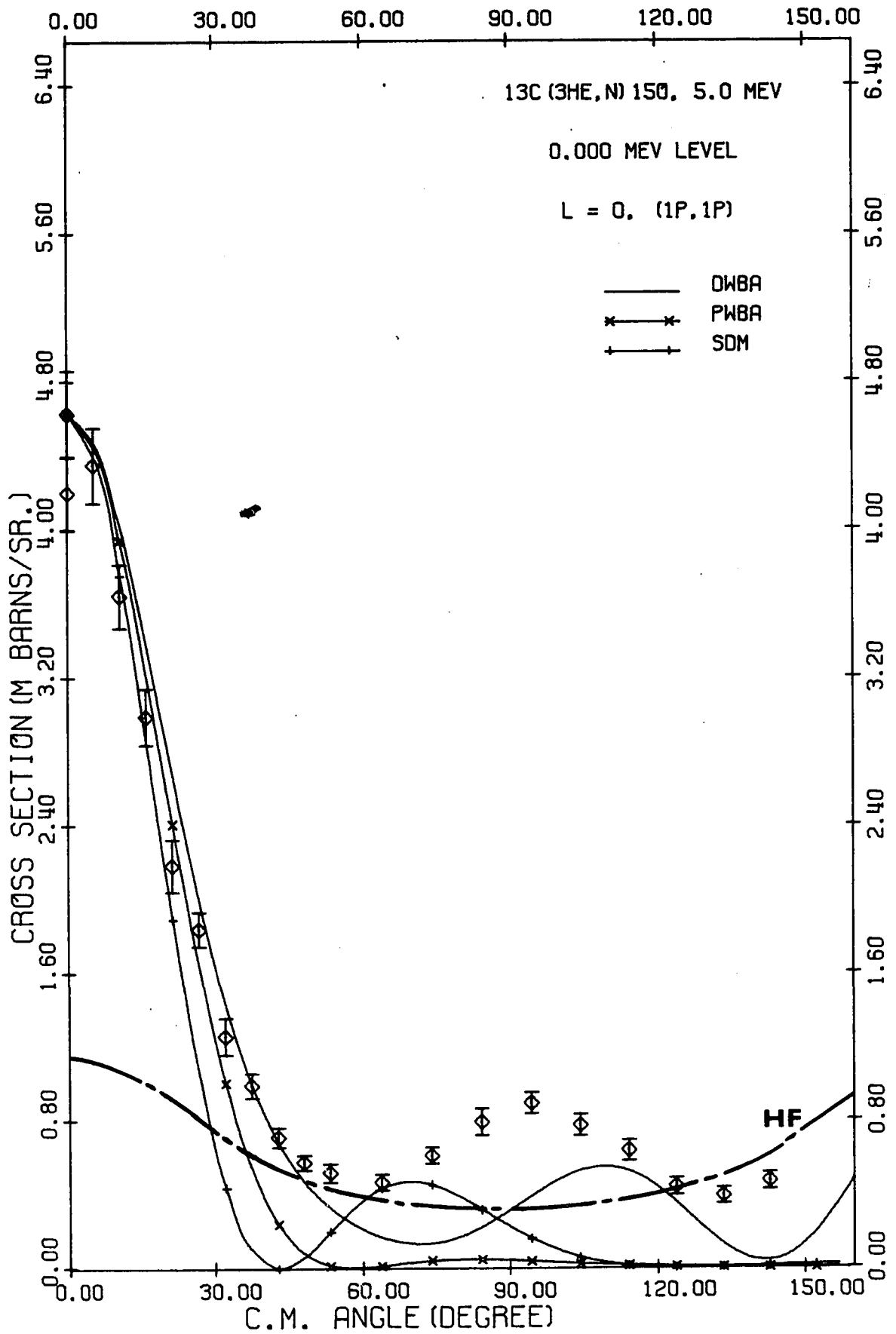
2. The 5.188 and 5.24 MeV Level (Unresolved)

In the present measurements these levels were unresolved except at angles of more than 110° . No attempts were made to determine the separate Q values for each level. The centroids of the peaks from the doublets were taken in the Q-value determinations. An average value of 5.232 MeV was used for the excitation energy of these two levels. The value 5.188 MeV and 5.240 MeV were taken from the work of Warburton et al. (WA 65A) who have measured the excitation energies of these levels using a Ge(Li) detector.

Figure 35. Angular distribution of the neutrons leading to the ground state of ^{15}O for $E_{3\text{He}} = 6.20$ MeV. See text for parameters used for DWBA calculation. $r_0 = 5$ fms, $\mu = 5$ fms were used for the plane wave Born approximation (PWBA) calculations. $r_0 = 5$ fms was also used for the simple diffraction model (SDM) calculations.

Figure 36. Angular distribution of the neutrons leading to the ground state of ^{15}O for $E_{3\text{He}} = 5.0$ MeV. (See also caption under figure 35).





The 5.188 and 5.240 MeV levels are known to have $J^\pi = \frac{1}{2}^+$ and $\frac{5}{2}^+$ respectively (WA 65A, HA 57B, GA 66). Bizzetti et al. (BI 67) have measured the life time of the 5.240 MeV level by Doppler-shift methods using a Ge(Li) detector. Their results also favored a $\frac{5}{2}^+$ assignment.

The selection rules for the present reaction restrict the L Values for transitions to these levels to 1 and 3 respectively. Figures 37 and 38 of the present results indicate that there is an L = 1 transition component in it, and also possibly there is a large contribution from transitions with $L > 2$. No attempts were made to fit the data. However, to show the L = 1 and 3 distributions, separate DWBA calculations with L = 1 (lp,2s) and L = 3 (lp,ld) were made, and are shown in figure 38. Comparing the measured cross sections to the HF cross section one notices that the compound formation to these levels is not negligible.

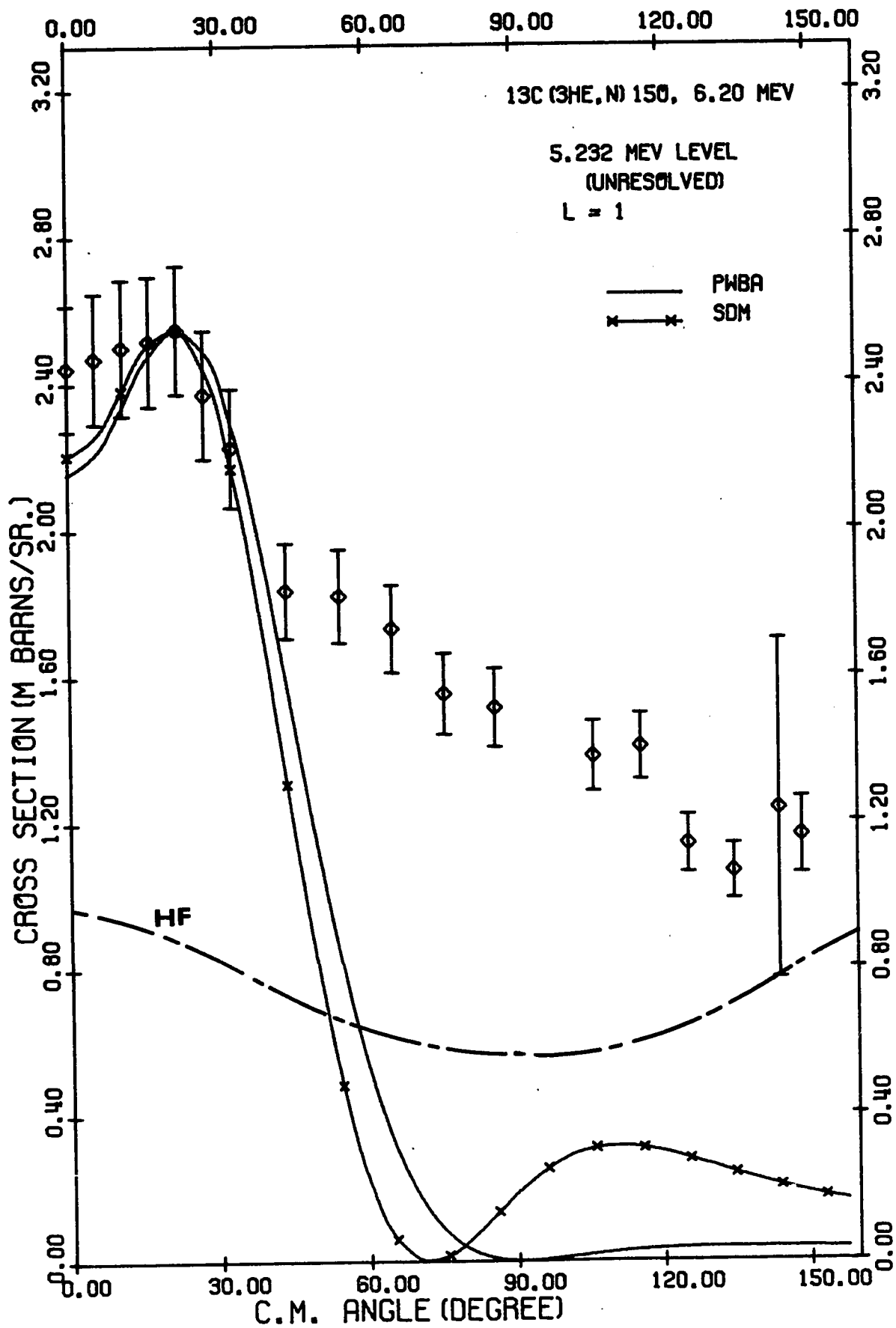
If the configuration of the 5.240 MeV level is as simple as predicted by Halbert et al. (HA 57B), then the (d,n) reaction should yield a good spectroscopic factor. However, the (d,n) results published to date are confined to low bombarding energies or have poor time resolutions (MU 67, LO 66, EL 60) and yield no additional information on these two levels. The present system could be used to resolve those two levels by (d,n) reaction.

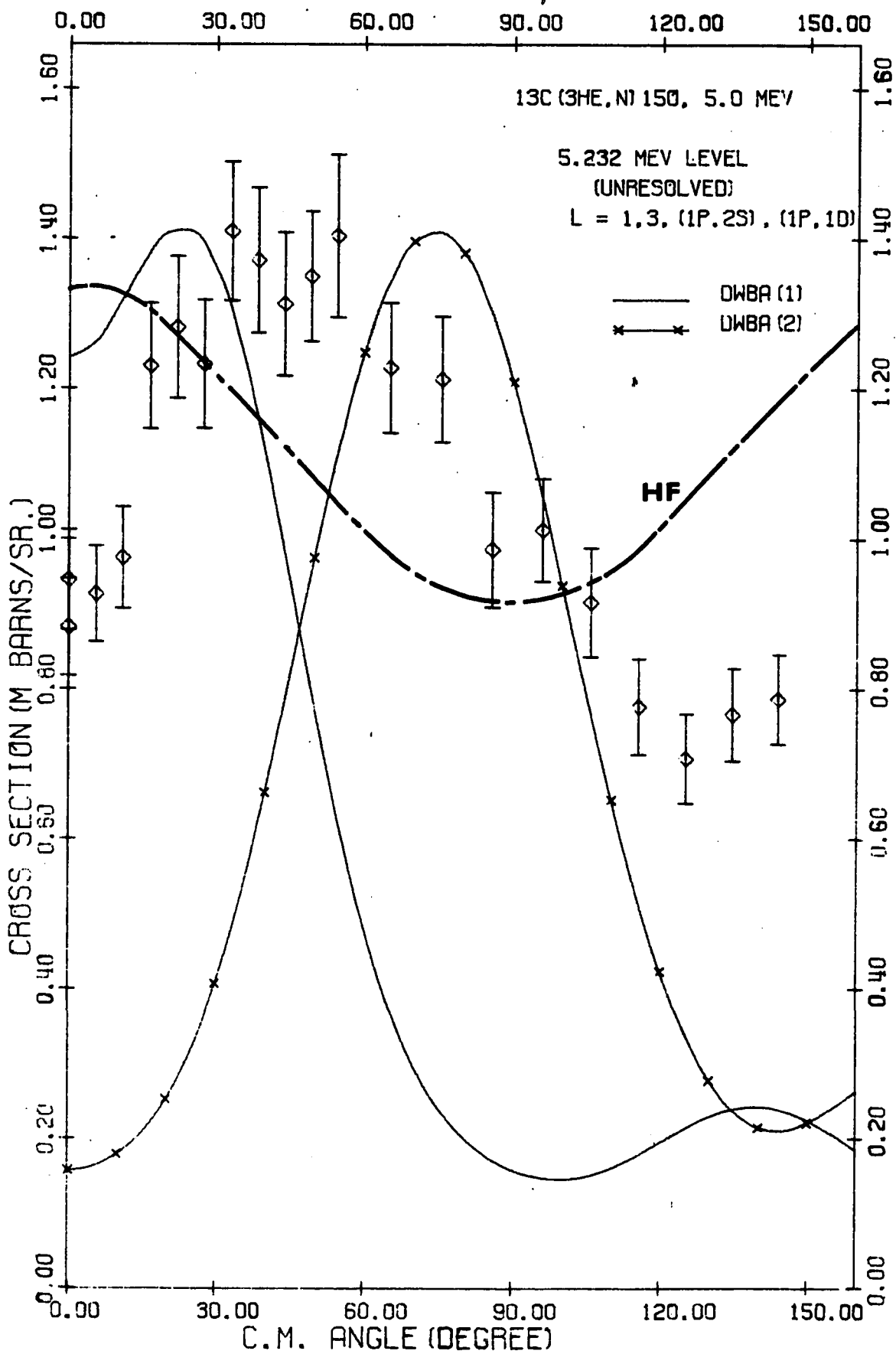
3. The 6.183 MeV level

Lane (LA 60) had shown from shell model calculations that there is only one normal (lp)¹¹ configuration state expected in this energy region for mass 15 nuclei.

Figure 37. Angular distribution of neutrons leading to the unresolved 5.188 and 5.240 MeV levels of ^{15}O for $E_{3\text{He}} = 6.2$ MeV. The HF calculations are the sum of those two levels. (See also caption under figure 35).

Figure 38. Angular distribution of neutrons leading to the 5.188 + 5.240 MeV levels of ^{15}O for $E_{3\text{He}} = 5.0$ MeV. DWBA(1) and DWBA(2) indicate results of $L = 1$ with configuration (1p,2s) and $L = 3$ with configuration (1p,1d) respectively. The HF calculations are the sum of these two levels.





Povh et al. (PO 59) from γ -ray measurements assigned the 6.183 MeV state a spin of $\frac{3}{2}$ and assumed the parity to be negative. This was in agreement with the previous (d,n) measurements of Evans (EV 53) who assigned a spin less than $\frac{5}{2}$ and negative parity to this level.

Later experimental results were all in favor of the $\frac{3}{2}^-$ assignment to this level, especially those given by Warburton et al. (WA 65) whose $^{16}\text{O}(^3\text{He}, \alpha)^{15}\text{O}$ spectrum strongly indicated that this is a $p_{3/2}^-$ hole state, if the ground state of the ^{16}O nucleus is a pure s^4p^{12} closed shell state. (However, there are some doubts about this statement. A shell model calculation of Wong* indicated that the s^4p^{12} contribution to the ^{16}O ground state configuration is no more than 70%). Recently Gill et al. (GI 68) have studied this particular level using the reaction $^{16}\text{O}(^3\text{He}, \alpha\gamma)^{15}\text{O}$. They concluded that this state is a mixture of a single-hole state with two-particle configurations.

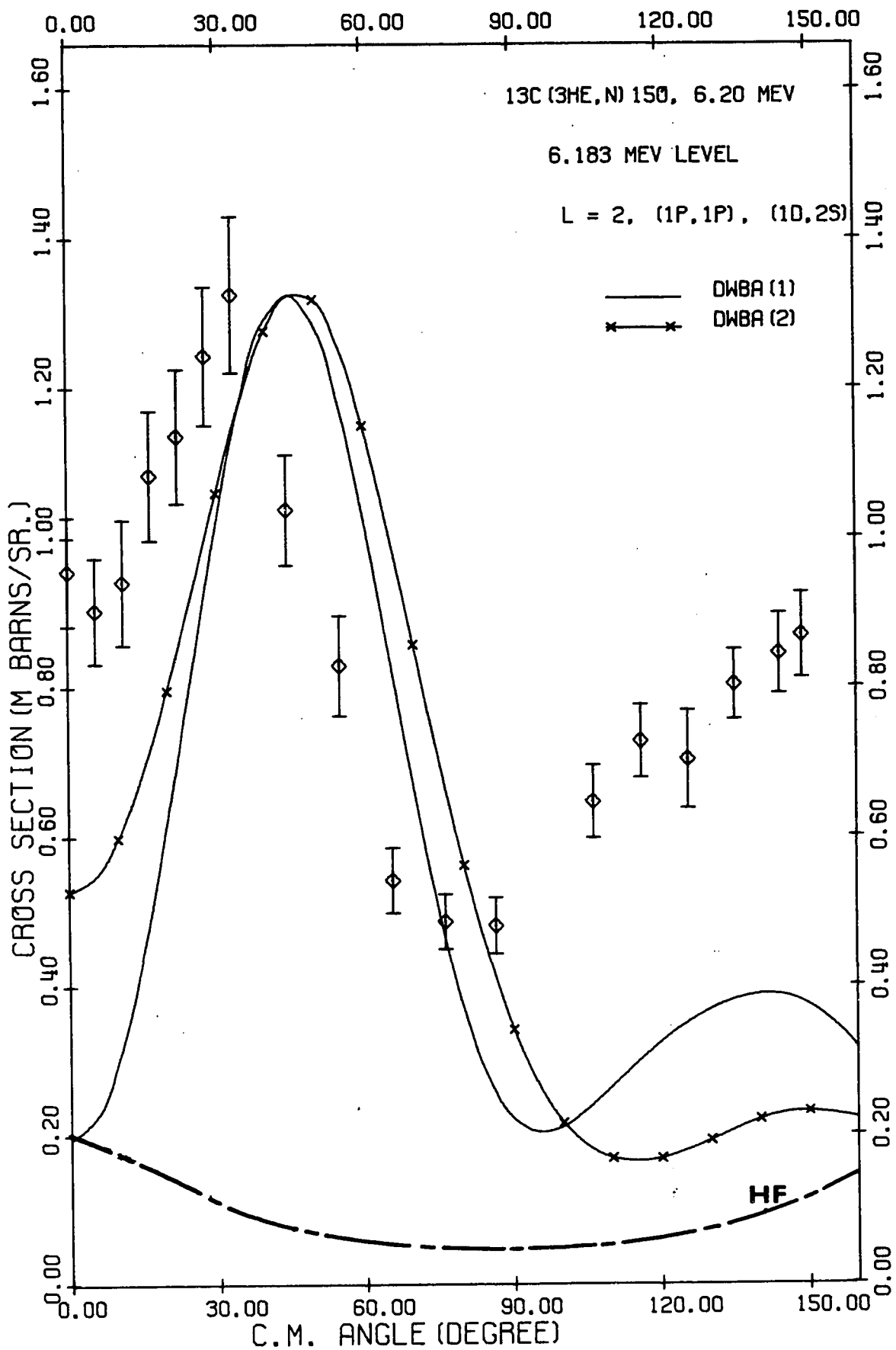
Judging from the excitation of Figure 31, which is flat and structureless for 6.183 MeV level, one might expect an angular distribution which is independent of energy. However, this is not the case.

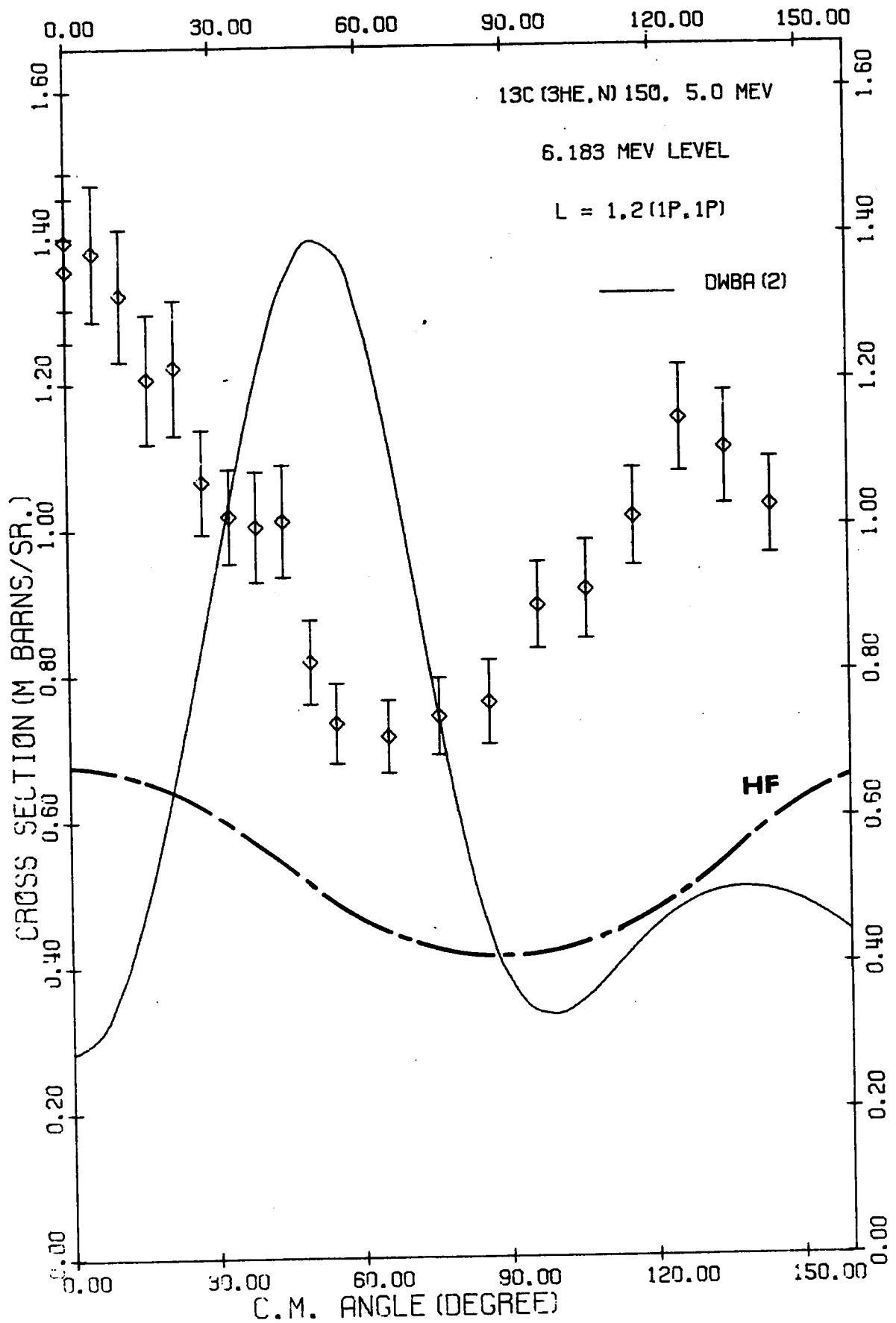
The angular distributions were strongly energy dependent (figures 39 and 40). By taking into consideration the HF cross sections, a reasonable fit to 6.2 MeV data was obtained, although the 5.0 MeV data has presented great difficulty for interpretation. One may assume that the interference term may play an important role in this case. More angular distri-

*S.S.M. Wong, private communication.

Figure 39. Angular distribution of neutrons leading to the 6.183 MeV level of ^{15}O for $E_{3\text{He}} = 6.2$ MeV. DWBA(1) and DWBA(2) represent results using (1p,1p) and (1d,2s) configurations respectively. $L = 2$ was assumed for both calculations. (See also caption under figure 35).

Figure 40. Angular distribution of neutrons leading to the 6.183 MeV level of ^{15}O for $E_{3\text{He}} = 5.0$ MeV. Only result of $L = 2$ with (1p,1p) configuration is presented for DWBA calculation. (See also caption under figure 35).





butions at other ^3He energies are needed to draw any conclusion about this level.

4. The 6.790 and 6.869 MeV levels

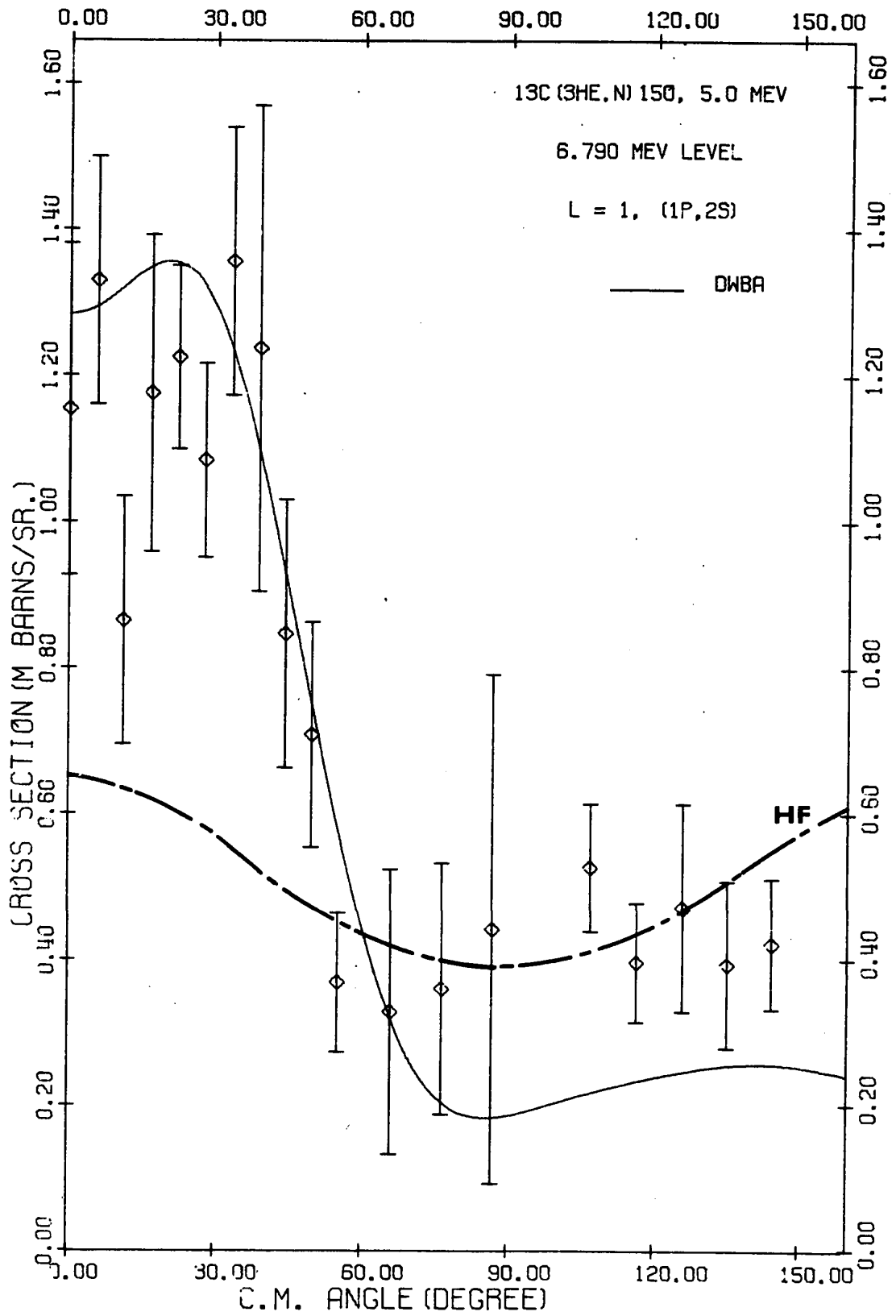
This pair of levels, in the present measurements were barely resolved in most of the 6.2 MeV data. However, they were resolved in the 5.0 MeV data. The large error bars indicated in figures 41 and 42 arise mostly from the peak fitting error. These two levels have been extensively studied by γ -ray measurements (WA 65A, GA 66, GO 66). The spins and parities are assigned as $\frac{3^+}{2}$ for the 6.790 MeV level and $\frac{3}{2}, (\frac{5}{2})$ for the 6.869 MeV level. The (d,n) measurement of Mubarakmand and Macefield (MU 67) also indicated that one of these levels (unresolved) should have an $L_p = 0$ transition and thus should have $J^\pi = \frac{3^+}{2}$.

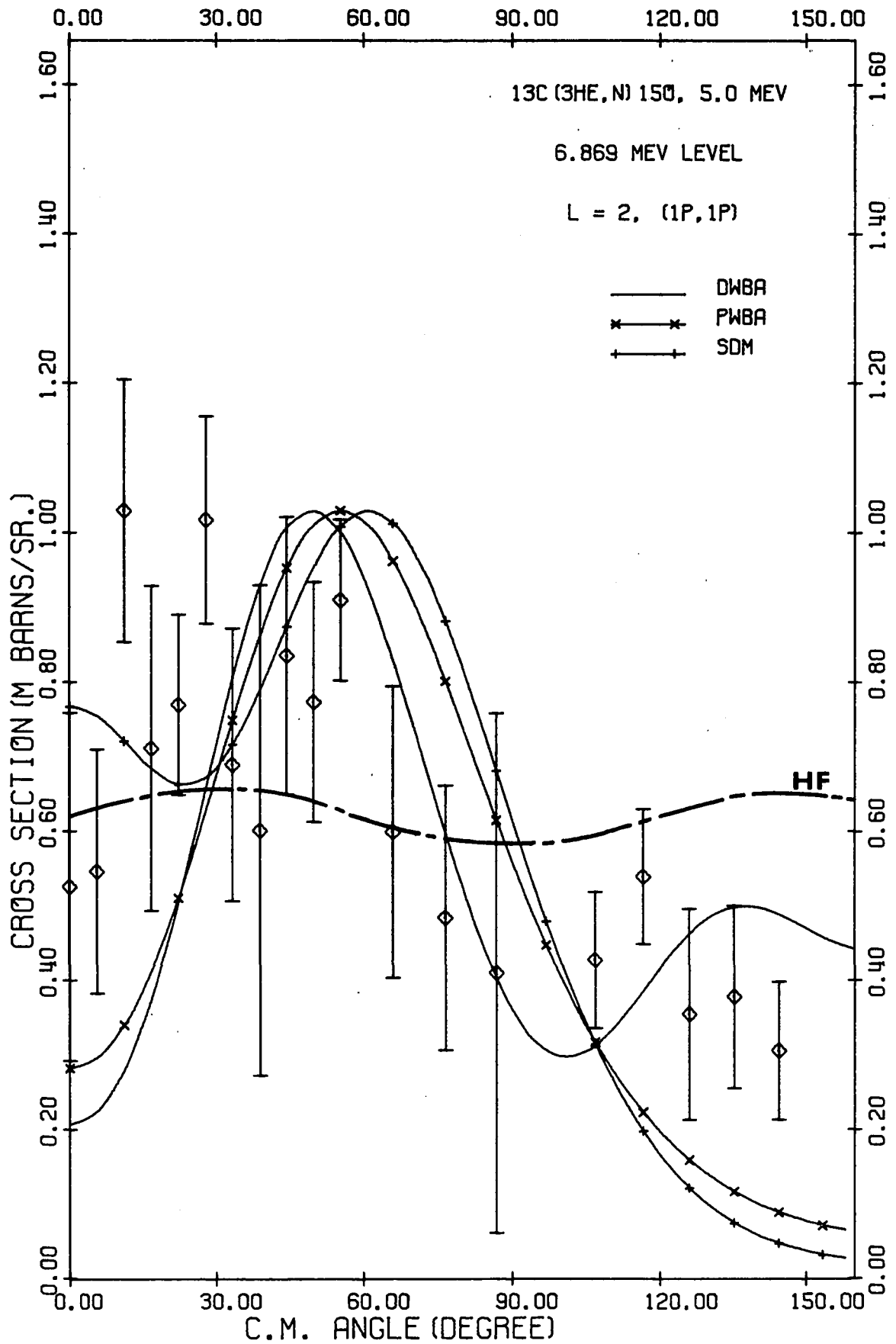
Halbert et al. (HA 57B) have predicted a composition of 85% $1s^4 1p^{10} 2s$ and 15% $1s^4 1p^{10} 1d$ for the 6.79 MeV $\frac{3^+}{2}$ level. As shown in figure 41, (1p,2s) DWBA gives a good fit to the data.

The measurement of Warburton et al. (WA 65A) indicated the 6.869 MeV level is a mirror level to the 7.15 MeV level of $^{15}\text{N}(\frac{5^+}{2})$. Although the data shown in figure 42 is in no way conclusive all calculations seem to favor an $L = 2$ transition. If this is the case, then the selection rule would rule out an even parity assignment for this level. The DWBA calculations also favored a (1p,1p) transition rather than a (1d,2s) transition. However this is in contradiction to Lane's calculation if one assumes the 6.183 MeV level as the pure normal configuration state (see subsection 3). Judging from the present neutron angular distributions one would assign a

Figure 41. Angular distribution of neutrons leading to 6.790 MeV level of ^{15}O for $E_{3\text{He}} = 5.0$ MeV. $L = 1$ was assumed for all calculations. (See also caption under figure 35).

Figure 42. Angular distribution of neutrons leading to 6.869 MeV level of ^{15}O for $E_{3\text{He}} = 5.0$ MeV. $L = 2$ was assumed for all calculations. (See also caption under figure 35).





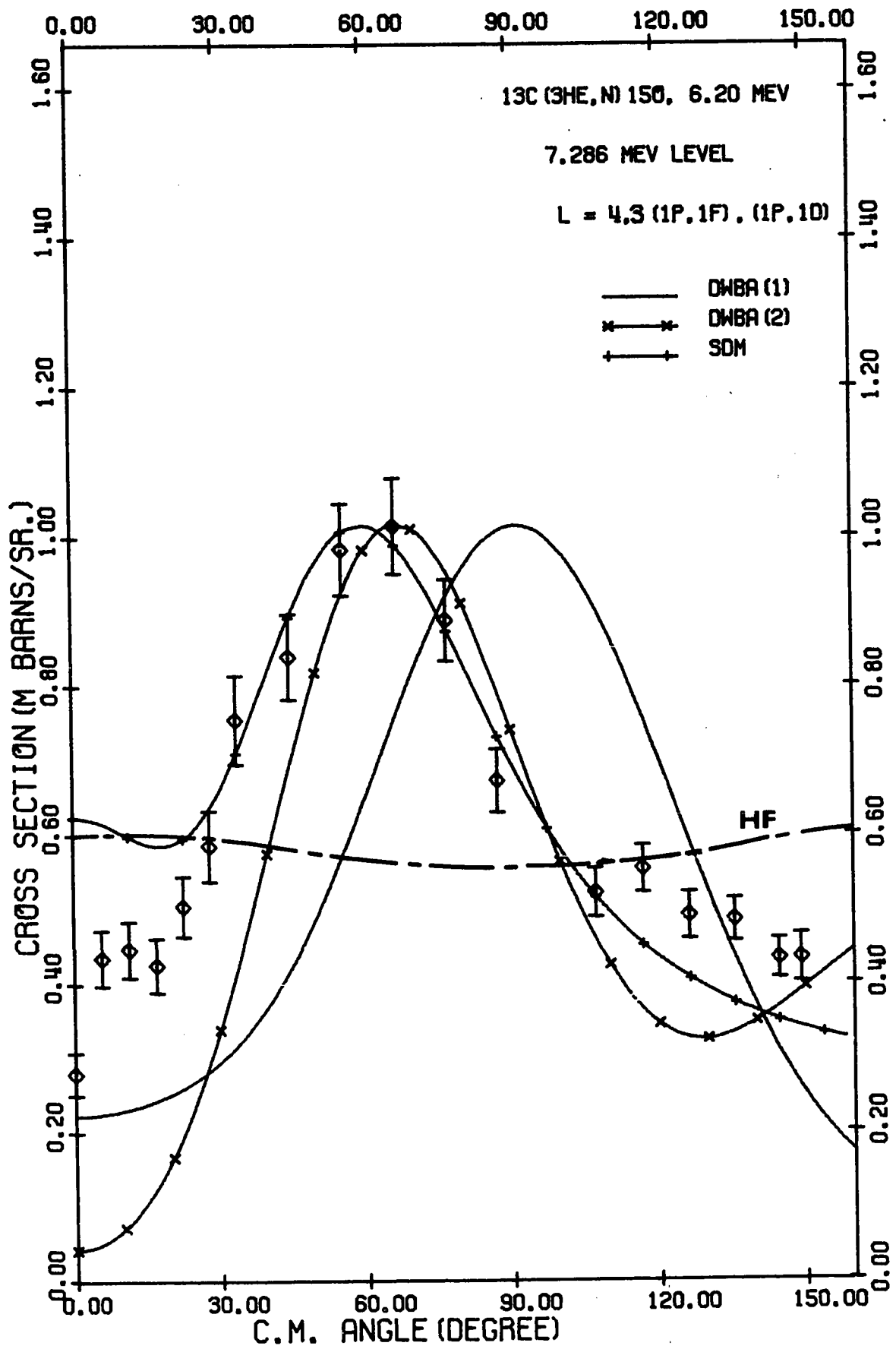
spin of $\frac{5}{2}$ or $\frac{3}{2}$ for this level.

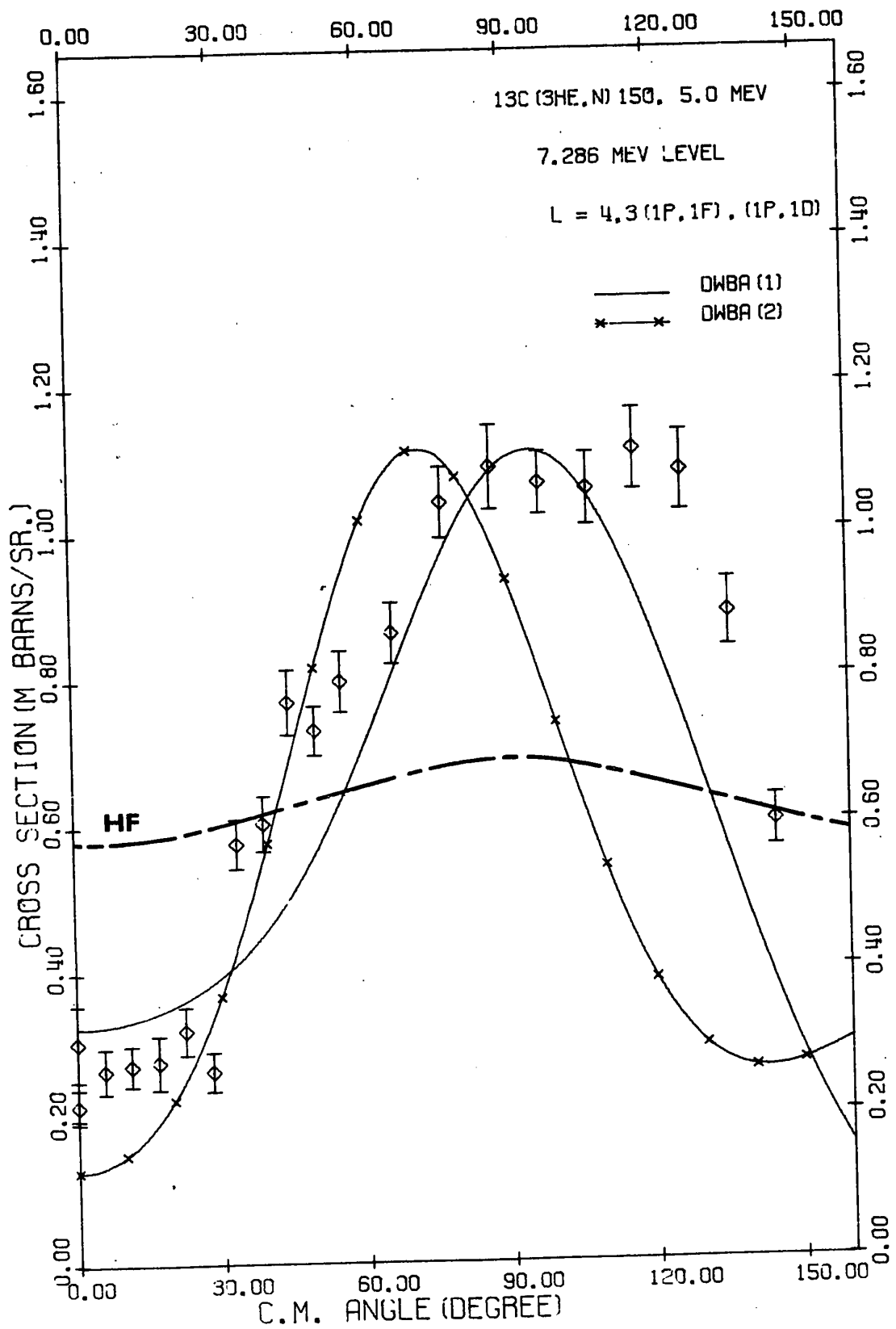
5. The 7.286 MeV level

A level at 7.16 MeV was reported by Hebbard and Povh (He 59) but later work of Warburton et al. (WA 65A) reported that there was no such level. Instead they found a level at excitation energy of 7.284 MeV. They also gave the possible spin for this new level as less than $\frac{9}{2}$. Mubarakrand and Macefield (MU 67) have measured this level by $^{14}\text{N}(d,n)^{15}\text{O}$ reaction. From the angular distributions they did obtain an excellent fit to their data with $\ell_p = 2$ transfer calculations, and thus a $\frac{7+}{2}$ assignment was given to this level. This level was then paired to the 7.56 MeV level of ^{15}N as its mirror level. The shell model calculation of Halbert and French (HA 57B) predicted the existence of a level consisting mainly of a $1s^4_1p^1_0_1d$ configuration at or near 6.39 MeV excitation for mass 15 nuclei. If this predicted level corresponds to the 7.286 MeV level of ^{15}O , then the selection rules allow only an $L = 3$ transition for the present transition. Various calculations together with the differential cross sections are shown in figures 43 and 44. The $E_{^3\text{He}} = 6.2$ MeV data indeed give a good fit to $(1p,1d)$ $L = 3$ DWBA calculation. The $L = 4$ SDM calculations also gives a good fit to the data, however, for such a high L value the results of the crude diffraction model are not to be trusted. The angular distribution at $E_{^3\text{He}} = 5.0$ MeV has a backward peaked distribution. The data did not differentiate between the $L = 3$ and $L = 4$ calculations. The above calculations lead one to assign the possible spin and parity

Figure 43. Angular distribution of neutrons leading to the 7.286 MeV level of ^{15}O for $E_{3\text{He}} = 6.2$ MeV. DWBA(1) and DWBA(2) represent calculations using $L = 4$ with (lp,lf) configuration and $L = 3$ with (lp,ld) configuration respectively. (See also caption under figure 35).

Figure 44. Angular distribution of neutrons leading to the 7.286 MeV level of ^{15}O for $E_{3\text{He}} = 5.0$ MeV. (See also caption under figure 35).





of this level as $\frac{5+}{2}$ or $\frac{7+}{2}$. This is in agreement with previous work (WA 65A, MU 67).

6. The 7.570 and 8.750 MeV level

Warburton et al. (WA 65A) and Evans et al. (EV 66) had paired the 7.570 MeV level to the mirror level of ^{15}N at 8.312 MeV leading to a spin and parity assignment of $\frac{1+}{2}$. The present ($^3\text{He},n$) reaction populates this level very weakly. The neutron angular distributions of figures 45 and 46 could not be explained by a direct reaction mechanism. It is therefore impossible to make any predictions for the spin and parity of this level from the present experimental evidence.

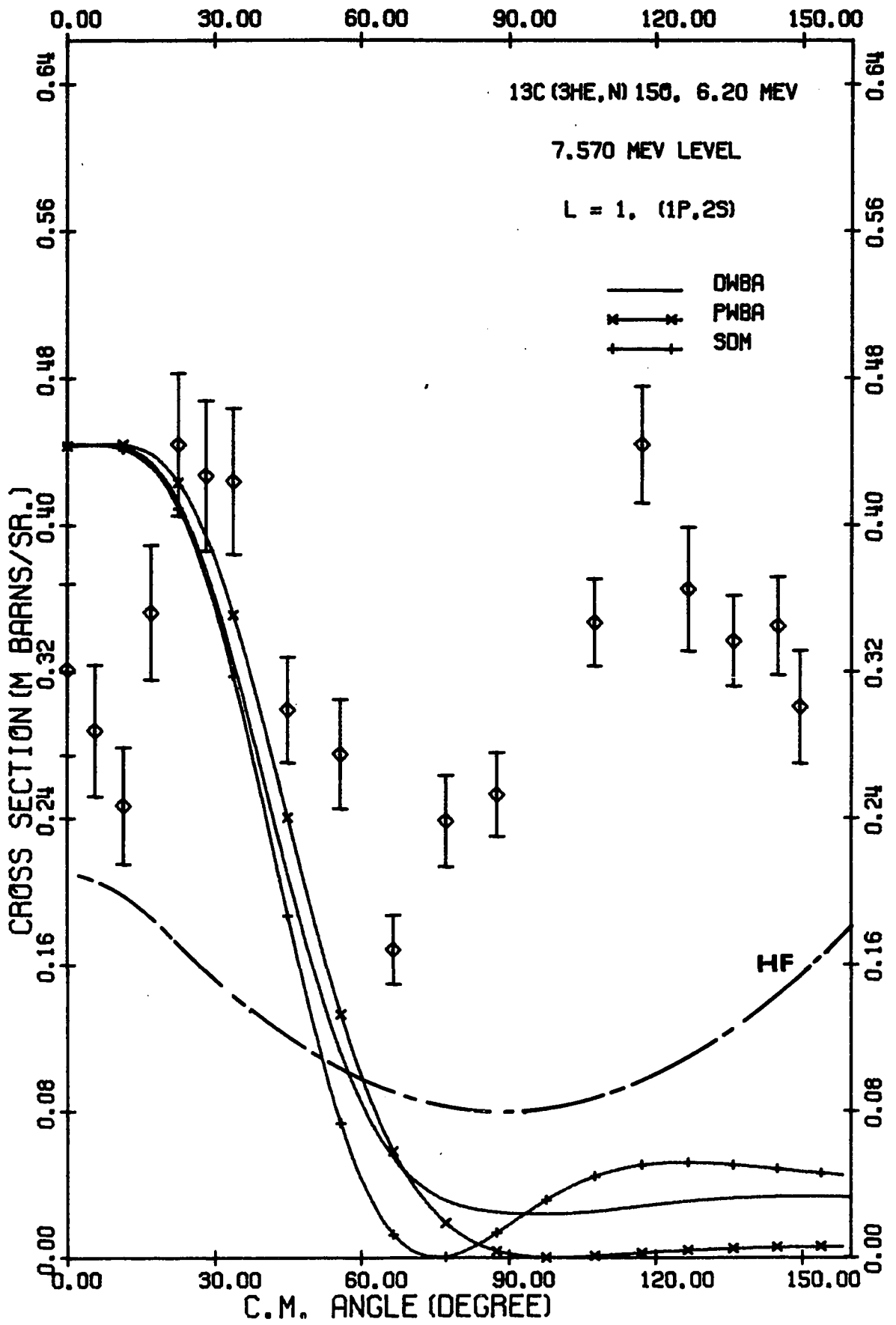
The 8.750 MeV level has been observed by proton elastic scattering on ^{14}N (HA 57A, GO 54, FE 59A), and by $^{14}\text{N}(p,\gamma)^{15}\text{O}$ (EV 66). All measurements have indicated this is a $\frac{1+}{2}$ level. The proton scattering of Hagedorn et al. (HA 57A) reported this level has a width of 34 ± 4 keV. Gove et al. (GO 54) also measured the proton scattering and have reported a level width of 53 keV. The present measurements confirm that this level has a large width but it was not possible to extract an accurate measurement of the width (see figure 30). The neutron angular distributions for this level are shown in figures 47 and 48. All calculations indicate that an $L = 1$ transition is involved, leading to an assignment for the spin and parity of this state of either $\frac{1+}{2}$ or $\frac{3+}{2}$.

7. 8.926 MeV and 8.974 MeV levels

Although in the present measurements these two levels were not well separated it was possible to extract angular

Figure 45. Angular distribution of neutrons leading to 7.570 MeV level of ^{15}O for $E_{3\text{He}} = 6.2$ MeV. $L = 1$ was assumed for all calculations. (See also caption under figure 35).

Figure 46. Angular distribution of neutrons leading to 7.570 MeV level of ^{15}O for $E_{3\text{He}} = 5.0$ MeV. DWBA(1) and DWBA (2) represent results of (1p,1d) and (1p,2s) configurations respectively. $L = 1$ was assumed for all calculations. (See also caption under figure 35).



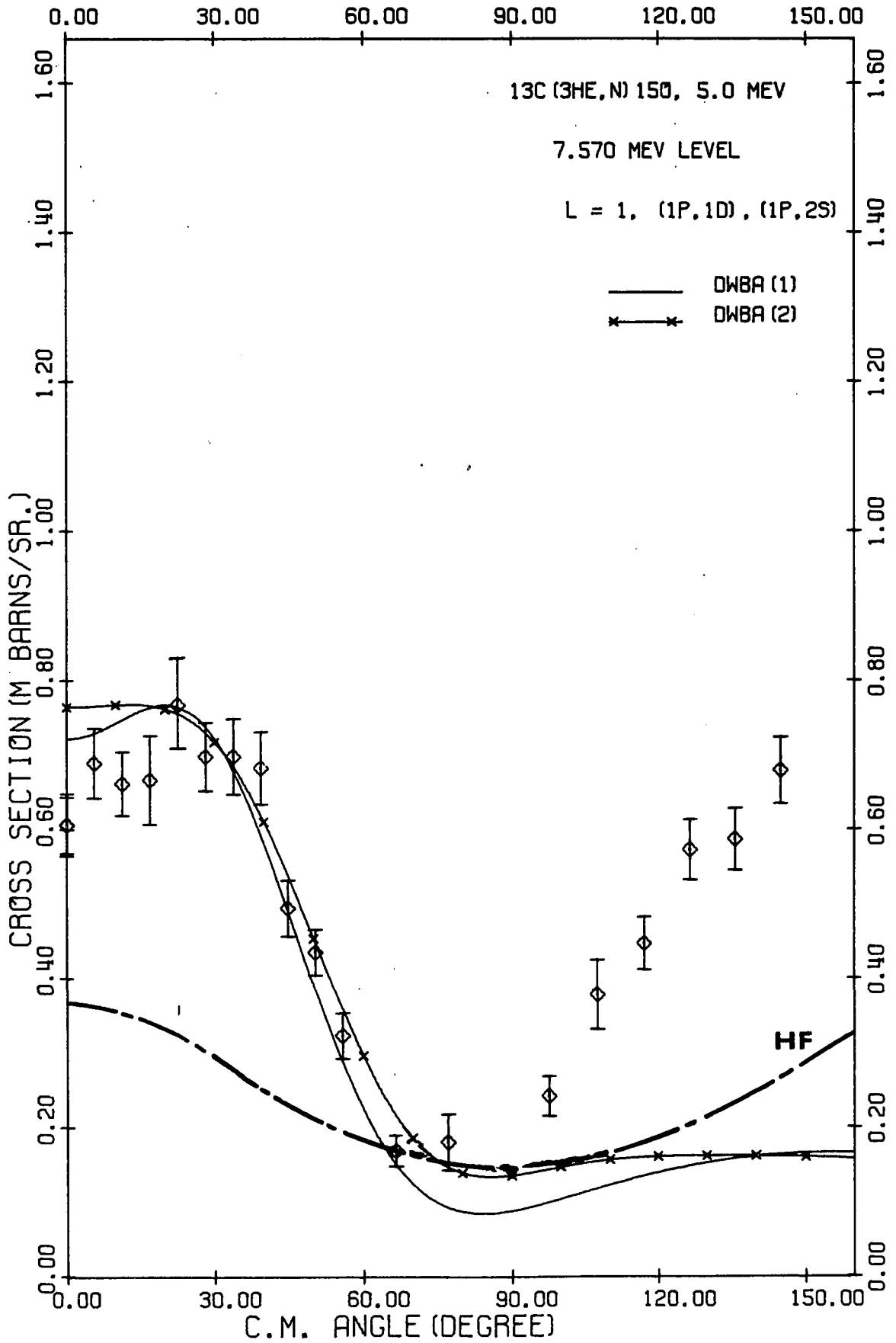
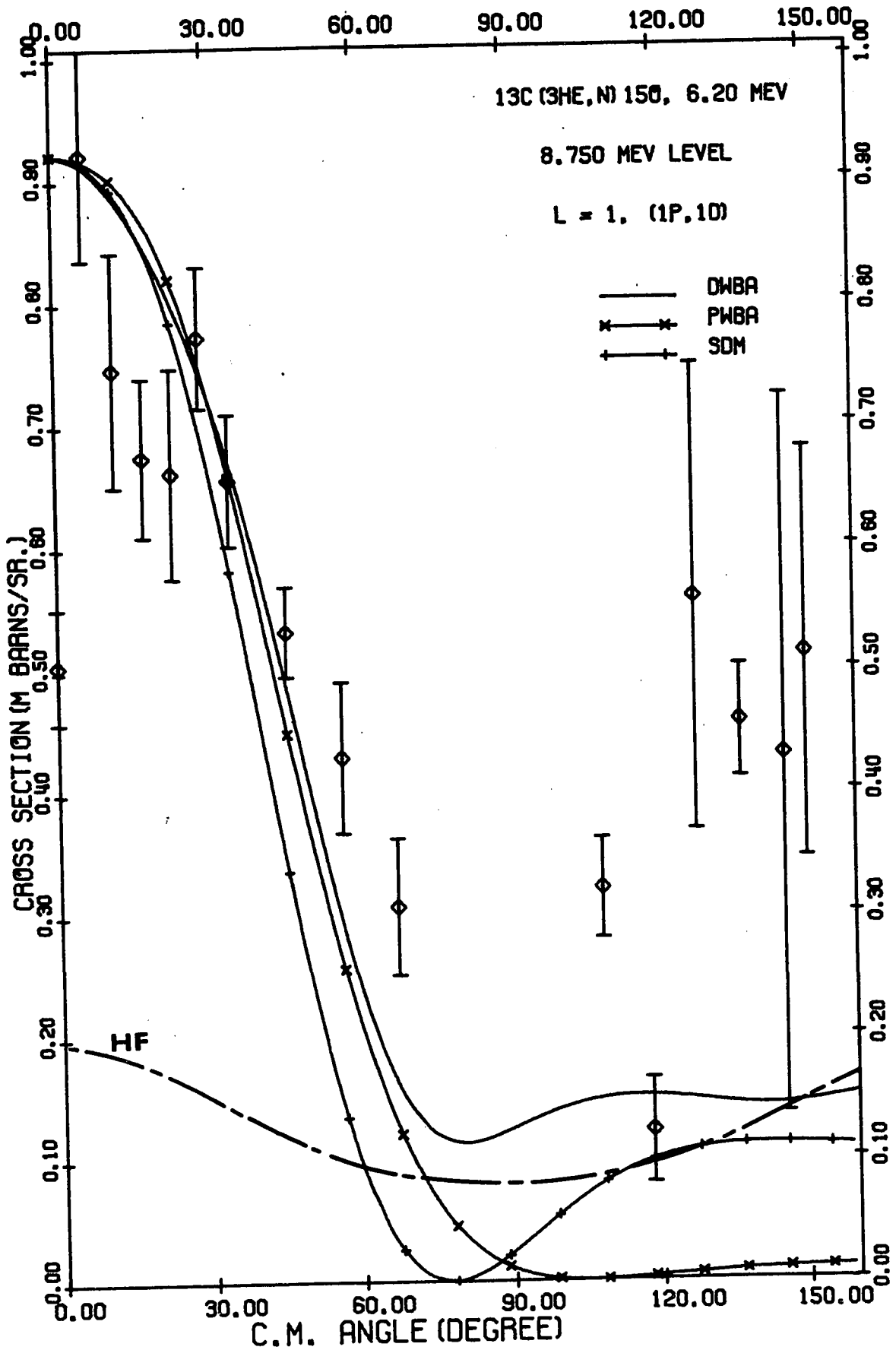
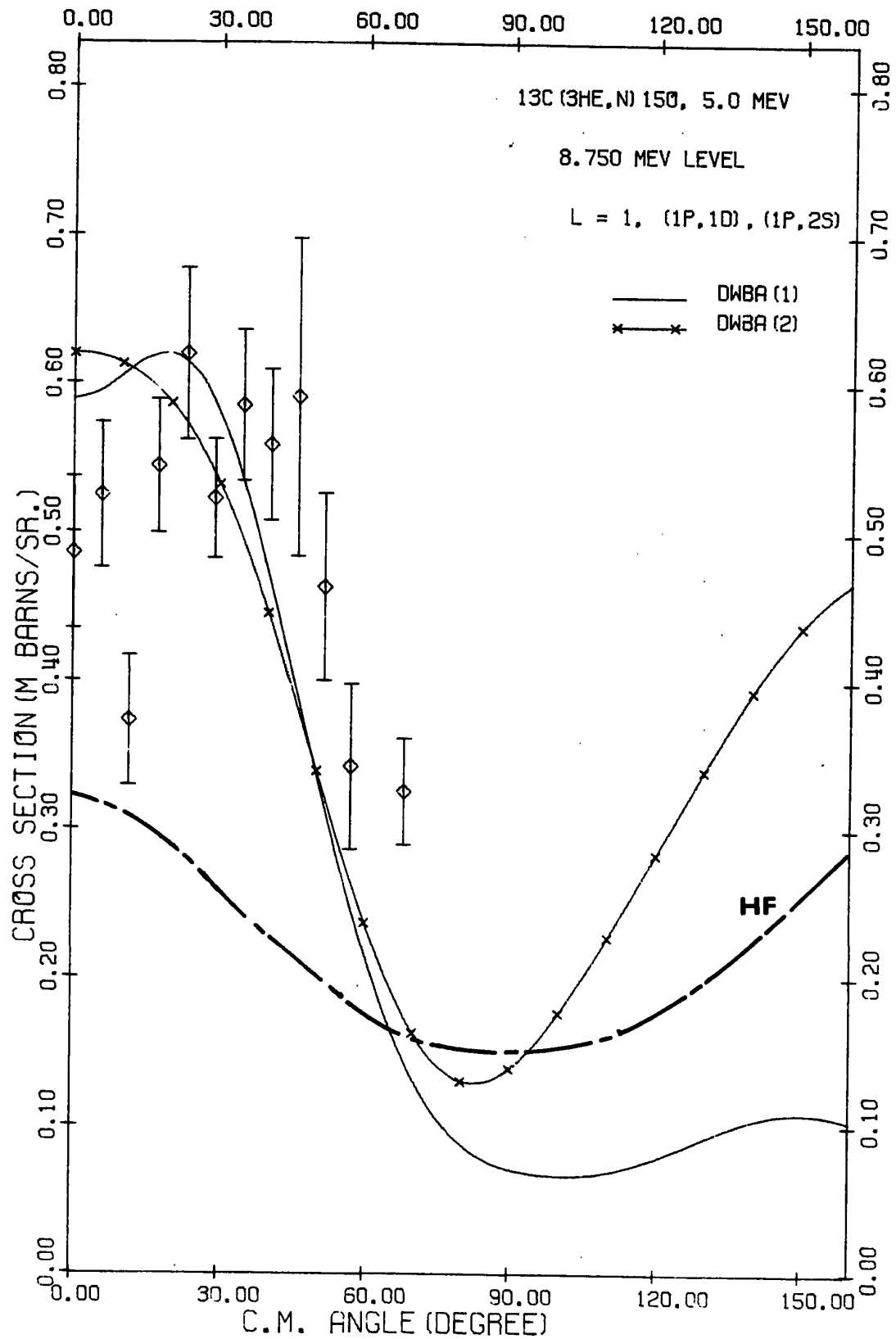


Figure 47. Angular distribution of neutrons leading to 8.750 MeV level of ^{15}O for $E_{^3\text{He}} = 6.2$ MeV. $L = 1$ was assumed for all calculations. (See also caption under figure 35).

Figure 48. Angular distribution of neutrons leading to 8.750 MeV level of ^{15}O for $E_{^3\text{He}} = 5.0$ MeV. DWBA(1) and DWBA(2) represent results of (lp,ld) and (lp,2s) calculations respectively. $L = 1$ was assumed for both calculations. (See also caption under figure 35).



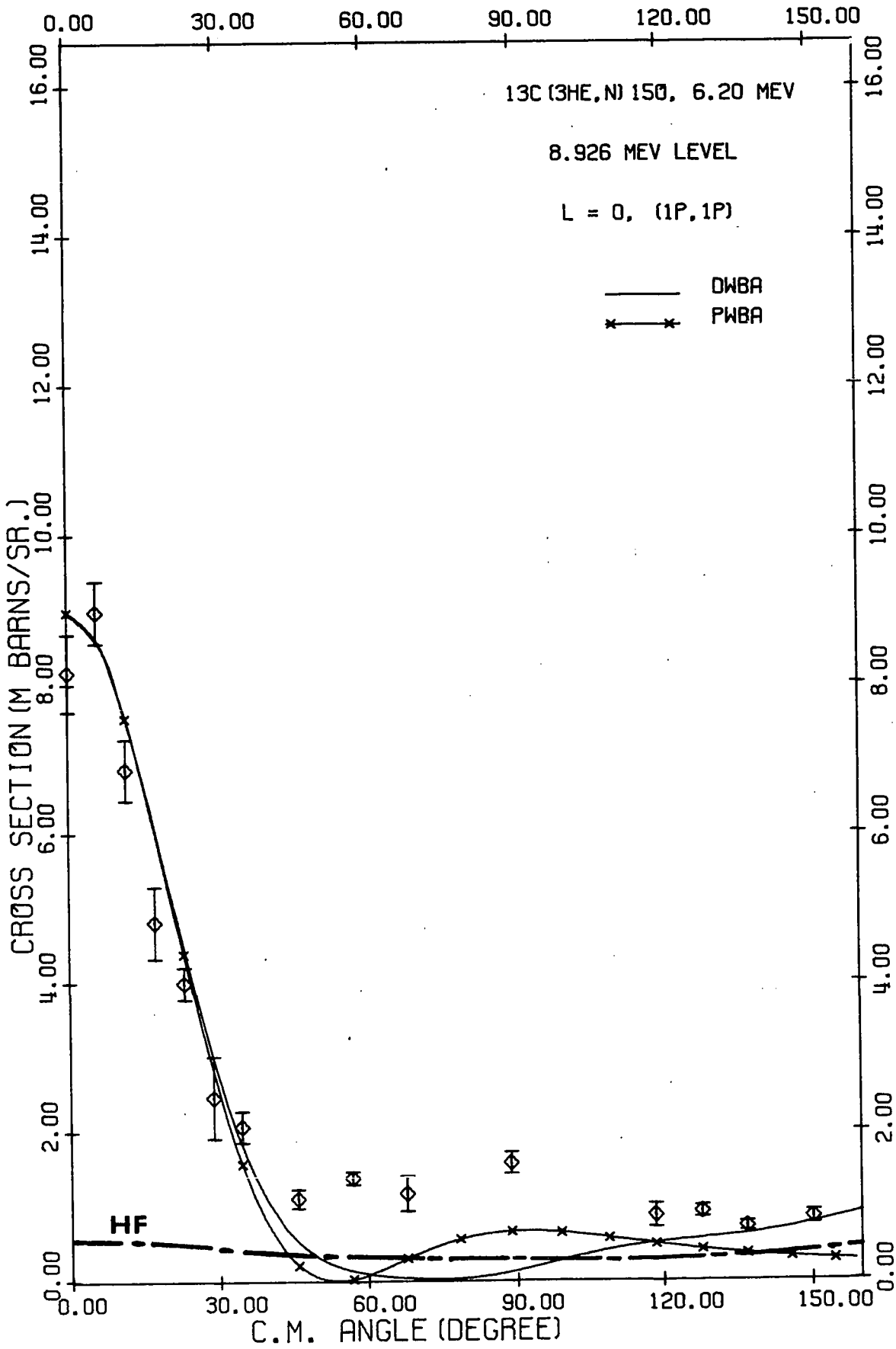


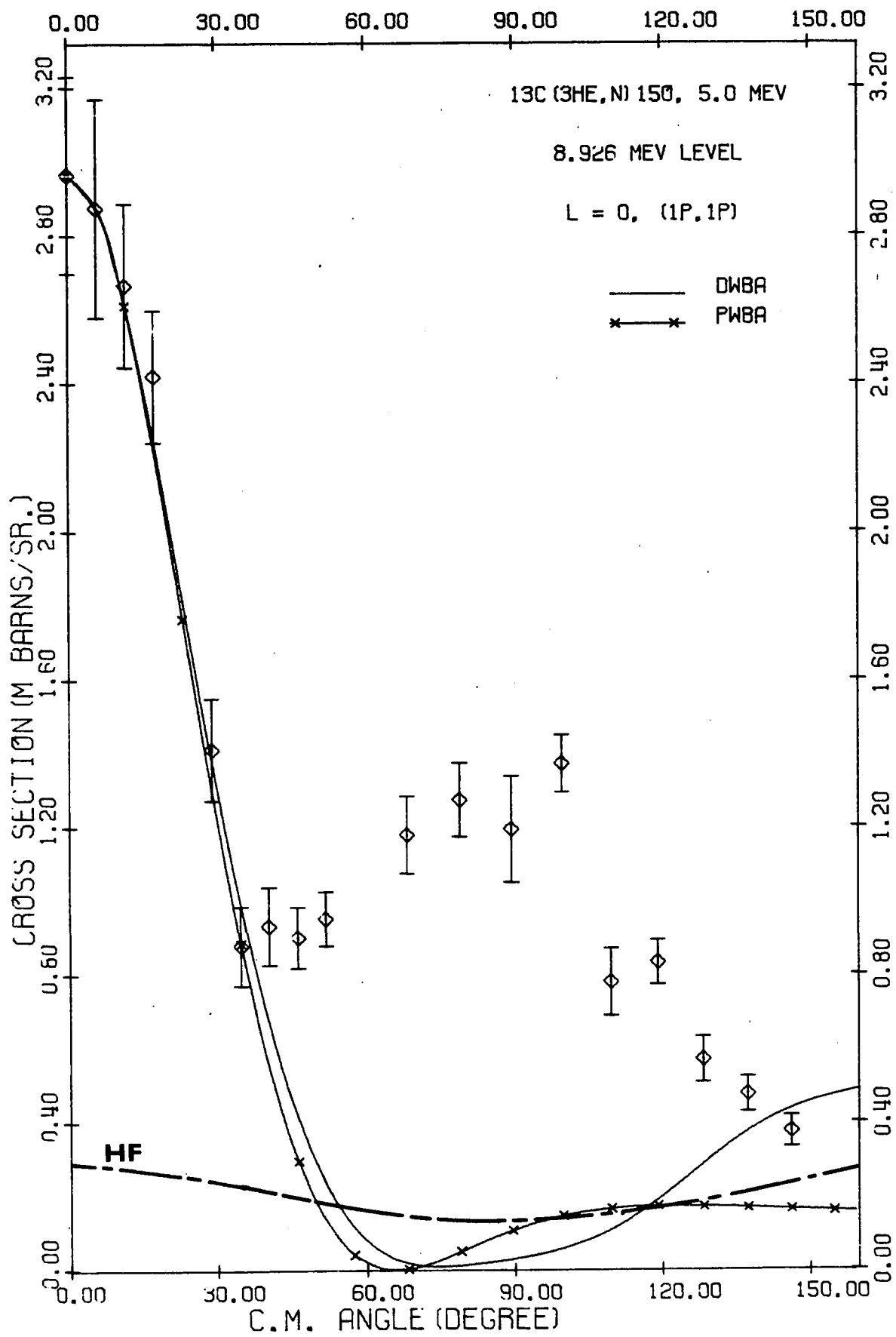
distributions for both transitions from the 5.0 and 6.2 MeV data. The 8.926 MeV level was more strongly populated than the 8.974 MeV level. The angular distributions for both levels are shown in figures 49 to 52.

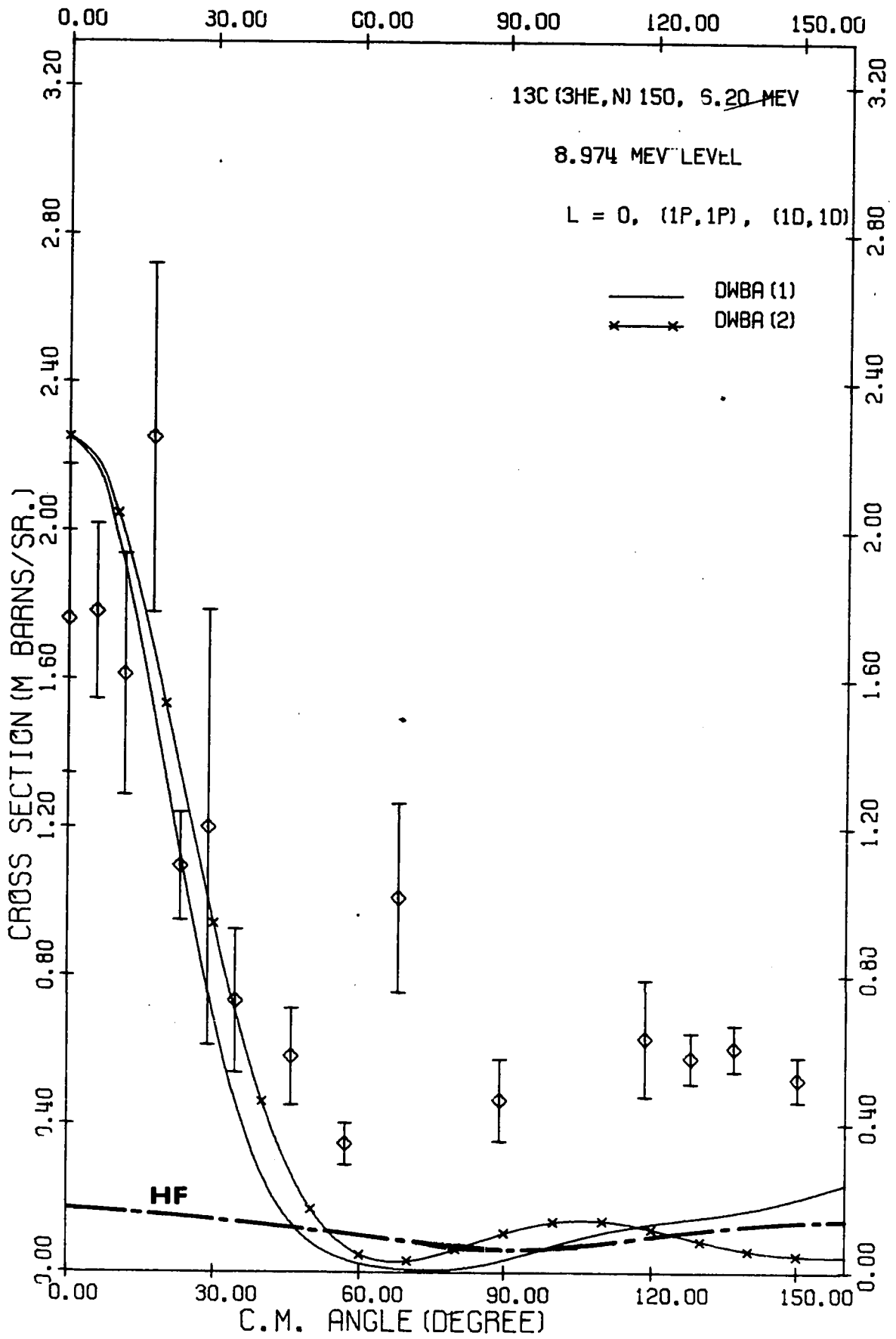
The 8.926 MeV level was known from the proton scattering measurements to be a $\frac{3^+}{2}$ level. Both d-wave and s-wave protons were involved in forming this state (HA 57A). The measurements of Evans et al. (EV 66) also indicate the angular distribution of the γ -rays decay to the ground state is consistent with the decay of a $\frac{3^+}{2}$ state formed with a d- to s-wave intensity ratio of 35%.

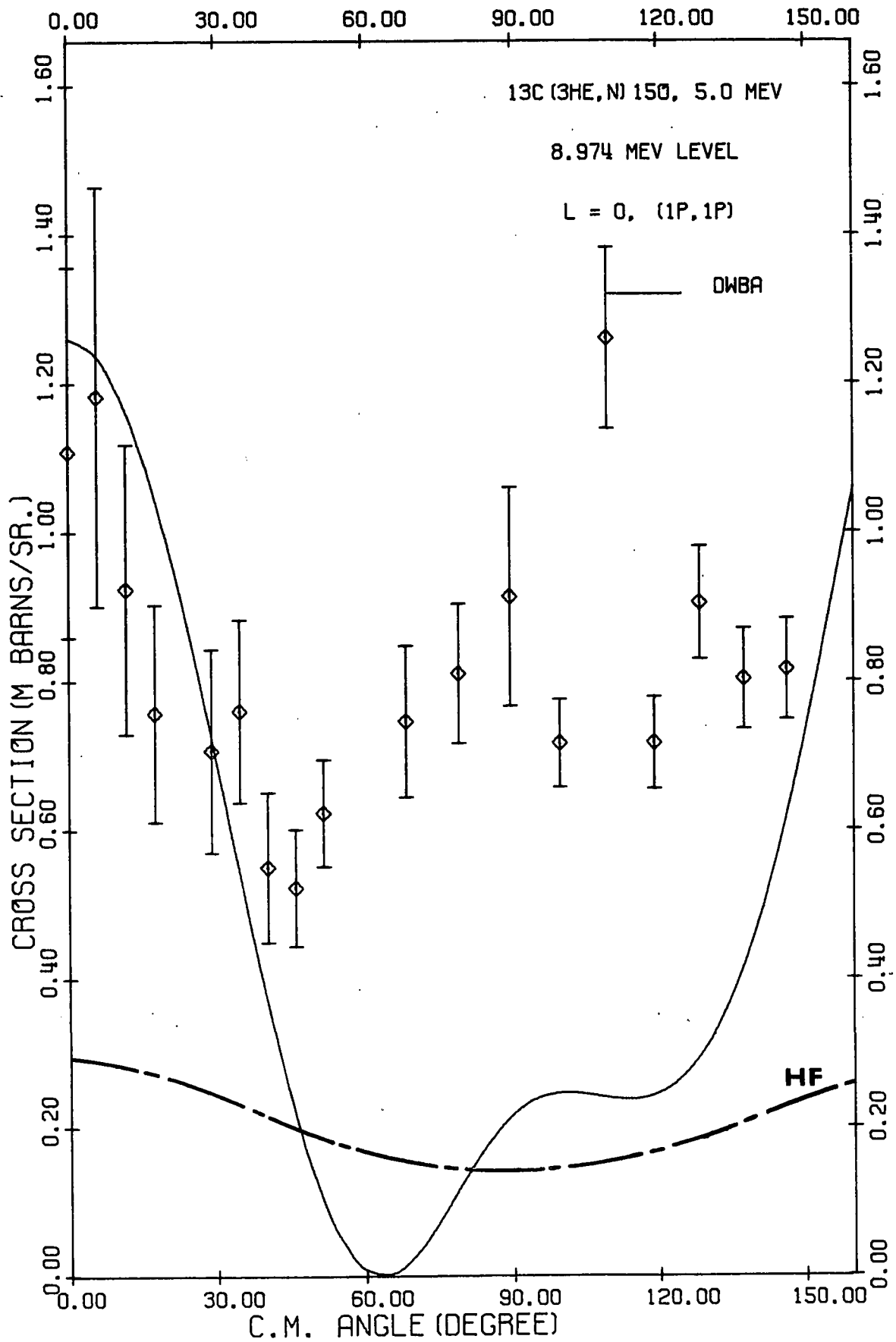
The spin and parity of the 8.97 MeV level was previously assigned by Cohen-Ganoura et al. (CO 63) and Evans et al. (EV 66) to be $\frac{5^-}{2}$. Assuming that these levels have spin and parity of $\frac{3^+}{2}$ and $\frac{5^-}{2}$ respectively, then the selection rules will permit an L = 1 transition for the 8.926 MeV level and an L = 2 transition for the 8.974 MeV level. The neutron angular distribution of present measurements indicate that this is not the case. A typical L = 0 transition was found for both levels (see figures 49 to 52). The strong transition to 8.974 MeV level may also indicate that this level is the $1p^{11}$ configuration level which was predicted by Lane et al. (LA 54) at 9.28 MeV. Since L equals zero, the only possible spin and parity can be assigned to those two levels is $\frac{1^-}{2}$. It was reported by Hagedon et al. (HA 57B) that a level at excitation energy 9.03 MeV can be assigned with a possible spin and parity of $\frac{3^-}{2}$ or $\frac{1^-}{2}$. One of the present observed levels may correspond to the 9.03 MeV level of Hagedon et al.

- Figure 49. Angular distribution of neutrons leading to the 8.926 MeV level of ^{15}O for $E_{3\text{He}} = 6.2$ MeV. $L = 0$ was assumed for all calculations. (See also caption under figure 35).
- Figure 50. Angular distribution of neutrons leading to the 8.926 MeV level of ^{15}O for $E_{3\text{He}} = 5.0$ MeV. $L = 0$ was assumed for all calculations. (See also caption under figure 35).
- Figure 51. Angular distribution of neutrons leading to the 8.974 MeV level of ^{15}O for $E_{3\text{He}} = 6.2$ MeV. DWBA (1) and DWBA (2) represent results of (lp,lp) and (ld,ld) calculations respectively. $L = 0$ was assumed for all calculations. (See also caption under figure 35).
- Figure 52. Angular distribution of neutrons leading to 8.974 MeV level of ^{15}O for $E_{3\text{He}} = 5.0$ MeV. $L = 0$ was assumed for all calculations. (See also caption under figure 35).









8. 9.498 MeV, 9.611 MeV and 9.665 MeV levels

Some of these levels of ^{15}O have been observed using proton scattering on ^{14}N by various groups (GO 54, BO 57, FE 59A). A broad state ($\frac{1}{2}^+$) at an excitation energy of 9.47 MeV is reported to decay entirely to the ground state. The present measurements of neutron angular distributions for these levels are shown in figures 53 to 57.

The strong transition to the 9.498 MeV corresponds to an $L = 2$ transition. Thus the possible spin and parity for this level is $\frac{3}{2}^-$ or $\frac{5}{2}^-$. Similar distributions were obtained for the 9.611 MeV level, therefore the only possible spin and parity assignment to this level is $\frac{3}{2}^-$ or $\frac{5}{2}^-$.

At these high excitation energies the CN formation decreases; on the other hand the DI increases substantially. This effect is seen in figures 53 to 56.

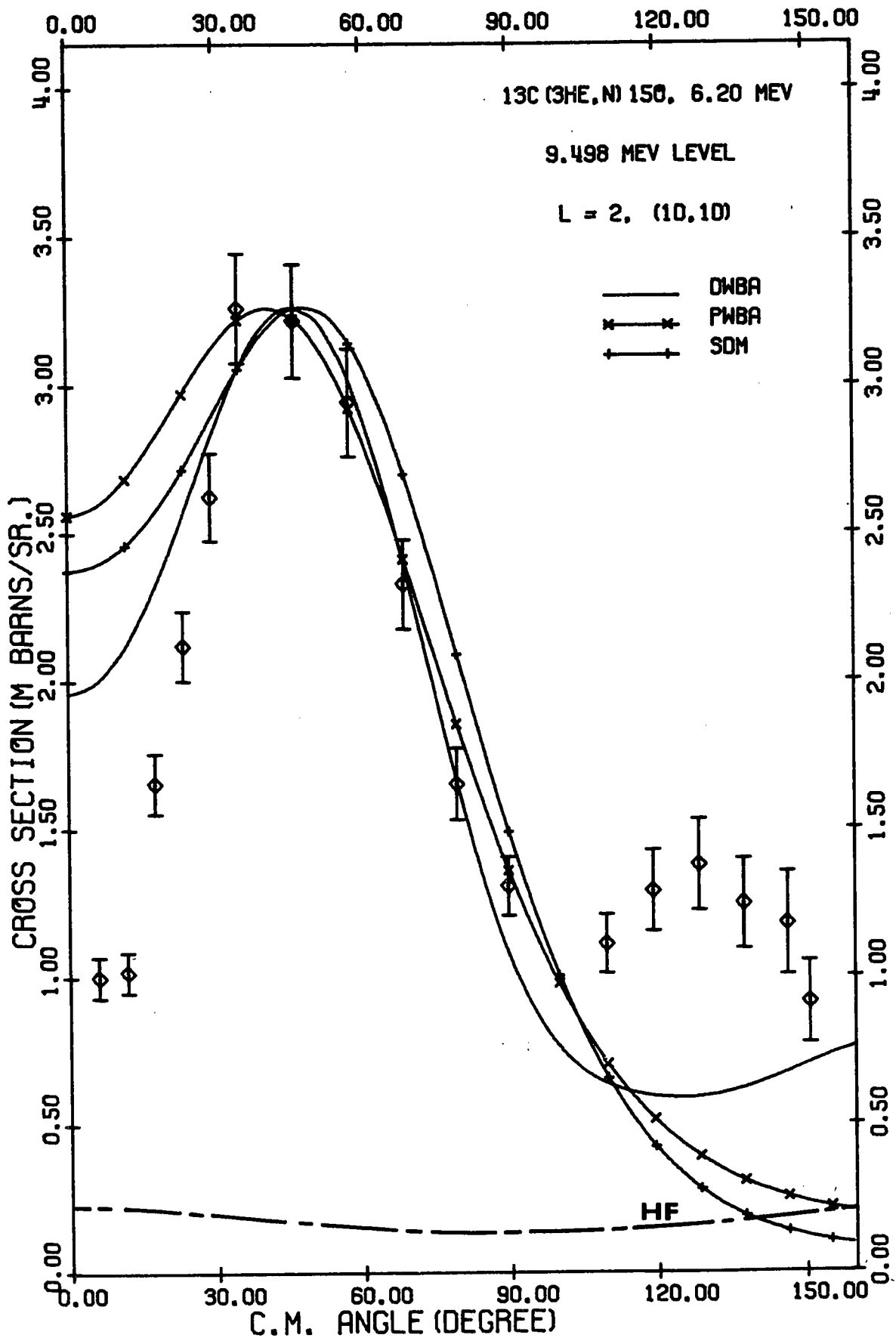
The neutron angular distribution for the 9.665 MeV is shown in figure 57. The calculations seem to favor an $L = 0$ transition. This suggests the spin and parity of this state may be assigned as $\frac{1}{2}^-$.

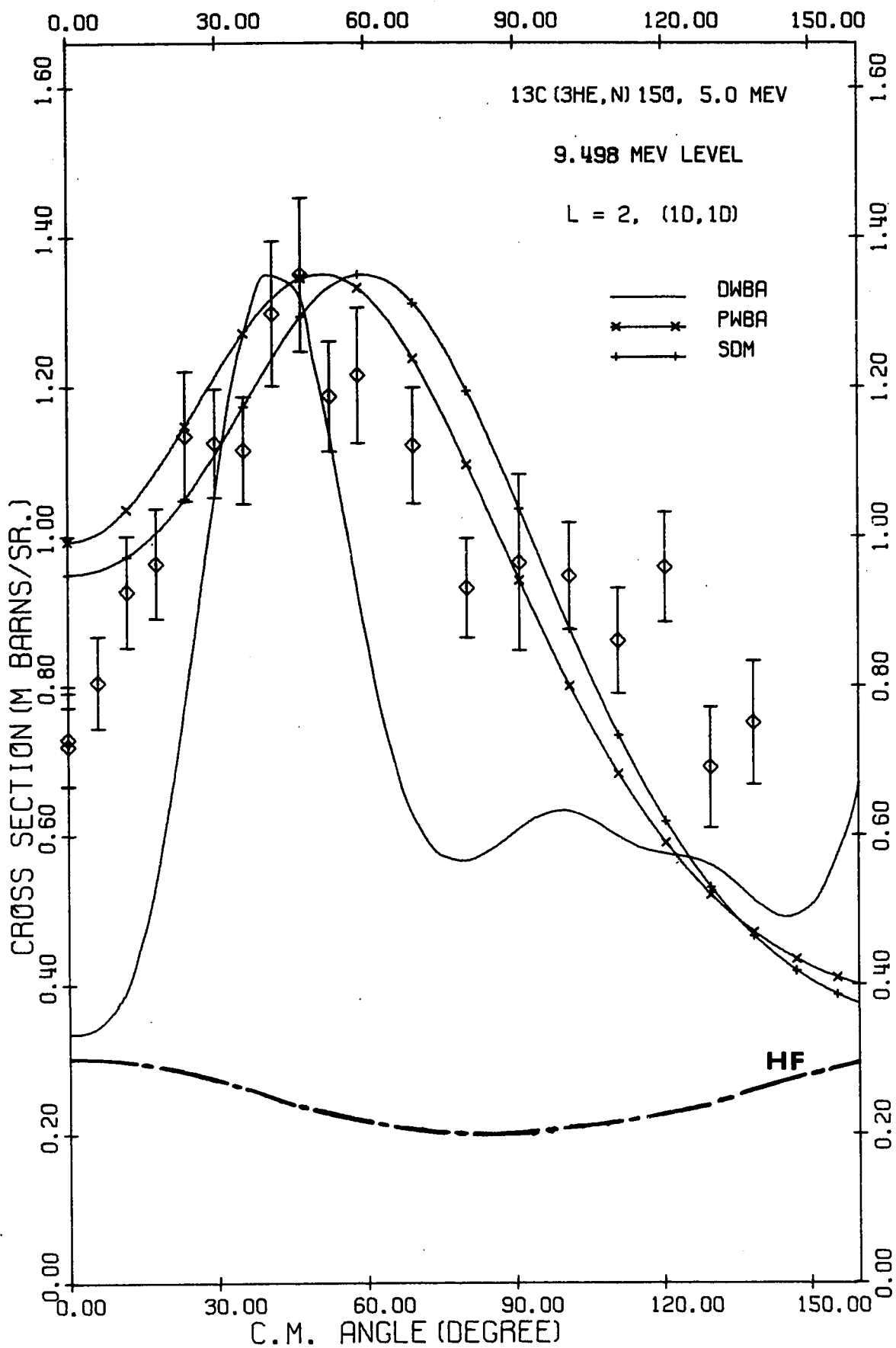
Figure 53. Angular distribution of neutrons leading to the 9.498 MeV level of ^{15}O for $E_{3\text{He}} = 6.2$ MeV. $L = 2$ was assumed for all calculations. (See also caption under figure 35).

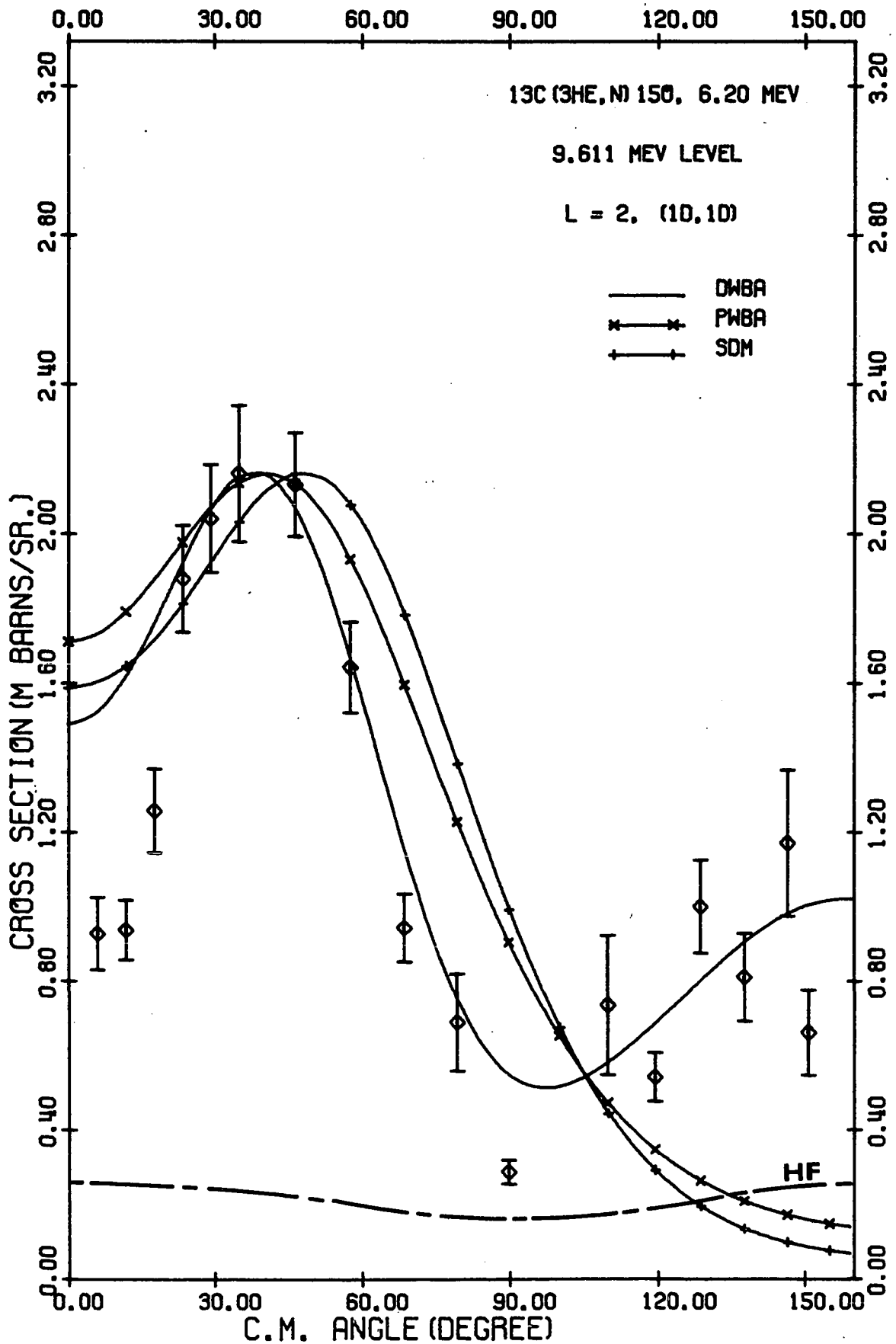
Figure 54. Angular distribution of neutrons leading to the 9.498 MeV level of ^{15}O for $E_{3\text{He}} = 5.0$ MeV. $L = 2$ was assumed for all calculations. (See also caption under figure 35).

Figure 55. Angular distribution of neutrons leading to the 9.611 MeV level of ^{15}O for $E_{3\text{He}} = 6.2$ MeV. $L = 2$ was assumed for all calculations. (See also caption under figure 35).

Figure 56. Angular distribution of neutrons leading to the 9.611 MeV level of ^{15}O for $E_{3\text{He}} = 5.0$ MeV. $L = 2$ was assumed for all calculations. (See also caption under figure 35).







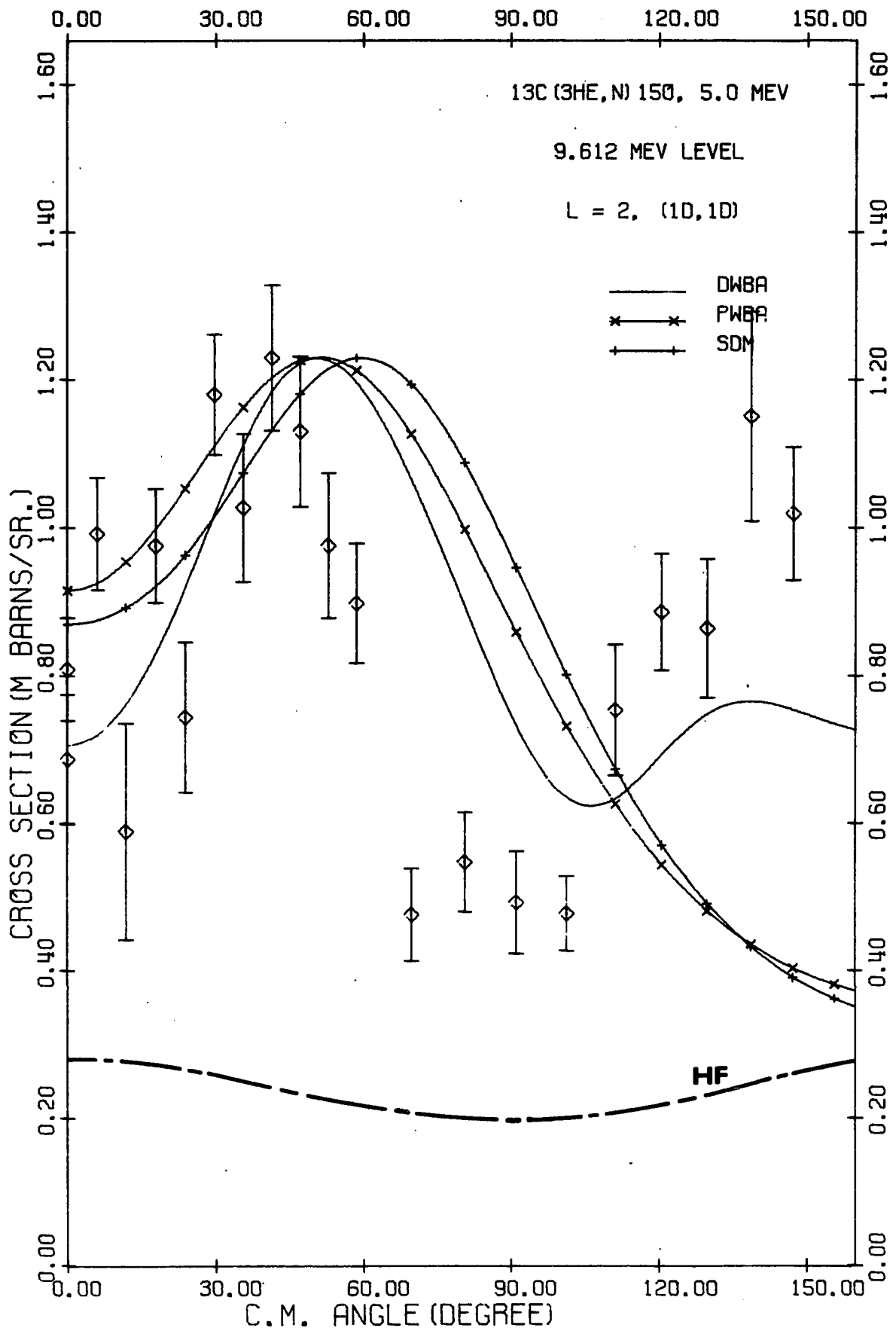
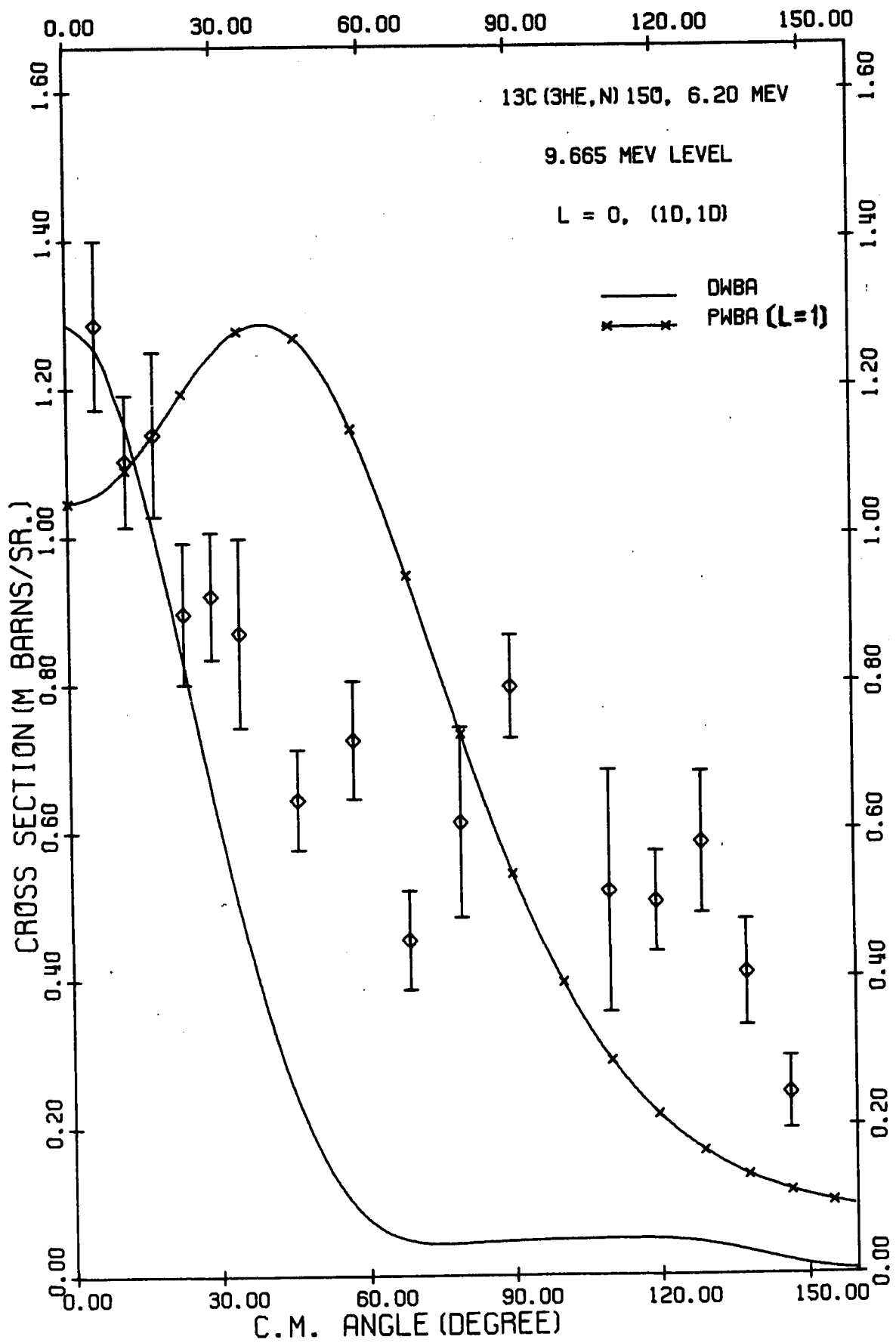


Figure 57: Angular distribution of neutrons leading to the 9.665 MeV level of ^{15}O for $E_{3\text{He}} = 6.2$ MeV. $L = 0$ with (1d,1d) configuration was used for DWBA calculation. $L = 1$ was also tried for PWBA calculation.



CHAPTER FIVE

CONCLUSIONS

The results shown in Chapters 3 and 4 present several significant features in common. To demonstrate this we assume that the maxima of individual angular distributions less contributions from HF cross section is a measure of the DI strength. DI and corresponding HF strengths are plotted versus their excitation energies in figures 58 and 59.

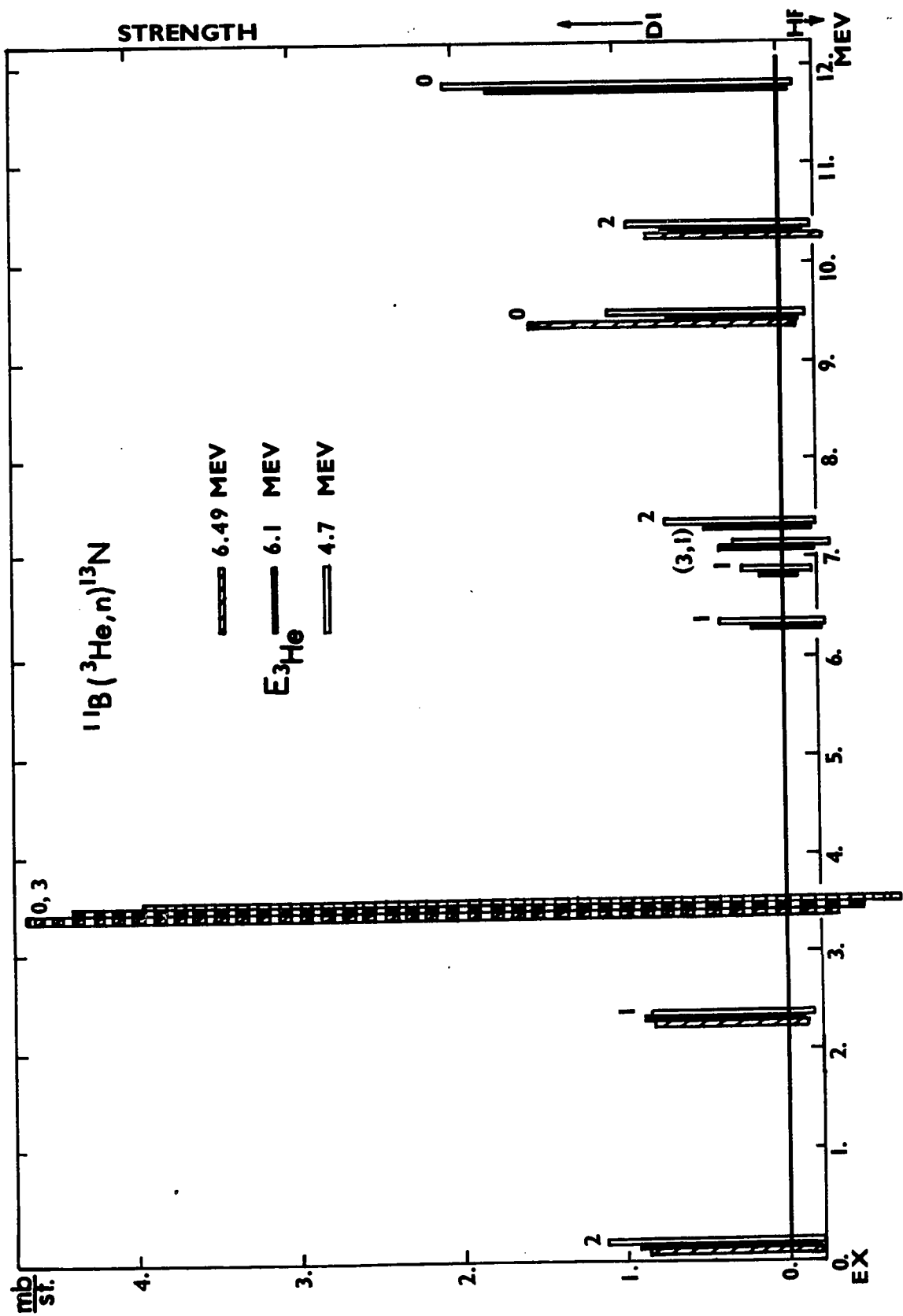
For a given nucleus, since the di-proton transfer probability is higher to the low Q values states (high-lying states) than those with high Q states, one would expect in general the DI transition strength will increase with the excitation energy. On the other hand, one would expect the CN cross section decreases as the excitation energy increases.

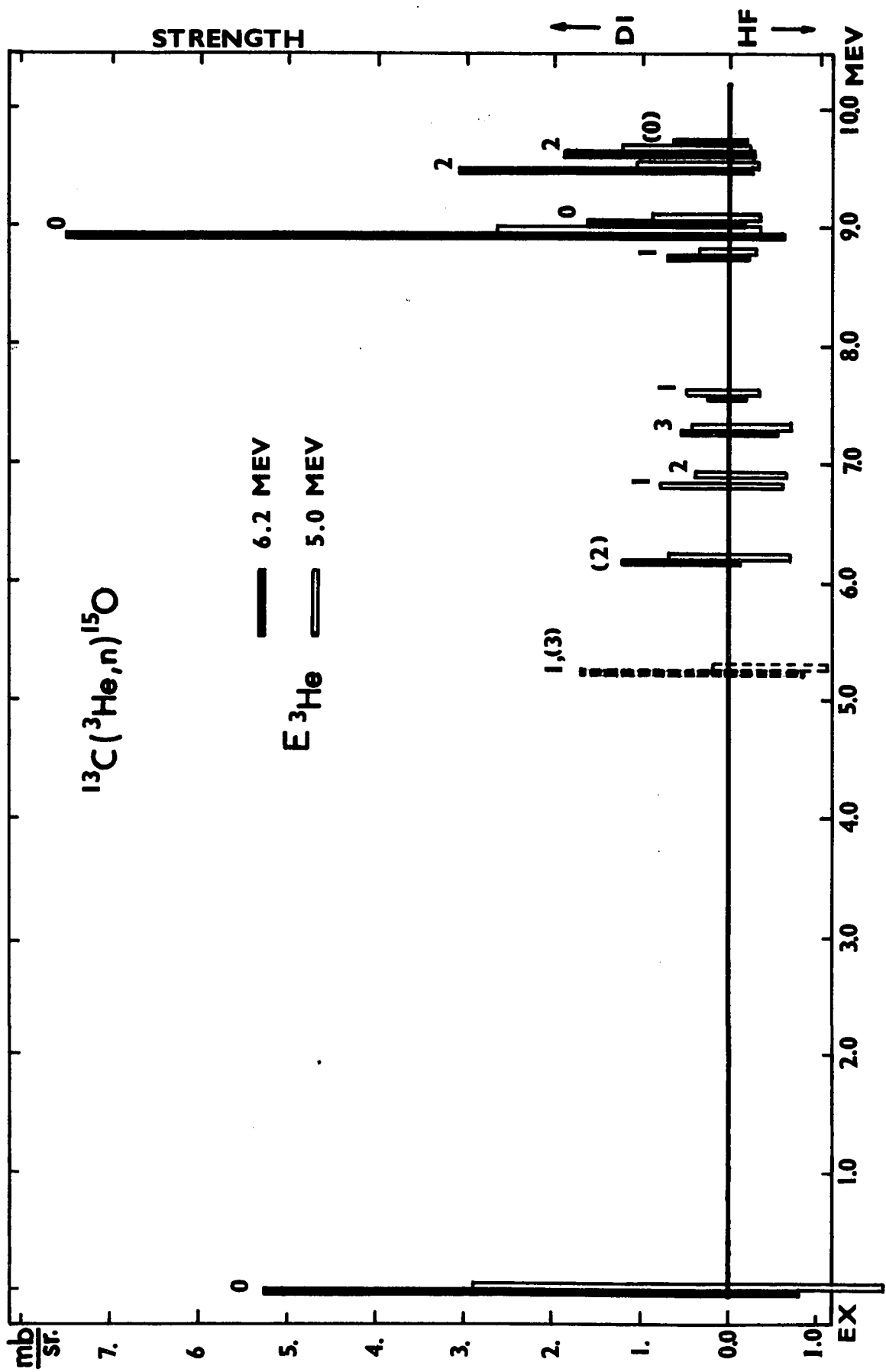
Glancing at figure 58 for $^{11}\text{B}(^3\text{He},n)^{13}\text{N}$ one notices that there is a minimum region of DI strength at $E_x \sim 7.0$ MeV regardless of ^3He bombarding energies. In case of $^{13}\text{C}(^3\text{He},n)^{15}\text{O}$ the trend shows a similar minimum at $E_x \sim 8$ MeV. The angular distributions for some of the transition to those minimum strength region states also indicated a strong energy dependence, which clearly is not characteristic of DI.

Feshbach (FE 58,62) has proposed that the CN states are the end product of a sequence of two body interactions. The first two-body interaction between the incident particle and a target nucleon leads to two-particle one hole states, which

Figure 58. Transition strength plotted vs excitation energy for reaction $^{11}\text{B}(^3\text{He},n)^{13}\text{N}$ (DI strength in positive and corresponding CN strength in negative direction). The 3.50 MeV data is for unresolved pair of levels.

Figure 59. Transition strength plotted vs excitation energy for reaction $^{13}\text{C}(^3\text{He},n)^{15}\text{O}$ (DI strength in positive and corresponding CN strength in negative direction). The 5.23 MeV data is for unresolved pair of levels.





were called doorways, and subsequently leading to three-particle and two-hole states and so on, until so called CN states are reached. For high Q states, although the CN vs DI strength ratio is great, the states consist mostly of simple single particle configurations and are easily formed by transferring protons from the projectile to the target nucleus with core excitations playing only a small part. Thus one sees a good strength of DI for those lowlying states. At the minimum strength region, however, most of the states are formed from more than simple single particle configurations, and are complicated. It then may need more than one step to form those states, thus one may see "doorway" states formed at this minimum strength region. The investigation of doorway states both at unbound, continuum region (SE 65) and at bound region (SE 66) are available. The present results may be useful from the point of view of CN theories.

This work has also demonstrated that:

1. At bombarding energy $5 \sim 6$ MeV, the DI is predominant for the most of transitions observed. Therefore the $(^3\text{He},n)$ is useful as a spectroscopic tool at these energies.
2. With a set of reasonable parameters, the prediction of the plane wave theory is still useful, i.e. a set of consistent parameters could be obtained.
3. The simple diffraction model gives surprisingly good predictions for the high Q transition states.
4. The DWBA theory with point ^3He approximation has given the most satisfactory explanations of the data of all DI theories used. However, in order to obtain the spectro-

scopic information which DWBA is potentially capable of giving one needs more sophisticated programs, such as the code developed by Glendenning et al. (FL 68) to include two body fraction of parentage coefficients or directly taking into account the wave function given directly from the shell model calculations.

5. Finally for the most states studied, the deduced L values from this work are in agreement with previous known spin and parity assignments. Disagreement was found in the case of the 8.926 MeV level of ^{15}O . This level was reassigned $\frac{1}{2}^-$ instead of $\frac{1}{2}^+$. The experimental data support the assignment $\frac{3}{2}^-$, or possibly $\frac{5}{2}^-$ to both 9.498 and 9.612 MeV levels of ^{15}O as suggested on the basis of L = 2 angular distributions obtained for those two levels.

APPENDIX I:

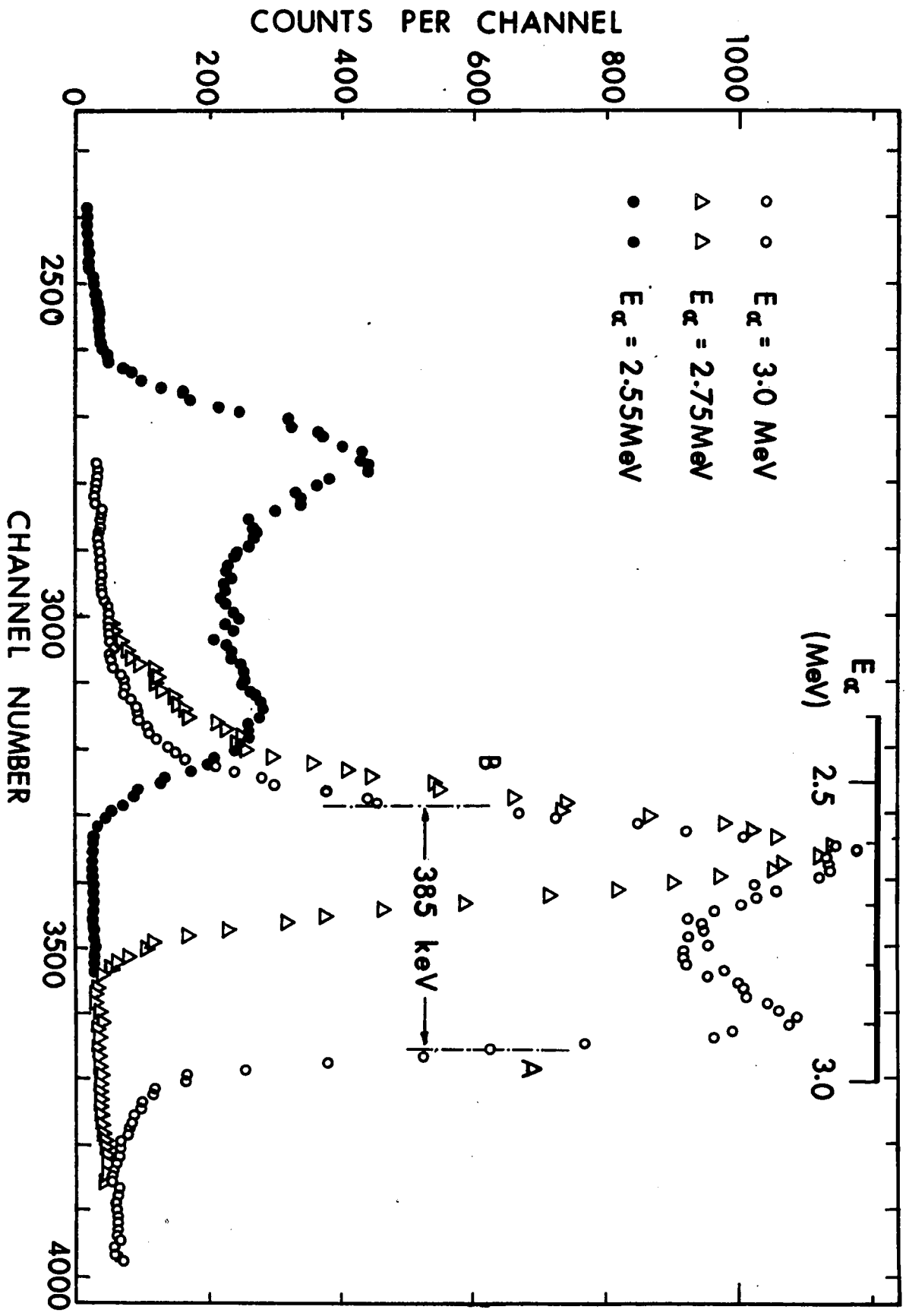
THE TARGET THICKNESS MEASUREMENTS

1. The Boron 11 target

The separated ^{11}B target, purchased from AERE, Harwell, England, was claimed to have a nominal loading of $100 \mu\text{g}/\text{cm}^2$ elementary ^{11}B on the gold foil backing. However, an unusually high yield of neutrons and γ -rays were observed from the bombardment of this target with ^3He . It was felt that a more accurate determination of the thickness on this particular target was needed. The method of measurement described in this subsection employed the neutron time-of-flight technique. Since the target thickness was measured at the spot of bombardment where cross sections for the reaction $^{11}\text{B}(^3\text{He},n)^{13}\text{N}$ were measured, the problem of the unevenness of the target surface was eliminated.

The ^{11}B target was mounted on the target holder previously described. The target holder surface was oriented at 75° with respect to the bombarding beam. The target was then bombarded by 3.0 MeV, 2.75 MeV and 2.55 MeV alpha beam. In order to gain energy resolution the neutron detector was placed at 140° (lab. angle). Neutron energy spectra were taken for the three different bombarding energies (see figure 60). The spectrum for $E_\alpha = 3.0$ MeV shows the 2.63 MeV and 3.0 MeV resonances [cf Mani et al. (MA 66)]. In the present measurements, due to energy cut-off at higher energy edge only the lower half of the 3.0 MeV resonance can be seen in the spectrum. This presented problems in obtaining infor-

Figure 60. Neutron time-of-flight spectra obtained from $^{11}\text{B}(\alpha, n)^{14}\text{C}$ for the ^{11}B target thickness determination. Spectra are obtained at $\theta_{\text{lab}} = 140^\circ$, flight path 2.5 meters, and bombarding energies at 3.0, 2.75, and 2.55 MeV.



mation of the natural width of the target from this spectrum. However, judging from the flat top of the 3.0 MeV run, the high energy edge of the $E_\alpha = 2.75$ MeV spectrum can be taken as the peak shape resulting from beam spread and spectrometer time resolution. Therefore the slope on the higher energy side of the 2.75 MeV run was used to determine the edge A (see figure 60). By comparing the 3.0 MeV, 2.75 MeV and the 2.55 MeV runs one also sees the lower energy edge of the peak is mostly from the contribution of 2.63 MeV resonance. However, careful inspection of the slope of the peak of 3.0 MeV run revealed that this slope consists of both lower energy slopes of the resonance edge and the beam energy spread. A symmetric peak was assumed for the beam spread and a similar amount to the high energy edge was subtracted from the lower energy of the peak of 3 MeV run and low energy edge of B of figure 60 was thus determined. The target thickness determined in this way was equivalent to 385 keV of 2.75 MeV α particles with an uncertainty of 32 keV which corresponds to $323 \pm 27 \mu\text{g}/\text{cm}^2$.

2. The Carbon 13 Target

Three different methods were used in measuring thickness of the carbon 13 target. The target was made by AERE at Harwell, England.

(a) The $^{13}\text{C}(p,\gamma)^{14}\text{N}$ resonance.

It is known there is a strong (p,γ) resonance near 1.75 MeV. This resonance was reported by Evans et al. (EV 66) to have a half width of less than 500 eV.

A 2 x 2 NaI(Tl) scintillation counter was mounted at $\theta_{\text{lab}} = 0^\circ$ at a distance of 1 meter from the target. Since

most of the γ -rays contributed to this resonance are known to be high energy γ -rays (4.8 MeV), a single channel analyzer was used to set up the counting threshold at approximately 4.0 MeV. As was expected a sharp resonance was observed at $E_p = 1.747$ MeV. The half width of this resonance including target thickness was 6.62 ± 0.7 keV (figure 61(a)) for the 1.75 MeV protons.

(b) The $^{13}\text{C}(\alpha, n)^{16}\text{O}$ resonance.

Bonner et al. (BO 56) by using long counter technique studied this reaction in great detail. They found there was a sharp resonance with a natural width of 5 keV at $E_\alpha = 3.73$ MeV. The present measurements were carried out using time-of-flight technique. With the neutron detector located at $\theta_{\text{lab}} = 0^\circ$, flight path = 3 meters. The half width was found to be 40 keV and thus the target thickness was estimated to be 39.2 ± 6 keV for 3.73 MeV α particles. This is equivalent to 5.29 ± 0.8 keV energy loss for 1.75 MeV protons.

(c) The $^{13}\text{C}(p, n)^{13}\text{N}$ threshold.

This well known threshold measurement was also used for the machine energy calibration. A McKibben long counter was placed at a detection angle of zero degrees at a distance of 1.5 meters from the target. The excitation curve presented in figure 61(C) was plotted by taking $\frac{2}{3}$ power of the total neutron yield against the proton energies, the width due to the target thickness was estimated to be approximately 3.45 ± 1 KeV for a proton energy of 3.235 MeV. This is equivalent to 6.38 ± 1.9 keV for 1.75 MeV protons.

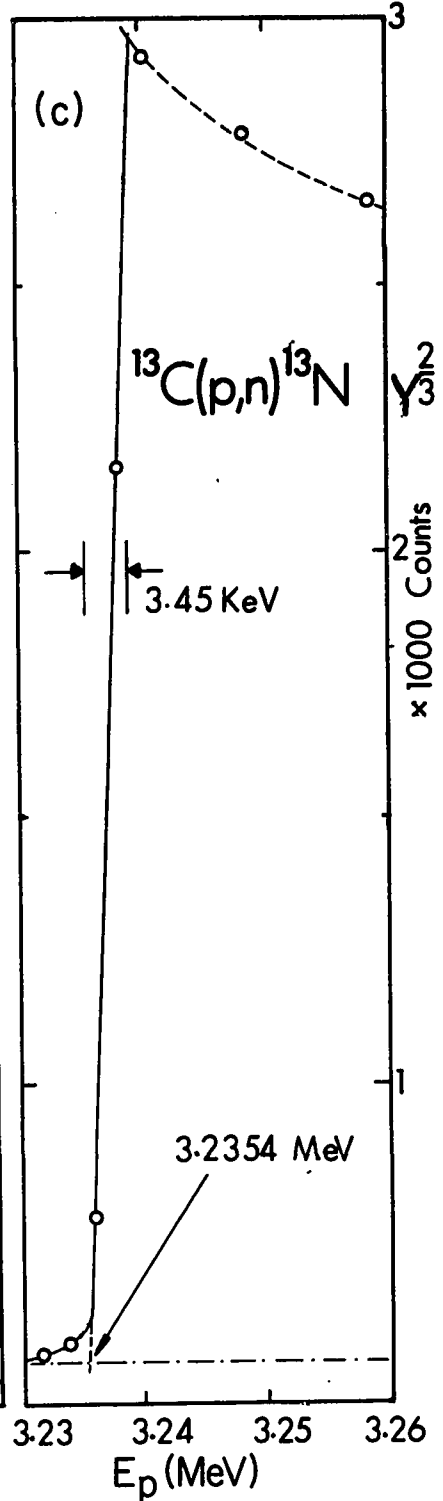
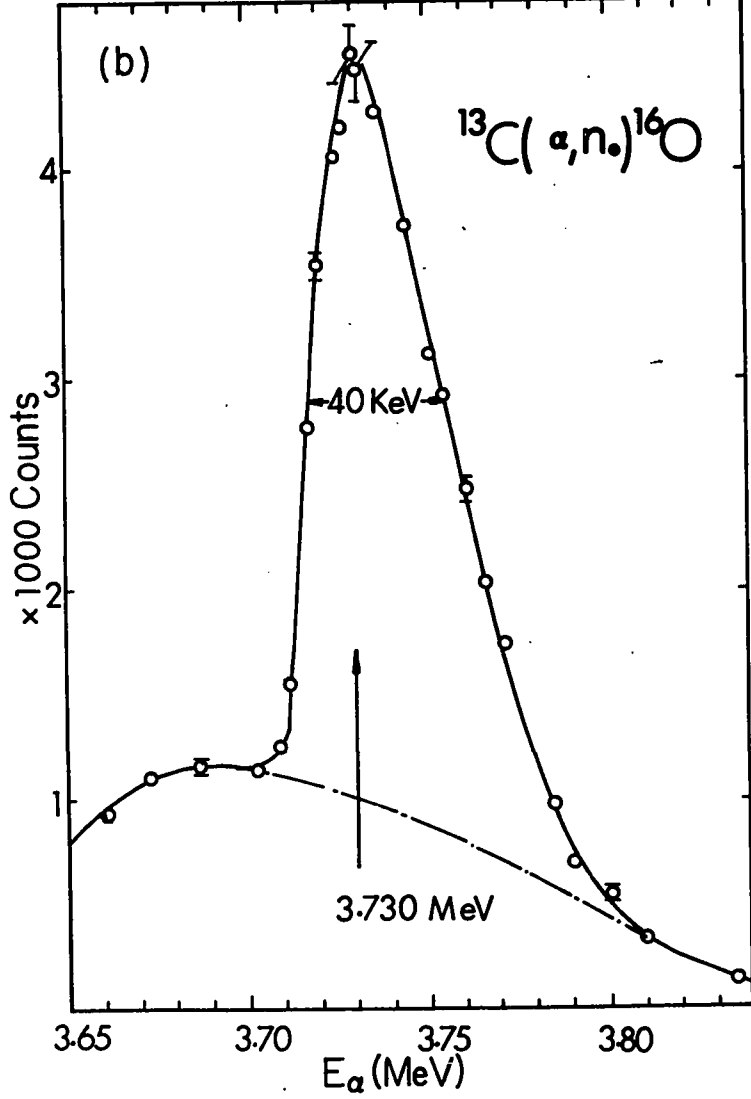
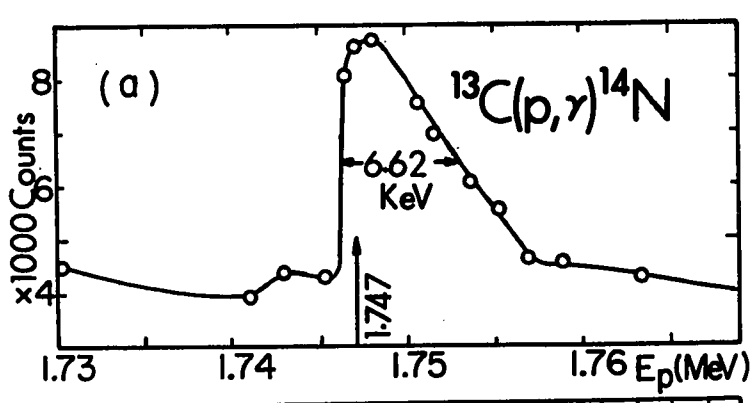
Since the measurements of (p, γ) resonance were done

Figure 61. Various methods used for the ^{13}C target thickness determinations.

(a) $^{13}\text{C}(p,\gamma)^{14}\text{N}$ resonance

(b) $^{13}\text{C}(\alpha,n_0)^{16}\text{O}$ resonance and

(c) $^{13}\text{C}(p,n)^{13}\text{N}$ threshold measurement.



right after the major ($^3\text{He},n$) measurements, it was considered the (p,γ) measurement carries more weight than other measurements.

A 6 : 3 : 1 weight average was taken, and the average target thickness was estimated to have an energy loss of 6.2 ± 0.8 keV for 1.75 MeV proton or 43 ± 6 $\mu\text{g}/\text{cm}^2$.

APPENDIX II

THE Q-VALUES MEASUREMENTS

The flight path from the target to centre of the detector was measured with a maximum error of ± 0.5 cm. The accelerator energies were calibrated by means of ${}^7\text{Li}(p,n){}^7\text{Be}$ and ${}^{13}\text{C}(p,n){}^{13}\text{N}$ threshold measurements. The threshold values 1880.56 keV, 3235.7 keV were taken from reference MA 66B. The overall long range stability in accelerator energies were also checked by various threshold resonance measurements.

The time calibration for the ${}^{11}\text{B}({}^3\text{He},n){}^{13}\text{N}$ measurements was obtained from the known Q values of the various levels of ${}^{11}\text{C}$ using the reaction ${}^9\text{Be}({}^3\text{He},n){}^{11}\text{C}$, which was reported earlier in reference SI 67. To check consistency the ${}^9\text{Be}({}^3\text{He},n){}^{11}\text{C}$ calibration runs were carried out before, in the middle, and at the end of the measurements. The calibration lines were least square fitted to straight lines, their slopes, intercepts at the time axis were compared, and a calibration value 0.22364 ± 0.00040 nsec/channel was obtained.

This value was also checked during a period of 6 months and only 0.2% of drift was observed. For the ${}^{15}\text{O}$ measurements, the time calibration was obtained from the ${}^{16}\text{O}(d,n){}^{17}\text{F}$ ground state and first excited state measurements. The ${}^{16}\text{O}(d,n){}^{17}\text{F}$ ground state adjusted Q value was taken from reference MA 65b, as -1623.95 ± 0.40 keV. Many runs were performed, by varying the detector angles, the flight paths, and the bombarding energies, until the observed peaks entirely covered the desired

time range. A least square fit to a straight line was obtained. A value -0.31866 ± 0.0049 was adapted as the time calibration for $^{13}\text{C}(^3\text{He},n)^{15}\text{O}$ at $E_{^3\text{He}} = 5$ MeV.

For the $^{11}\text{B}(^3\text{He},n)^{13}\text{N}$ the half width of the entire target thickness was estimated as 55 KeV for 6.1 MeV ^3He and the carbon deposit on the surface was estimated from the known cross section $^{12}\text{C}(^3\text{He},n)^{14}\text{O}$ reaction (TO 61) to be 15 keV.

Since there is some doubt about the linearity of the calibration for the electronics system II, and also in order to avoid electronics drifts, $^{12}\text{C}(^3\text{He},n)^{14}\text{O}$ ground state, which appears very strongly due to the carbon contamination on the ^{11}B target, was used as the time reference peak. By introducing the time reference peak the effect of the small drift in electronics system was then minimized. A Q value of -1148.10 ± 0.39 keV was also found from MTW tables (MA 65B).

In the case of $^{13}\text{C}(^3\text{He},n)^{15}\text{O}$ reactions the half width of the entire target was estimated as 12.5 keV and the total width of the ^{12}C deposits was estimated as less than 6.5 keV at the ^3He bombarding energy of 5.0 MeV.

All calculation of the Q values were done relativistically using a computer code written for the purpose.

$$Q = E_n + E_R - E_{^3\text{He}}$$

where E_n is the neutron energy

E_R is the energy of recoil nucleus

$E_{^3\text{He}}$ is the effective bombarding ^3He energy.

E_R can be solved from the following equation

$$E_{3\text{He}}^2 + 2M_{3\text{He}} c^2 E_{3\text{He}} - 2\sqrt{(E_{3\text{He}}^2 + 2M_{3\text{He}} c^2 E_{3\text{He}})(E_n^2 + 2M_n c^2 E_n)} \\ \times \cos\theta + E_n^2 + 2M_n c^2 E_n = E_R^2 + 2M_R c^2 E_R$$

The final Q for various small levels were obtained by weighted mean from the measurements.

The standard deviations of the mean σ_m were calculated

$$\sigma_m^2 = \frac{\sum \omega_i \delta_i^2}{(n-1) \sum \omega_i}$$

where δ_i are the deviations of each measurement from the mean, n is the number of measurements, ω_i is the weighting factors estimated from the internal error of each measurement.

The overall uncertainty of the measurements were estimated from errata arising from distance measurements, ~ 0.5 cm; $E_{3\text{He}}$, ~ 5 keV; time calibration of the TAC, ~ 0.00049 nsec/channel; angle measurement, 0.30 degrees and the averaged peak channel determination.

In Table 10 the calculated ground state Q was then compared from the known mass measurement results of MTW (MA 65A).

Table 10. Ground State Q Values (MeV)

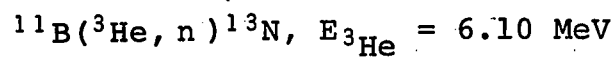
Reactions	Calculate from		Present Measurements	
	MTW	Q	Standard Deviation	Overall Error
$^{11}\text{B}(^3\text{He},n)^{13}\text{N}$	10.182	10.183	0.002	0.011
$^{13}\text{C}(^3\text{He},n)^{15}\text{O}$	7.125	7.123	0.003	0.007

The excited states measurements for both ^{13}N and ^{15}O especially the higher states presented by this calculation are believed to be the most accurate measurements to date.

APPENDIX III
TABLES OF CROSS SECTIONS

C.M.Angle (degree)	Sigma (mb/se.)	Error (mb/sr.)	C.M.Angle (degree)	Sigma (mb/sr)	Error (mb/sr.)
-----------------------	-------------------	-------------------	-----------------------	------------------	-------------------

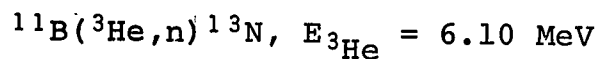
<u>0.0 MeV State</u>			<u>2.358 MeV State</u>		
0.0	1.078	0.036	0.0	0.283	0.020
0.0	1.046	0.036	0.0	0.274	0.024
5.42	1.057	0.036	5.45	0.375	0.056
10.83	1.067	0.044	10.90	0.509	0.024
16.24	1.073	0.040	16.35	0.663	0.040
21.63	0.994	0.040	21.78	0.824	0.032
32.39	0.979	0.032	32.60	0.981	0.044
43.07	0.950	0.036	53.98	0.586	0.028
53.66	0.859	0.032	59.26	0.592	0.048
58.92	0.911	0.044	64.51	0.486	0.024
64.14	0.802	0.028	69.71	0.478	0.020
69.33	0.764	0.036	74.89	0.415	0.024
74.29	0.619	0.024	80.02	0.292	0.016
79.62	0.527	0.036	85.12	0.266	0.024
94.78	0.415	0.016	95.20	0.126	0.024
104.71	0.449	0.024	105.12	0.179	0.012
104.71	0.405	0.020	105.12	0.240	0.028
114.49	0.490	0.016	114.88	0.171	0.016
124.14	0.570	0.032	124.50	0.223	0.016
133.66	0.530	0.024	133.98	0.247	0.012
138.37	0.600	0.028	138.67	0.187	0.028
143.07	0.540	0.028	143.34	0.230	0.016
147.74	0.580	0.028	147.98	0.264	0.016



C.M.Angle (degree)	Sigma (mb/sr.)	Error (mb/sr.)	C.M.Angle (degree)	Sigma (mb/sr.)	Error (mb/sr.)
<u>3.502 + 3.55 MeV States</u>			<u>6.353 MeV State</u>		
0.0	5.074	0.164	0.0	0.333	0.016
5.48	5.173	0.160	0.0	0.312	0.016
10.95	4.908	0.164	5.55	0.346	0.020
16.41	4.095	0.140	11.09	0.364	0.020
32.73	2.293	0.076	16.62	0.397	0.024
43.51	1.812	0.060	22.15	0.411	0.024
54.18	1.281	0.048	33.14	0.400	0.024
59.47	1.358	0.052	44.04	0.310	0.012
64.73	1.232	0.040	54.81	0.254	0.012
69.95	1.364	0.060	60.15	0.214	0.016
75.13	1.210	0.040	65.44	0.256	0.016
80.27	1.203	0.044	70.70	0.160	0.012
85.37	1.181	0.036	75.91	0.161	0.012
95.46	1.264	0.044	81.07	0.136	0.012
105.37	1.248	0.044	86.19	0.175	0.012
105.37	1.283	0.052	96.28	0.145	0.012
115.12	1.316	0.056	106.19	0.182	0.016
124.72	1.116	0.044	106.19	0.173	0.012
134.17	1.011	0.036	115.90	0.190	0.012
138.85	0.901	0.036	125.44	0.224	0.016
143.50	0.861	0.036	134.81	0.246	0.016
148.12	0.799	0.036	139.44	0.221	0.016
			144.03	0.278	0.016
			148.60	0.317	0.016

$${}^{11}\text{B}({}^3\text{He},n){}^{13}\text{N}, E_{{}^3\text{He}} = 6.10 \text{ MeV}$$

C.M.Angle (degree)	Sigma (mb/sr.)	Error (mb/sr.)	C.M.Angle (degree)	Sigma (mb/sr.)	Error (mb/sr.)
<u>6.875 MeV State</u>			<u>7.363 MeV State</u>		
0.0	0.163	0.020	0.0	0.655	0.036
5.56	0.159	0.020	0.0	0.638	0.028
11.12	0.184	0.016	11.16	0.637	0.032
16.68	0.103	0.036	16.73	0.433	0.032
22.22	0.236	0.020	22.29	0.561	0.028
33.24	0.211	0.016	33.35	0.369	0.024
44.17	0.197	0.020	44.30	0.381	0.028
54.97	0.205	0.016	55.13	0.298	0.020
60.31	0.218	0.032	65.80	0.384	0.024
65.62	0.218	0.016	76.30	0.479	0.028
76.10	0.173	0.016	81.47	0.513	0.036
81.27	0.167	0.016	86.60	0.479	0.028
86.39	0.234	0.016	96.70	0.557	0.032
96.49	0.124	0.012	106.60	0.557	0.028
106.39	0.203	0.028	106.60	0.583	0.036
106.39	0.223	0.036	116.29	0.549	0.036
116.09	0.163	0.024	125.80	0.599	0.040
125.61	0.171	0.028	135.13	0.589	0.036
134.96	0.170	0.016	139.73	0.685	0.048
144.16	0.194	0.020	144.30	0.629	0.036
148.71	0.294	0.028	148.83	0.849	0.052
<u>7.145 MeV State</u>			<u>8.918 MeV State</u>		
0.0	0.465	0.024	0.0	0.682	0.060
0.0	0.490	0.024	0.0	0.580	0.036
11.15	0.556	0.024	11.29	0.391	0.048
16.71	0.560	0.032	22.55	0.570	0.108
22.26	0.525	0.024	44.79	0.315	0.024
33.30	0.588	0.028	55.71	0.308	0.052
44.25	0.462	0.028	66.46	0.318	0.036
55.06	0.497	0.024	87.35	0.392	0.032
65.72	0.439	0.024	126.46	0.461	0.056
76.21	0.337	0.020	144.79	0.636	0.052
81.39	0.332	0.024	149.27	0.521	0.060
86.51	0.379	0.024			
96.91	0.326	0.020			
106.51	0.344	0.020			
106.51	0.386	0.028			
116.21	0.403	0.028			
125.72	0.507	0.032			
135.06	0.442	0.024			
139.67	0.430	0.032			
144.24	0.560	0.032			
148.78	0.579	0.032			



C.M. Angle (degree)	Sigma (mb/sr.)	Error (mb/sr.)	C.M. Angle (degree)	Sigma (mb/sr.)	Error (mb/sr.)
------------------------	-------------------	-------------------	------------------------	-------------------	-------------------

9.476 MeV State

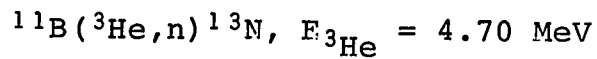
0.0	1.043	0.016
0.0	0.867	0.416
11.36	0.765	0.036
17.03	0.614	0.036
22.68	0.426	0.028
33.92	0.249	0.020
45.04	0.207	0.024
56.01	0.208	0.020
61.43	0.120	0.024
66.80	0.198	0.020
77.38	0.137	0.020
82.59	0.085	0.024
87.74	0.221	0.072
107.73	0.123	0.024
117.38	0.122	0.016
125.79	0.231	0.048
136.01	0.144	0.024
145.04	0.123	0.020
149.49	0.243	0.032

11.878 MeV State

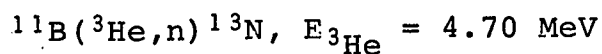
0.0	1.124	0.180
0.0	1.653	0.248
5.91	1.859	0.272
11.81	1.947	0.288
17.70	1.223	0.184
23.57	1.173	0.172
35.22	0.943	0.136
46.72	0.758	0.112
58.01	0.229	0.036
69.06	0.605	0.092
79.84	0.500	0.076
100.48	0.735	0.124
129.06	0.384	0.092
146.71	0.405	0.116
150.98	0.471	0.104

10.381 MeV State

0.0	0.232	0.028
0.0	0.331	0.024
5.74	0.376	0.040
11.48	0.293	0.040
17.21	0.404	0.040
22.92	0.491	0.032
34.28	0.682	0.048
45.50	0.847	0.068
56.56	0.785	0.056
62.02	0.688	0.060
67.42	0.729	0.060
78.05	0.672	0.060
83.28	0.512	0.048
88.44	0.604	0.056
98.57	0.438	0.044
108.44	0.491	0.052
118.05	0.564	0.068
127.41	0.602	0.072
136.55	0.610	0.080
141.05	0.893	0.124
145.50	0.831	0.116
149.90	0.893	0.128



C.M.Angle (degree)	Sigma (mb/sr.)	Error (mb/sr.)	C.M.Angle (degree)	Sigma (mb/sr.)	Error (mb/sr.)
<u>0.0 MeV State</u>			<u>3.502 + 3.55 MeV State</u>		
0.0	1.338	0.052	0.0	4.629	0.140
10.76	1.282	0.050	10.87	4.134	0.127
21.49	1.162	0.042	21.71	3.278	0.106
32.18	1.101	0.046	32.49	2.550	0.087
42.80	0.975	0.056	43.21	1.973	0.068
53.34	0.988	0.057	53.82	1.833	0.078
63.77	0.884	0.048	64.32	1.790	0.069
74.09	0.641	0.051	74.69	1.629	0.057
84.29	0.533	0.038	84.91	1.625	0.067
94.35	0.582	0.046	94.99	1.594	0.063
104.29	0.761	0.041	104.91	1.350	0.059
114.09	0.879	0.056	114.69	1.332	0.077
123.77	0.847	0.045	124.32	1.362	0.080
133.33	0.902	0.045	133.82	1.237	0.096
142.79	0.966	0.131	143.20	1.286	0.096
<u>2.358 MeV State</u>			<u>6.353 MeV State</u>		
0.0	0.310	0.020	0.0	0.360	0.043
10.83	0.473	0.026	11.02	0.450	0.043
21.63	0.806	0.038	22.02	0.542	0.046
32.39	0.990	0.044	32.95	0.591	0.048
43.07	0.840	0.049	43.79	0.646	0.055
53.66	0.720	0.042	54.72	0.559	0.054
64.13	0.621	0.033	65.11	0.538	0.053
74.49	0.490	0.043	75.55	0.548	0.057
84.70	0.390	0.027	85.81	0.504	0.055
94.77	0.332	0.022	95.90	0.485	0.059
104.70	0.366	0.027	105.81	0.462	0.047
114.48	0.330	0.032	115.54	0.459	0.048
124.13	0.326	0.029	125.11	0.434	0.054
133.65	0.336	0.027	134.51	0.382	0.045
143.06	0.668	0.202	143.79	0.454	0.060



C.M.Angle (degree)	Sigma (mb/sr.)	Error (mb/sr.)	C.M.Angle (degree)	Sigma (mb/sr.)	Error (mb/sr.)
-----------------------	-------------------	-------------------	-----------------------	-------------------	-------------------

6.875 MeV State

0.0	0.285	0.112
11.06	0.676	0.406
22.09	0.502	0.059
33.06	0.468	0.043
43.93	0.373	0.064
54.69	0.376	0.042
65.30	0.243	0.059
75.75	0.278	0.060
86.03	0.545	0.088
96.12	0.340	0.194
115.75	0.219	0.176
143.93	0.602	0.081

7.363 MeV State

0.0	0.530	0.068
11.10	0.545	0.072
22.17	0.532	0.052
33.18	0.587	0.053
44.08	0.787	0.073
54.87	0.739	0.063
65.50	0.785	0.068
75.97	0.836	0.070
86.26	0.883	0.076
96.36	0.892	0.075
106.26	0.804	0.070
115.97	0.680	0.061
125.50	0.663	0.111
134.86	0.574	0.066
144.08	0.707	0.078

7.145 MeV State

0.0	0.490	0.179
11.08	0.312	0.139
22.13	0.304	0.041
33.11	0.359	0.040
44.00	0.383	0.044
54.77	0.388	0.038
65.60	0.593	0.057
75.86	0.544	0.049
86.14	0.526	0.051
96.23	0.477	0.045
106.14	0.597	0.053
115.85	0.523	0.048
125.39	0.500	0.051
134.77	0.549	0.063
144.00	0.483	0.059

9.476 MeV State

0.0	1.223	0.105
11.33	1.012	0.092
22.63	0.581	0.055
33.84	0.424	0.049
44.94	0.287	0.047
55.89	0.453	0.066
66.67	0.461	0.051
77.24	0.473	0.076
87.58	0.574	0.060
97.70	0.506	0.051
107.58	0.451	0.050
117.23	0.414	0.050
135.89	0.462	0.058
144.94	0.647	0.072
144.94	0.647	0.072

$^{11}\text{B}(^3\text{He},n)^{13}\text{N}, E_{^3\text{He}} = 4.70 \text{ MeV}$

C.M.Angle (degree)	Sigma (mb/sr.)	Error (mb/sr.)	C.M.Angle (degree)	Sigma (mb/sr.)	Error (mb/sr.)
-----------------------	-------------------	-------------------	-----------------------	-------------------	-------------------

10.381 MeV State

22.94	0.437	0.049
45.53	0.824	0.077
56.59	0.884	0.082
78.09	0.878	0.086
88.48	1.129	0.101
98.61	0.895	0.077
108.48	0.926	0.094
118.09	0.989	0.091
127.45	0.790	0.075
136.59	0.818	0.074
145.52	0.810	0.076

11.878 MeV State

0.0	2.150	0.328
11.98	1.837	0.268
23.90	1.473	0.216
35.70	1.454	0.216
47.34	0.545	0.084

11.53 MeV State

0.0	2.020	0.316
11.82	1.627	0.248
23.60	1.483	0.228
35.26	1.553	0.236

$^{12}\text{C}(^3\text{He},n)^{14}\text{O}$, $E_{^3\text{He}} = 6.10 \text{ MeV}$

C.M. Angle (degree)	Cross Section (Arbitrary Unit)	Error
<u>0.0 MeV State</u>		
0.0	2.854	0.252
0.0	3.371	0.296
5.82	3.380	0.304
11.64	3.314	0.292
17.45	2.560	0.224
23.24	2.036	0.204
34.73	0.825	0.084
46.09	0.321	0.036
57.26	0.388	0.044
62.77	0.260	0.048
68.22	0.379	0.040
78.92	0.351	0.044
84.17	0.216	0.032
89.35	0.209	0.028
109.35	0.150	0.024
109.35	0.262	0.040
118.92	0.300	0.044
128.21	0.421	0.064
137.26	0.741	0.108
141.70	0.813	0.120
146.08	0.831	0.124
150.43	0.943	0.140

$^{13}\text{C}(^3\text{He},n)^{15}\text{O}, E_{^3\text{He}} = 6.2 \text{ MeV}$

C.M.Angle (degree)	Sigma (mb/sr.)	Error (mb/sr.)	C.M.Angle (degree)	Sigma (mb/sr.)	Error (mb/sr.)
<u>0.0 MeV State</u>			<u>6.182 MeV State</u>		
0.0	6.110	0.228	0.0	0.958	0.074
5.40	6.194	0.285	5.57	0.905	0.071
10.81	4.699	0.265	11.15	0.943	0.084
16.20	3.836	0.186	16.71	1.087	0.088
21.59	2.861	0.167	22.26	1.139	0.090
26.96	1.914	0.107	27.79	1.247	0.094
32.32	1.377	0.084	33.30	1.329	0.105
42.99	0.956	0.065	44.24	1.041	0.074
53.56	0.642	0.041	55.06	0.832	0.067
64.03	0.341	0.030	65.72	0.543	0.044
74.37	0.265	0.028	76.21	0.488	0.037
84.58	0.452	0.036	86.51	0.482	0.038
* → 104.58	→ 0.592	→ 0.043	→ 106.51	→ 0.649	→ 0.049
* → 124.02	→ 0.334	→ 0.032	→ 125.72	→ 0.705	→ 0.067
133.56	0.304	0.033	135.06	0.805	0.047
142.98	0.560	0.045	144.24	0.846	0.054
147.66	0.716	0.059	148.78	0.871	0.057
* 114.37	0.403	0.032	116.21	0.729	0.049
<u>5.232 MeV State</u>			<u>7.286 MeV State</u>		
0.0	2.444	0.172	0.0	0.280	0.029
5.53	2.470	0.179	5.64	0.435	0.038
11.06	2.500	0.186	11.27	0.447	0.038
16.59	2.517	0.178	16.89	0.426	0.037
22.10	2.548	0.176	22.50	0.504	0.041
27.59	2.370	0.176	28.09	0.585	0.048
33.06	2.224	0.162	33.65	0.755	0.060
43.94	1.834	0.130	44.70	0.839	0.058
54.70	1.819	0.128	55.60	0.984	0.062
65.31	1.729	0.120	66.33	1.014	0.065
75.76	1.551	0.111	76.87	0.888	0.055
86.04	1.513	0.108	87.20	0.673	0.043
106.04	1.380	0.096	107.20	0.522	0.033
115.76	1.406	0.091	116.87	0.554	0.032
125.31	1.140	0.079	126.33	0.491	0.032
134.69	1.064	0.076	135.60	0.485	0.029
143.94	1.235	0.464	144.69	0.433	0.027
148.51	1.162	0.105	149.19	0.434	0.033

$^{13}\text{C}(^3\text{He},n)^{15}\text{O}, E_{^3\text{He}} = 6.2 \text{ MeV}$

C.M.Angle (degree)	Sigma (mb/sr.)	Error (mb/sr.)	C.M.Angle (degree)	Sigma (mb/sr.)	Error (mb/sr.)
<u>7.570 MeV State</u>			<u>8.926 MeV State</u>		
0.0	0.321	0.047	0.0	8.187	0.524
5.65	0.288	0.036	11.55	6.881	0.416
11.30	0.247	0.032	17.32	4.826	0.488
16.94	0.352	0.037	23.06	4.010	0.221
22.57	0.444	0.039	28.79	2.472	0.554
28.18	0.427	0.041	34.48	2.078	0.215
33.76	0.424	0.040	45.76	1.108	0.132
44.83	0.299	0.029	56.87	1.384	0.091
55.76	0.275	0.030	67.78	1.172	0.242
66.52	0.168	0.019	88.85	1.584	0.151
77.07	0.239	0.025	118.44	0.880	0.160
87.41	0.253	0.023	127.77	0.928	0.084
107.41	0.347	0.024	136.87	0.724	0.065
117.07	0.444	0.032	150.14	0.843	0.089
126.51	0.365	0.034			
135.76	0.337	0.025			
144.83	0.345	0.027			
149.31	0.301	0.031			
<u>8.750 MeV State</u>			<u>8.974 MeV State</u>		
0.0	0.505	0.047	0.0	1.765	0.417
5.76	0.922	0.086	5.79	1.786	0.238
11.51	0.746	0.096	11.57	1.617	0.327
17.25	0.675	0.065	17.34	2.257	0.472
22.98	0.662	0.086	23.09	1.098	0.146
28.68	0.773	0.058	28.82	1.203	0.590
34.36	0.656	0.054	34.52	0.735	0.194
45.61	0.532	0.037	45.82	0.585	0.131
56.69	0.429	0.062	56.94	0.347	0.057
67.56	0.306	0.056	67.85	1.013	0.257
108.60	0.321	0.041	88.93	0.466	0.112
118.21	0.122	0.043	118.52	0.632	0.158
127.56	0.558	0.190	127.85	0.579	0.069
136.68	0.457	0.046	136.93	0.606	0.063
145.60	0.429	0.293	150.19	0.523	0.062
150.00	0.512	0.167			

$^{13}\text{C}(^3\text{He},n)^{15}\text{O}, E_{^3\text{He}} = 6.2 \text{ MeV}$

C.M.Angle (degree)	Sigma (mb/sr.)	Error (mb/sr.)	C.M.Angle (degree)	Sigma (mb/sr.)	Error (mb/sr.)
-----------------------	-------------------	-------------------	-----------------------	-------------------	-------------------

9.499 MeV State

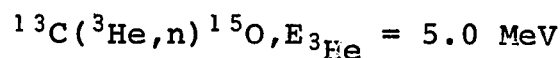
5.86	1.001	0.070
11.71	1.018	0.069
17.54	1.656	0.102
23.36	2.121	0.119
29.16	2.625	0.149
34.92	3.263	0.185
46.33	3.220	0.192
57.55	2.943	0.183
68.54	2.329	0.151
79.27	1.654	0.122
89.72	1.308	0.100
109.72	1.112	0.100
119.27	1.292	0.138
128.54	1.378	0.155
137.54	1.247	0.153
146.32	1.180	0.175
150.64	0.914	0.140

9.665 MeV State

5.88	1.286	0.114
11.75	1.102	0.089
17.61	1.138	0.111
23.45	0.896	0.096
29.26	0.920	0.086
35.04	0.869	0.128
46.49	0.643	0.068
57.74	0.724	0.080
68.75	0.453	0.067
79.51	0.612	0.129
89.97	0.796	0.070
109.96	0.519	0.164
119.50	0.505	0.068
128.75	0.584	0.096
137.73	0.408	0.072
146.48	0.244	0.049

9.612 MeV State

5.87	0.928	0.098
11.73	0.938	0.081
17.57	1.259	0.113
23.40	1.881	0.143
29.20	2.042	0.144
34.97	2.162	0.183
46.40	2.133	0.139
57.63	1.644	0.122
68.64	0.945	0.092
79.38	0.690	0.131
89.83	0.288	0.033
109.83	0.736	0.188
119.37	0.542	0.066
128.63	1.001	0.126
146.40	1.172	0.197
150.70	0.662	0.115



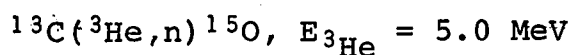
C.M.Angle (degree)	Sigma (mb/sr.)	Error (mb/sr.)	C.M.Angle (degree)	Sigma (mb/sr.)	Error (mb/sr.)
<u>0.0 MeV State</u>			<u>6.183 MeV State</u>		
0.0	4.628	0.236	0.0	1.396	0.094
0.0	4.200	0.201	0.0	1.357	0.099
5.38	4.349	0.205	5.56	1.380	0.094
10.75	3.644	0.173	11.12	1.322	0.091
16.12	2.990	0.153	16.67	1.207	0.089
21.49	2.184	0.142	22.21	1.223	0.093
26.84	1.838	0.095	27.73	1.065	0.072
32.17	1.257	0.101	33.23	1.018	0.065
37.49	0.990	0.068	38.71	1.004	0.076
42.79	0.709	0.054	44.15	1.012	0.077
48.07	0.574	0.041	49.57	0.818	0.058
53.33	0.518	0.051	54.95	0.734	0.055
63.77	0.466	0.044	65.60	0.715	0.050
74.09	0.613	0.045	76.08	0.742	0.053
84.28	0.795	0.074	86.37	0.761	0.058
94.35	0.897	0.058	96.47	0.893	0.060
104.28	0.776	0.059	106.37	0.915	0.068
114.08	0.638	0.057	116.08	1.013	0.067
123.76	0.442	0.047	125.60	1.148	0.073
133.33	0.389	0.044	134.95	1.107	0.078
142.79	0.469	0.047	144.15	1.027	0.066
<u>5.232 MeV State</u>			<u>6.790 MeV State</u>		
0.0	0.945	0.067	0.0	1.155	0.227
0.0	0.882	0.065	5.60	1.331	0.170
5.52	0.926	0.064	11.20	.865	0.170
11.03	0.975	0.068	16.79	1.176	0.217
16.53	1.231	0.084	22.36	1.225	0.126
22.03	1.282	0.095	27.92	1.084	0.133
27.51	1.233	0.086	33.45	1.357	0.184
32.96	1.410	0.093	38.96	1.238	0.333
38.40	1.371	0.097	44.44	0.847	0.184
43.81	1.313	0.096	49.89	0.709	0.155
49.19	1.350	0.087	55.30	0.369	0.096
54.54	1.404	0.109	65.99	0.328	0.196
65.14	1.229	0.087	76.50	0.360	0.173
75.58	1.213	0.084	86.81	0.442	0.350
85.85	0.986	0.077	106.81	0.527	0.088
95.93	1.013	0.069	116.50	0.396	0.082
105.84	0.916	0.073	125.98	0.472	0.143
115.57	0.777	0.064	135.29	0.394	0.115
125.14	0.708	0.060	144.44	0.422	0.090
134.54	0.766	0.062			
143.81	0.787	0.060			

$^{13}\text{C}(^3\text{He},n)^{15}\text{O}, E_{^3\text{He}} = 5.0 \text{ MeV}$

C.M.Angle (degree)	Sigma (mb/sr.)	Error (mb/sr.)	C.M.Angle (degree)	Sigma (mb/sr.)	Error (mb/sr.)
<u>6.869 MeV State</u>			<u>7.570 MeV State</u>		
0.0	0.526	0.234	0.0	0.607	0.038
5.61	0.546	0.164	0.0	0.607	0.042
11.21	1.030	0.176	5.66	0.690	0.047
16.80	0.712	0.218	11.32	0.662	0.043
22.38	0.770	0.121	16.96	0.667	0.060
27.94	1.018	0.139	22.60	0.768	0.052
33.48	0.690	0.183	28.21	0.698	0.046
38.99	0.602	0.329	33.80	0.698	0.051
44.47	0.836	0.186	39.36	0.683	0.049
49.92	0.774	0.161	44.88	0.495	0.038
55.33	0.910	0.108	50.37	0.435	0.031
66.03	0.600	0.196	55.82	0.324	0.031
76.54	0.484	0.178	66.58	0.169	0.021
86.86	0.411	0.349	77.15	0.180	0.038
106.86	0.428	0.092	97.61	0.242	0.027
116.54	0.540	0.091	107.49	0.378	0.047
126.03	0.355	0.142	117.14	0.447	0.036
135.33	0.379	0.123	126.58	0.573	0.041
144.47	0.306	0.093	135.82	0.587	0.042
			144.88	0.680	0.045
<u>7.286 MeV State</u>			<u>8.750 MeV State</u>		
0.0	0.219	0.024	0.0	0.486	0.051
0.0	0.305	0.052	5.81	0.525	0.049
5.63	0.268	0.031	11.61	0.374	0.044
11.25	0.274	0.028	17.39	0.544	0.045
16.87	0.279	0.037	23.17	0.620	0.058
22.47	0.321	0.033	28.91	0.523	0.040
28.05	0.265	0.027	34.63	0.586	0.051
33.61	0.576	0.034	40.31	0.559	0.051
39.15	0.604	0.038	45.96	0.591	0.107
44.65	0.770	0.045	51.56	0.464	0.063
50.11	0.730	0.034	57.10	0.343	0.056
55.54	0.798	0.042	68.04	0.326	0.036
66.26	0.863	0.042			
76.80	1.041	0.049			
87.13	1.088	0.058			
97.24	1.067	0.043			
107.13	1.058	0.050			
116.80	1.112	0.056			
126.26	1.082	0.055			
135.54	0.886	0.047			
144.64	0.599	0.035			

$$^{13}\text{C}(^3\text{He},n)^{15}\text{O}, E_{^3\text{He}} = 5.0 \text{ MeV}$$

C.M. Angle (degree)	Sigma (mb/sr.)	Error (mb/sr.)	C.M. Angle (degree)	Sigma (mb/sr.)	Error (mb/sr.)
<u>8.926 MeV State</u>			<u>9.498 MeV State</u>		
0.0	2.965	0.267	0.0	0.719	0.053
5.84	2.875	0.296	0.0	0.729	0.063
11.67	2.666	0.222	5.97	0.805	0.062
17.49	2.420	0.179	11.93	0.926	0.075
29.07	1.412	0.139	17.88	0.964	0.074
34.81	0.879	0.108	23.80	1.135	0.087
40.52	0.933	0.106	29.70	1.125	0.073
46.19	0.902	0.083	35.57	1.116	0.072
51.81	0.953	0.074	41.39	1.298	0.097
68.35	1.180	0.106	47.16	1.350	0.103
79.07	1.275	0.101	52.89	1.187	0.074
89.51	1.195	0.145	58.55	1.216	0.091
99.65	1.373	0.078	69.67	1.122	0.078
109.51	0.780	0.092	80.50	0.931	0.067
119.07	0.834	0.061	91.01	0.965	0.118
128.35	0.571	0.062	101.18	0.947	0.072
137.38	0.477	0.048	111.01	0.860	0.071
146.19	0.376	0.043	120.50	0.959	0.074
			129.67	0.691	0.081
			138.54	0.751	0.083
<u>8.974 MeV State</u>			<u>9.612 MeV State</u>		
0.0	1.108	0.249	0.0	0.810	0.070
5.85	1.183	0.282	0.0	0.687	0.088
11.69	0.924	0.195	5.98	0.992	0.076
17.52	0.758	0.146	11.95	0.589	0.147
29.12	0.707	0.137	17.91	0.976	0.077
34.88	0.761	0.123	23.85	0.744	0.102
40.60	0.550	0.101	29.76	1.181	0.082
46.27	0.523	0.079	35.63	1.027	0.100
51.90	0.624	0.072	41.47	1.230	0.099
68.47	0.747	0.102	47.25	1.131	0.102
79.19	0.811	0.094	52.98	0.977	0.098
89.64	0.913	0.147	58.65	0.899	0.081
99.79	0.717	0.059	69.79	0.476	0.063
109.64	1.261	0.122	80.63	0.548	0.068
119.19	0.717	0.062	91.15	0.493	0.070
128.46	0.905	0.076	101.32	0.478	0.051
137.48	0.803	0.068	111.15	0.754	0.089
146.27	0.816	0.068	120.63	0.887	0.079
			129.79	0.865	0.094
			138.65	1.151	0.142
			147.25	1.019	0.090



C.M. Angle (degree)	Sigma (mb/sr.)	Error (mb/sr.)	C.M. Angle (degree)	Sigma (mb/sr.)	Error (mb/sr.)
<u>8.926 MeV State</u>			<u>9.498 MeV State</u>		
0.0	2.965	0.267	0.0	0.719	0.053
5.84	2.875	0.296	0.0	0.729	0.063
11.67	2.666	0.222	5.97	0.805	0.062
17.49	2.420	0.179	11.93	0.926	0.075
29.07	1.412	0.139	17.88	0.964	0.074
34.81	0.879	0.108	23.80	1.135	0.087
40.52	0.933	0.106	29.70	1.125	0.073
46.19	0.902	0.083	35.57	1.116	0.072
51.81	0.953	0.074	41.39	1.298	0.097
68.35	1.180	0.106	47.16	1.350	0.103
79.07	1.275	0.101	52.89	1.187	0.074
89.51	1.195	0.145	58.55	1.216	0.091
99.65	1.373	0.078	69.67	1.122	0.078
109.51	0.780	0.092	80.50	0.931	0.067
119.07	0.834	0.061	91.01	0.965	0.118
128.35	0.571	0.062	101.18	0.947	0.072
137.38	0.477	0.048	111.01	0.860	0.071
146.19	0.376	0.043	120.50	0.959	0.074
			129.67	0.691	0.081
			138.54	0.751	0.083
<u>8.974 MeV State</u>			<u>9.612 MeV State</u>		
0.0	1.108	0.249	0.0	0.810	0.070
5.85	1.183	0.282	0.0	0.687	0.088
11.69	0.924	0.195	5.98	0.992	0.076
17.52	0.758	0.146	11.95	0.589	0.147
29.12	0.707	0.137	17.91	0.976	0.077
34.88	0.761	0.123	23.85	0.744	0.102
40.60	0.550	0.101	29.76	1.181	0.082
46.27	0.523	0.079	35.63	1.027	0.100
51.90	0.624	0.072	41.47	1.230	0.099
68.47	0.747	0.102	47.25	1.131	0.102
79.19	0.811	0.094	52.98	0.977	0.098
89.64	0.913	0.147	58.65	0.899	0.081
99.79	0.717	0.059	69.79	0.476	0.063
109.64	1.251	0.122	80.63	0.548	0.068
119.19	0.717	0.062	91.15	0.493	0.070
128.46	0.905	0.076	101.32	0.478	0.051
137.48	0.803	0.068	111.15	0.754	0.089
146.27	0.816	0.068	120.63	0.887	0.079
			129.79	0.865	0.094
			138.65	1.151	0.142
			147.25	1.019	0.090

REFERENCES

- AB 66 A.Y.ABUL-MAGD & M.EL NADI, NUCL. PHYS.,
1966, <77>, 182.
- AD 61 H.S.ADAMS, J.D.FOX, N.P.HEYDENBERG & G.M.TEMMER,
PHYS. REV., 1961, <124>, 1899.
- AJ 62 F.A.AJZENBERG-SELOVE, ENERGY LEVELS OF LIGHT NUCLEI
(NATIONAL ACADEMY OF SCIENCE - NRC, WASHINGTON,
D.C., 1962).
- BA 61A F.C.BARKER, NUCL. PHYS., 1961, <28>, 96.
- BA 63A J.B.BALL, C.B.FULMER, AND C.D.GOODMAN, PHYS. REV.,
1963, <130>, 2342.
- BA 63B F.C.BARKER, G.D.SYMONS, N.W.TANNER & P.B.TREACY,
NUCL. PHYS., 1963, <45>, 449.
- BA 63C F.C.BARKER, NUCL. PHYS., 1963, <45>, 467.
- BA 66 D.BACHELIER, M.BERNAS, I.BRISSAUD, P.RADVANYI AND
M.ROY, NUCL. PHYS., 1966, <88>, 307.
- BA 67 J.BANG, N.S.ZELENKAYA, E.Z.MAGZUMOV,
V.G.NEUDACHIN, JNP(U.S.S.R.), 1966, <4>, 962.
SOVIET PHYS. JNP, 1966, <4>, 688.
- BE 66 G.BENCZE & J.ZIMANYI, NUCL. PHYS., 1966, <81>, 76.
- BI 67 P.G.BIZZETI, A.M.BIZZETI-SONA, S.KALBITZER & B.POVH,
NUCL. PHYS., 1967, <A104>, 577.
- BJ 59 F.BJORKLUND, PROCEEDING OF THE INTERNATIONAL CONF.
ON NUCLEAR OPTICAL MODEL, (FLORIDA STATE UNIV., 1959) P1.
- BL 52 J.M.BLATT & L.C. BEIDENHARN, REV. MOD. PHYS., 1952,
<24>, 258.
- BL 57 J.S.BLAIR, PHYS. REV., 1957, <108>, 827.
- BO 56 T.W.BONNER, A.A.KRAUS, J.B.MARION & J.P.SCHIFFER,
PHYS. REV., 1956, <102>, 1348.
- BO 57 C.R.BOLMGREN, G.D.FREIER, J.G.LIKELY, AND
K.F.FAMULARO, PHYS. REV., 1957, <105>, 210.
- BR 57 D.A.BROMLEY, E.ALMQVIST, H.E.GOVE, A.E.LITHERLAND,
E.B.PAUL & J.J.FERGUSON, PHYS. REV., 1957,
<105>, 957.
- BR 60 D.A.BROMLEY & E.ALMQVIST, REPORTS ON PROGRESS IN
PHYSICS, 1960, <23>, 544.

BR 68 K.H.BRAY, J.NURZYNSKI & W.P.BAURKE, NUCL. PHYS.,
1968, <A114>, 309.

BU 57 S.T.BUTLER, PHYS. REV., 1957, <106>, 272.

CD 63 J.COHEN-GANDOURA, M.LAMBERT, & J. SCHMOUKER,
J. PHYS. RADIUM, 1963, <24>, 43.

DA 64 A.DAR, NUCL.PHYS., 1964, <55>, 305.

DA 68 N.E.DAVISON, PRIVATE COMMUNICATION.

DE 64A J.DELAUNAY, NUCLEAR STRUCTURE AND NUCLEAR
REACTIONS, PROC. OF THE 9TH SUMMER MEETING OF
NUCLEAR PHYSICISTS, ZAGREB, 1964.

DE 64B V.K.DESHPANDE, H.W.FULBRIGHT & J.W.VERBA,
NUCL. PHYS., 1965, <52>, 457.

DE 64C V.K.DESPANDE AND H.W.FULBRIGHT, UNIV. OF ROCHESTER
REPORT, 1964, UR-875-61.

DI 61 G.U.DIN, H.KUAN & T.W.BONNER, PROC. RUTHERFORD INT.
LONDON JUBILEE CONF., MANCHESTER, ED. BY J.B.BIRKS,
(HEYWOOD & CO., LONDON) 1961, P.499.

DI 64 G.U.DIN, H.M.KUAN & T.W.BONNER, NUCL. PHYS.,
1964, <50>, 267.

DI 65 G.U.DIN & J.L.WEIL, NUCL. PHYS., 1965, <73>, 161.

DI 66 G.U.DIN & J.L.WEIL, NUCL. PHYS., 1966, <86>, 509.

DU 63 J.L.DUGGAN, P.D.MILLER & R.F.GABBARD, NUCL. PHYS.,
1963, <46>, 336.

EA 67 L.G.EARWAKER, NUCL. PHYS., 1967, <A90>, 56.

EL 57 M.EL NADI, PROC. PHYS. SOC., 1957, <A70>, 62.

EL 60 A.L.ELWYN, J.V.KANE, S.OFER & R.PIXLEY,
PHYS. REV., 1960, <120>, 2207.

EL 66 F.EL BATANONI & A.A.KRESNIN, NUCL. PHYS., 1966,
<89>, 577.

EV 53 W.H.EVANS, T.S.GREEN & R.MIDDLETON,
PROC. PHYS. SOC. (LONDON), 1953, <A66>, 108.

EV 66 A.E.EVANS, E.BROWN & J.B.MARION, PHYS. REV., 1966,
<149>, 863.

FE 58 H.FESHBACH, ANN. PHYS. 1958, <5>, 357.

FE 59A A.J.FERGUSON, R.L.CLARKE & H.E.GOVE, PHYS. REV.,
1959, <115>, 1655.

FE 59B A.J.FERGUSON, PHYS. REV., 1959, <115>, 1660.

FE 62 H.FESHBACH, ANN. PHYS. 1962, <19>, 287.

FI 65 F.W.K.FIRK, FAST NEUTRON PHYSICS (PART II), ED. BY
J.B.MARION & J.L.FOWLER, INTERSCIENCE PUB.,
1965, P.2237.

FI 67 A.A.FIFE, G.C.NEILSON & W.K.DAWSON, NUCL. PHYS.,
1967, <A94>, 561.

FL 68 D.G.FLEMING, J.CERNY, C.C.MAPLES, & N.K.GLENDENNING,
PHYS. REV., 1968, <166>, 1012.

FR 68 G.FRANCK, M.SC. THESIS, UNIV. OF ALBERTA, 1968.

FU 65 H.W.FULBRIGHT, W.PARKER ALFORD, O.M.BILANIUK,
V.K.DESHPANDE & J.W.VERBA, NUCL. PHYS., 1965,
<70>, 553.

GA 60 N.H.GALE, J.B.GARG, J.M.CALVERT AND K.RAMAVATRAM,
NUCL. PHYS., 1960, <20>, 313.

GA 62 A.GARCIA, J.KIRK, J.B.A.ENGLAND & P.E.HODGSON,
NUCL. PHYS., 1962, <38>, 372.

GA 63 A.GALLMAN, D.E.ALBURGER, D.H.WILKINSON & F.HIBOU,
PHYS. REV., 1963, <129>, 1765.

GA 66 A.GALLMAN, F.HAAS, AND N.BALAUX, PHYS. REV., 1966,
<151>, 735.

GE 67 D.A.GEDCKE AND W.J.MCDONALD, NUCL. INSTR. & METS.,
1967, <56>, 148.

GI 68 R.D.GILL, J.S.LOPES, B.C.ROBERTSON, R.A.I.BELL AND
H.J.ROSE, NUCL. PHYS., 1968, <A106>, 678.

GL 62 N.K.GLENDENNING, NUCL. PHYS., 1962, <29>, 109.

GL 63 N.K.GLENDENNING, ANN. REV. OF NUCL. SCI.,
1963, <13>, 191.

GL 65 N.K.GLENDENNING, PHYS. REV., 1965, <137>, B102.

GL 66 R.N.GLOVER & A.D.W.JONES, NUCL. PHYS., 1966,
<81>, 277.

- GL 67 N.K.GLENDENNING, PHYS. REV., 1967, <156>, 1344.
- GO 54 H.E.GOVE, A.J.FERGUSON & J.T.SAMPLE, PHYS. REV., 1954, <93>, A928.
- GO 66 S.GORODETZKY, R.M.FREEMAN, A.GALLMANN AND F.HAAS, PHYS. REV., 1966, <149>, 801.
- GR 67 T.B.GRANDY, PH.D. THESIS, UNIV. OF ALBERTA, 1967.
- GU 51 J.B.GUNN & J.IRVING, PHIL. MAG., 1951, <42>, 1353.
- HA 52 W.HAUSER & H.FESHBACH, PHYS. REV., 1952, <87>, 366.
- HA 57A F.HAGEDORN, F.MOZER, T.WEBB, W.FOWLER & C.LAURITSEN, PHYS. REV., 1957, <105>, 219.
- HA 57B E.C.HALBERT & J.B.FRENCH, PHYS. REV., 1957, <105>, 1563.
- HE 59 D.F.HEBBARD & B.POVH, NUCL. PHYS., 1959, <13>, 642.
- HE 64A E.M.HENLEY & D.U.L.YU, PHYS. REV., 1964, <133>, B1445.
- HE 64B E.M.HENLEY & D.U.L.YU, PHYS. REV., 1964, <135>, B1152.
- HI 67 J.C.HIEBERT, E.NEWMAN & R.H.BASSEL, PHYS. REV., 1967, <154>, 898.
- HI 68 H.F.HINDERLITER, W.A.LOCHSTET, BULL. AM. PHYS. SOC., 1968, <13>, 606.
- HO 61 P.E.HODGSON, PROC. PHYS. SOC., 1961, <77>, 997.
- HO 63 P.E.HODGSON, SELECTED TOPICS IN NUCLEAR SPECTROSCOPY, PROC. OF THE NUFFIC CONFERENCE 1963.
- HO 63A P.E.HODGSON, THE OPTICAL MODEL OF ELASTIC SCATTERING (OXFORD UNIV. PRESS, LONDON, 1963), P119.
- HU 53 R.HUBY, PROGR. NUCL. PHYS., 1953, <3>, 177.
- HU 62 J.R.HUIZENGA & G.I.IGO, NUCL. PHYS., 1962, <29>, 462.
- IN 53 D.R.INGLIS, REV. MOD. PHYS., 1953, <25>, 390.
- JA 53A H.L.JACKSON, A.I.GALONSKY, F.J.EPPLING, R.W.HILL, E.GOLDBERG & J.R.CAMERON, PHYS. REV., 1953, <89>, 365.
- JA 53B H.L.JACKSON & A.I.GALONSKY, PHYS. REV., 1953, <89>, 370.

JD 61 R.G. JOHNSON, L.F. CHASE, JR. & F.J. VAUGHN,
PROC. RUTHERFORD INT. JUBILEE CONF., MANCHESTER,
1961. ED. BY J.B. BIRKS, (HEYWARD, LONDON) 1961, P.591

KO 67 R.L. KOZUB, L.A. KULL & E. KASHY, NUCL. PHYS.,
1967, <A99>, 540.

KU 56 D. KURATH, PHYS. REV., 1956, <101>, 216.

KU 60 J.A. KUEHNER, E. ALMQUIST & D.A. SROMLEY, NUCL. PHYS.,
1960, <21>, 555.

KU 61 D. KURATH & R.D. LAWSON, NUCL. PHYS., 1961, <23>, 5.

KU 67 H.M. KUAN & S.S. HANNA, PHYS. LETT., 1967, <248>, 566.

LA 54 A.M. LANE, PROC. PHYS. SOC., 1954, <A67>, 167.

LA 55 A.M. LANE, PROC. PHYS. SOC., 1955, <A68>, 197.

LA 60 A.M. LANE, REV. OF MOD. PHYS., 1960, <32>, 519.

LA 67A B. LAWERGREN & I.V. MITCHELL, NUCL. PHYS., 1967,
<A98>, 481.

LA 67B B. LAWERGREN, G.C. MORRISON, & A.T.G. FERGUSON, NUCL.
PHYS., 1967, <A106>, 455.

LE 61 J.J. LEIGH, PHYS. REV., 1961, <123>, 2145.

LI 64 C.L. LIN & S. YOSHIDA, PROGR. THEOR. PHYS. (KYOTO),
1964, <32>, 885.

LI 66 C. LIN & S. YOSHIDA, PROGR. THEOR. PHYS. (KYOTO),
1966, <36>, 251.

LO 66 A. LOUIS & C. NUSSBAUM, HELV. PHYS. ACTA, 1966,
<39>, 574.

MA 63 J.H. MANLEY, PHYS. REV., 1963, <130>, 1475.

MA 65A J.H.E. MATTAUCH, W. THIELE AND A.H. WAPSTRA, NUCLEAR
PHYSICS, 1965, <67>, 1.

MA 65B J.H.E. MATTAUCH, W. THIELE AND A.H. WAPSTRA, NUCLEAR
PHYSICS, 1965, <67>, 73.

MA 66A G.S. MANI & G.C. DUTT, NUCL. PHYS., 1966, <78>, 613.

MA 66B J.B. MARION, PHYS. LETT., 1966, <21>, 61.

MA 66C S.K. MARK, K.G. STANDING & Y.I. WU,
BULL. AM. PHYS. SOC., 1966, <12>, 52.

MC 67A W.J.MCDONALD AND D.A.GEDCKE, "DETECTION SYSTEM FOR A FAST NEUTRON TIME-OF-FLIGHT SPECTROMETER", UNIV. OF ALBERTA, NUCLEAR RESEARCH CENTRE REPORT, SEPT., 1967.

ME 60 J.B.MEAD & B.L.COHEN, PHYS. REV. LETT., 1960, <5>, 105.

MU 67 S.MUBARAKMAND AND B.E.F.MACEFIELD, NUCL. PHYS., 1967, <A98>, 82.

NE 56 T.D. NEWTON, CAN. J. PHSY., 1956, <34S>, 804.

NE 60 H.C.NEWS, PROC .PHYS. SOC., 1960, <A76>, 489.

NI 61 N.M.NIKOLIC, L.J.LIDOFKY & T.H.KRUSE, BULL. AM. PHYS. SOC., 1961, <6>, 25.

NO 62 M. NOMOTO, NUCL. PHYS., 1962, <30>, 514.

OB 66 A.OBST, M.SC. THESIS, UNIVERSITY OF ALBERTA, 1966.

PO 59 B.POVH & D.F.HEBBARD, PHYS. REV., 1959, <115>, 608.

RE 56 C.W.REICH, G.C.PHILLIPS & J.L.RUSSELL, PHYS. REV., 1956, <104>, 143.

RE 66 W.B.REID AND R.H.HUMMEL, CAN. NUCL. TECH., JAN. -FEB., 1966.

RI 64 G.RIPKA, COMP.REND.COG.INT. DE PHYSIQUE NUCLEAIRE, PARIS, VOL 2, 1964, P.390.

RO 61 D.ROBSON, NUCL. PHYS., 1961, <22>, 34.

RO 64A J.R.ROOK & D.MITRA, NUCL. PHYS., 1964, <51>, 96.

RO 64B M.L.ROUSH, M.A.WILSON AND W.F.HORNYAK, NUCL. INSTR. AND METHODS, 1964, <31>, 112.

RO 65 J.R.ROOK, NUCL. PHYS., 1965, <61>, 219.

RO 66 L.ROSEN, PROC. SECOND INTER. SYMP. ON POLARIZATION PHENOMENA OF NUCLEONS, ED. BY P.HUBER & H.SCHOPPER (BIRKHAUSEN VERLAG BASEL, BERN), 1966, P.253.

RO 67 J.R.ROOK, NUCL. PHYS., 1967, <A97>, 217.

SE 62A H.M.SEN GUPTA, J.ROTLAT, P.E.HODGSON & J.B.A.ENG- LAND, NUCL. PHYS., 1962, <38>, 361.

SE 65 K.K.SETH, PHYS. LETTERS, 1965, <16>, 306.

SE 66 K.K. SETH, R.G. COUCH, J.A. BIGGERSTAFF & P.D. MILLER,
PHYS. LETTERS, 1966, <17>, 1294.

SH 62 G.G. SHUTE, D. ROBSON, V.R. MCKENNA & A.T. BERZTISS,
NUCL. PHYS., 1962, <37>, 535.

SH 65 I.S. SHAPIRO & S.F. TIMASHEV, NUCL. PHYS.,
1965, <79>, 46.

SI 67 J.W.D. SINCLAIR, M.SC. THESIS, UNIV. OF ALTA., 1967.

SM 65 W.R. SMITH, ORK RIDGE NATIONAL LABORATORY REPORT,
ORNL-TM-1117, 1965.

TA 60 I. TALMI & I. UNNA, ANN. REV. OF NUCL. SCIENCE,
1960, <10>, 353.

TE 66 J.W. TEPEL, NUCL. INSTR. AND METHODS, 1966, <40>, 100.

TH 55 R.G. THOMAS, PHYS. REV., 1955, <100>, 25.

TO 56 W. TOBOCMAN, TECH. REP. NO. 29, CASE INSTITUTE OF
TECH., 1956.

TO 61 J.H. TOWLE AND B.E.F. MACEFIELD, PROC. PHYS. SOC.,
1961, <77>, 399.

WA 65A E.K. WARBURTON, J.W. OLNESS & D.E. ALBURGER, PHYS. REV.,
1965, <140>, B1202.

WA 65B E.K. WARBURTON, P.D. PACKER & P.F. DONOVAN, PHYS. LETT.,
1965, <19>, 397.

WI 63 D.L. WIEBER, NUCL. INSTR. AND METH., 1963, <24>, 269.

WO 51 L. WOLFENSTEIN, PHYS. REV., 1951, <82>, 690.

YO 60 H. YOSHIKI & N. NIKOLIC, BULL. AM. PHYS. SOC.,
1960, <5>, 46.